Universidad de Huelva

Departamento Ciencias Integradas

Bifurcaciones locales y globales en sistemas dinámicos y autónomos

Memoria para optar al grado de doctora
presentada por:

María de la Cinta Domínguez Moreno

Fecha de lectura: 23 de enero de 2024

Bajo la dirección de los doctores:

Antonio Algaba Durán

Manuel Merino Morlesín

Huelva, 2024

UNIVERSIDAD DE HUELVA
Departamento de Ciencias Integradas

BIFURCACIONES LOCALES Y GLOBALES EN SISTEMAS DINÁMICOS AUTÓNOMOS

Mª de la Cinta Domínguez Moreno

Julio 2023

UNIVERSIDAD DE HUELVA
Departamento de Ciencias Integradas

BIFURCACIONES LOCALES Y GLOBALES EN SISTEMAS DINÁMICOS AUTÓNOMOS

Programa de Ciencia y Tecnología Industrial y Ambiental

Directores de tesis:
Antonio Algaba Durán
Manuel Merino Morlesín

Doctorando:
Mª de la Cinta Domínguez Moreno

Julio 2023

BIFURCACIONES LOCALES Y GLOBALES EN SISTEMAS DINÁMICOS AUTÓNOMOS

Memoria presentada por D[a]. María de la Cinta Domínguez Moreno para optar al grado de Doctor por la Universidad de Huelva.

DOMINGUEZ MORENO MARIA DE LA CINTA - 48922342P

Firmado digitalmente por DOMINGUEZ MORENO MARIA DE LA CINTA - 48922342P
Fecha: 2023.07.26 18:58:55 +02'00'

Fdo.: María de la Cinta Domínguez Moreno.

Huelva, Julio de 2023.

Agradecimientos

Quisiera expresar mi más sincero agradecimiento por el apoyo y la ayuda recibida durante estos años de trabajo.

En primer lugar, a mis directores de tesis, D. Antonio Algaba Durán y D. Manuel Merino Morlesín, por introducirme en el campo de los sistemas dinámicos, y por su incondicional ayuda a lo largo de todos estos años. También quisiera agradecer al profesor D. Manuel Reyes Columé por todos los seminarios que impartió en el inicio de mi formación.

Debo mencionar a los compañeros y compañeras del Departamento de Matemática Aplicada II de la Universidad de Sevilla, con quienes he compartido muchos momentos, y en especial a D. Alejandro José Rodríguez Luis, con quien he colaborado en mis trabajos; agradecerle su ayuda desinteresada y su apoyo incondicional durante todos estos años.

Me gustaría dar las gracias a todos mis compañeros y compañeras del área de Matemáticas del Departamento de Ciencias Integradas de la Universidad de Huelva, por sus consejos y palabras de ánimo durante la realización de este trabajo; en especial a D. Antonio Lozano, Dª. Mónica Esquivel, Dª. Natalia Fuentes, Dª. Begoña Marchena y Dª. Irene García, que me recibieron con los brazos abiertos desde el primer día que llegué a esta universidad y que, junto al compañero D. Antonio Carlos Alarcón, hemos compartido tantas charlas durante la hora del café.

No se me puede olvidar todo el apoyo recibido por quienes pasaron por este Departamento; en especial a mi compañera Dª. Isabel Checa, quien iniciara este camino conmigo.

Agradecer de corazón a mis padres, pues sin su ayuda y su apoyo esto no hubiera sido posible; a mis hermanos, quienes me animaron a estudiar las matemáticas desde siempre; y a Boni, mi compañero de vida, por haber creído en mí desde el principio.

Y por último, y no menos importante, siempre llevaré en mi recuerdo al profesor D. Cristóbal García. Nunca olvidaré tu amabilidad y disponibilidad en todo momento. Muchas gracias allá donde estés.

A mis padres Antonio y Mari,
A Boni, mi compañero.

ÍNDICE GENERAL

Introducción: objetivos, metodología, resultados y conclusiones.

La teoría de bifurcaciones forma parte de la teoría general de sistemas dinámicos y se originó junto con la teoría cualitativa moderna a finales del siglo XIX, cuando Jules Henri Poincaré introdujo las ideas topológicas y geométricas en el estudio de la dinámica [27]. El concepto de bifurcación se formaliza al relacionarlo con el concepto de estabilidad estructural, que fue introducido por Andronov y Pontriaguin en 1937 [11].

Los avances más significativos se han producido en el contexto de la llamada teoría local de bifurcaciones, en la que se hace uso de dos herramientas básicas como son la reducción mediante el teorema de la variedad de centros y la simplificacion mediante formas normales [25, 43, 53, 67, 86].

Se ha constatado durante la segunda mitad del siglo XX, gracias a la colaboración de diversas disciplinas, que la conducta dinámica de los sistemas deterministas es extremadamente compleja. Para comprender dicha complejidad un primer paso consiste en proporcionar una descripción del "esqueleto" de un sistema dinámico: equilibrios y órbitas periódicas. Se trata de conocer la dinámica local en torno a las soluciones más simples (estacionarias y periódicas) y, además, mediante la prolongación de sus variedades estables e inestables indagar sobre sus intersecciones, lo que conduce a fenómenos de dinámica global.

El estudio de la dinámica global de un sistema Poincaré con el problema de los tres cuerpos [69]. Este problema lo comenzó estudiando Isaac Newton (1687) y posteriormente siguieron trabajando en él científicos como Euler y Lagrange. Fue Poincaré quien sentó las bases de la teoría que describe el comportamiento caótico y la dinámica compleja en el problema de los tres cuerpos e introdujo los conceptos de órbita homoclina y órbita heteroclina. Como consecuencia de las ideas aportadas por Poincaré aparecieron nuevos trabajos de la mano de George D. Birkhoff, que no tuvieron gran repercusión, pero que fueron completados a mediados de los años 60 por Stephen Smale, quien introdujo un modelo matemático conocido con el nombre de "herradura de Smale" en el que demostró que la existencia de órbitas homoclinas transversales implica la presencia de conjuntos invariantes [81].

En la misma década aparecen en Rusia los trabajos pioneros de Shilnikov sobre órbitas homoclinas en sistemas dinámicos autónomos [76–79], y la aportación de Melnikov [61] y Arnold [13], quienes proporcionaron el "método de Poincaré-Melnikov-Arnold" (más brevemente conocido como método de Melnikov) para poder estudiar las curvas de homoclinas y heteroclinas, lo cual ha permitido entender mejor el comportamiento de los sistemas dinámicos complejos.

Entre 1950 y 1970, Kolmogorov, Arnold y Moser aportaron un importante conjunto de resultados que actualmente se conoce con el nombre de teoría KAM [12, 51, 52, 64] que trata de explicar cómo son modificadas las trayectorias de un sistema integrable bajo pequeñas perturbaciones en las condiciones iniciales del sistema.

También cabe destacar la aportación del matemático y meteorólogo americano Edward Lorenz en 1963 [58] quien trabajando en un sistema simple de tres ecuaciones diferenciales, pensado como modelo atmosférico, observó que una pequeña variación en los valores iniciales en las ecuaciones del sistema mostraba unos pronósticos del estado del tiempo totalmente diferentes, con lo que detectó que pequeñas variaciones en los datos de partida generaban una gran dispersión de los escenarios finales. Este fenómeno se dio a conocer más adelante con el nombre de "efecto mariposa", a raíz de una conferencia que impartió en 1972 (véase [40]).

A finales del siglo XX, los resultados obtenidos anteriormente tienen continuación en Europa occidental, con trabajos sobre el comportamiento periódico en torno a una órbita homoclina por parte de Glendinning y Sparrow [41, 42], y de Gaspard, Kapral y Nicolis [36]. Ello da lugar a la aparición de nuevos trabajos sobre órbitas heteroclinas de codimensión dos en sistemas de dimensión mayor o igual que tres donde caben destacar las consecuencias sobre la dinámica periódica y no periódica debido a la existencia de bifurcaciones globales [20, 42]. Al trabajar con una familia de sistemas parametrizados, los resultados generalmente se obtienen en forma de diagramas y conjuntos de bifurcaciones.

En el marco de varias tesis doctorales desarrolladas en nuestro grupo [1, 32, 35, 62, 68, 72], así como en los proyectos de investigación correspondientes, hemos considerado familias de sistemas dinámicos tridimensionales como son el sistema de Lorenz y otros de tipo cuasi-Lorenz. Un primer objetivo de este trabajo, que se encuentra en su origen y motivación, es el estudio del comportamiento dinámico y de bifurcaciones de dichos sistemas. La aplicación de ideas y técnicas propias de la teoría geométrica y de bifurcaciones de sistemas dinámicos genera una variedad de problemas y cuestiones de interés general y cuya resolución constituye un segundo objetivo fundamental en esta memoria.

Entre las hipótesis de partida se encuentra el hecho de que mediante el análisis de las posibles bifurcaciones es factible obtener información valiosa sobre el comportamiento dinámico, a menudo complejo, de sistemas concretos. Por lo tanto, la teoría de bifurcaciones constituye una herramienta fundamental para el estudio de los sistemas dinámicos.

El estudio de bifurcaciones de una familia parametrizada de sistemas dinámicos se centra en aquellos valores de los parámetros donde se producen pérdidas de estabilidad estructural. Se generan problemas locales en caso de se trate la pérdida de hiperbolicidad (degeneración lineal) de equilibrios u órbitas periódicas que da origen a fenómenos de bifurcación local (inestabilidad estructural local), y problemas globales que están caracterizados por la inestabilidad estructural de las órbitas homoclinas que da lugar a variados y complejos fenómenos de bifurcación global.

La forma de aplicar la teoría local de bifurcaciones aparece de forma recurrente en esta memoria y consiste en buscar las situaciones de mayor degeneración de los elementos críticos (preferentemente equilibrios, ocasionalmente órbitas periodicas) en los sistemas parametrizados. Para ello se comienzan analizando las posibles degeneraciones en las partes lineales (no hiperbolicidad), lo que permite obtener un primer conjunto de parámetros de bifurcación de entre los parámetros propios del sistema. El estudio de las correspondientes conductas de bifurcación se lleva a cabo mediante técnicas analíticas tales como la reducción del sistema mediante el teorema de la variedad de centros y el cálculo de formas normales. Con tal fin se precisa el concurso de algoritmos de computación simbólica desarrollados en trabajos anteriores.

El cálculo de las formas normales nos proporciona información sobre aquellos términos no lineales esenciales para la conducta de bifurcación. Nos planteamos, en este punto, analizar las posibles degeneraciones de las partes no lineales. Con ello, pondremos en evidencia el papel como parámetros de bifurcación de nuevos parámetros del sistema.

En síntesis, habremos encontrado situaciones altamente degeneradas y se pretende describir las correspondientes bifurcaciones multiparamétricas. Dichas situaciones de degeneración actúan como centros organizadores de la dinámica, por lo que podemos detectar una variedad de comportamientos dinámicos y de bifurcaciones mediante un análisis local adecuado. Los resultados de este análisis local serán válidos, en principio, en un entorno del elemento crítico en el espacio de órbitas y en un entorno de los valores críticos de bifurcación en el espacio de parámetros. Sin embargo, de la observación experimental o la simulación numérica se deduce, con frecuencia, que los resultados del estudio local se conservan *lejos* de la situaciones de bifurcación (los entornos predichos por la teoría tienen en todo caso un tamaño concreto, aun cuando no sea conocido, en general, a priori).

Por lo tanto, nos planteamos *extender* los resultados locales mediante el uso de métodos de continuación numérica. La valiosa información obtenida en el estudio de una bifurcación local será el adecuado punto de partida para la aplicación de las técnicas numéricas: aproximaciones locales bien en el espacio de órbitas (por ejemplo, condiciones iniciales aproximadas de órbitas periódicas u homoclinas), bien en el espacio de parámetros (por ejemplo, aproximaciones a curvas de bifurcación). Así que se trata de una buena muestra de la conjunción de técnicas analíticas y numéricas para estudiar los sistemas dinámicos tridimensionales.

A lo largo de esta memoria vamos a estudiar la dinámica de diversos sistemas dinámicos tridimensionales. Específicamente analizaremos el modelo planteado por Lorenz que viene dado por las ecuaciones

$$\dot{x} = \sigma(y - x), \quad \dot{y} = \rho x - y - xz, \quad \dot{z} = -bz + xy, \tag{1}$$

siendo σ, ρ y β parámetros que determinan las propiedades dinámicas del sistema.

El comportamiento de este sistema ha sido estudiado en centenares de artículos, pero en la mayoría de ellos se ha hecho desde un punto de vista físico y, debido a ello, se han elegido los parámetros estrictamente positivos [5, 16–18, 24, 29, 38, 42, 54, 55, 82, 84]. En cambio, es interesante conocer el comportamiento del modelo cuando los parámetros toman cualquier valor real, ya sean positivos o negativos [21,50,56,57,63], pues nos interesa el comportamiento del sistema desde un punto de vista dinámico.

El estudio del sistema de Lorenz ha originado, en buena medida, el trabajo desarrollado en esta memoria y ha suscitado una gran parte de los problemas y cuestiones generales abordados.

Esta memoria está organizada en cinco capítulos; cuatro de ellos son artículos ya publicados y el último es un trabajo que actualmente está sometido a revisión.

En el capítulo 1 llevamos a cabo un análisis completo de la bifurcación de Hopf y de sus degeneraciones en el sistema de Lorenz, tanto del equilibrio en el origen como de los equilibrios no triviales. En primer lugar, determinamos los valores de los parámetros para los que el equilibrio en el origen experimenta una bifurcación de Hopf. A partir de este primer conjunto de valores, y con técnicas analíticas tales como variedad de centros y cálculo de formas normales, encontramos una degeneración de codimensión dos de dicha bifurcación, degeneración que finalmente se comprueba que es de codimensión infinita y se demuestra la existencia de un centro sobre la variedad de centros, evidenciando la falta de estabilidad estructural del modelo de Lorenz.

Por otro lado, el análisis de la bifurcación de Hopf de los equilibrios no triviales también ha sido completado a pesar de su complejidad. Hemos logrado determinar todas las degeneraciones posibles: varias curvas en el espacio triparamétrico correspondientes a una degeneración de codimensión dos; dos puntos diferentes correspondientes a una degeneración de codimensión tres; y una semirrecta correspondiente a una degeneración de codimensión infinita.

A partir de los resultados teóricos obtenidos y mediante las técnicas de continuación numérica, comprobamos que las degeneraciones encontradas en la bifurcación de Hopf constituyen importantes centros organizadores de la dinámica del sistema de Lorenz.

Hay otros sistemas tridimensionales cuadráticos cuyo interés ha aumentado considerablemente en las últimas décadas. En la parte final de este capítulo hemos analizado dos de estos sistemas: el sistema de Chen [23] y el sistema de Lü [59]. Se han considerado los resultados obtenidos al respecto en publicaciones previas (ver [3, 4]) donde se demuestra que estos sistemas son casos particulares del sistema de Lorenz. Con los

resultados obtenidos en este capítulo hemos encontrado toda la información posible respecto a la bifurcación de Hopf en ambos sistemas.

En el capítulo 2 analizamos la bifurcación de Takens–Bogdanov en el sistema de Lorenz. La contribución a la teoría de sistemas dinámicos por parte de F. Takens y R.I. Bogdanov fue el estudio del primer despliegue universal en una singularidad de codimensión dos [14, 44], que aparece cuando un autovalor cero doble tiene multiplicidad geométrica uno. Esta bifurcación ha sido encontrada en un gran número de sistemas de distintos campos de aplicaciones (véase [6–8, 10, 19, 33, 34, 60, 70, 83]).

En raras ocasiones es posible demostrar la existencia de una órbita homoclina o heteroclina. Uno de los aspectos más importantes de la bifurcación de Takens–Bogdanov es que garantiza la existencia de conexiones globales en una región del espacio de parámetros, que pueden ser órbitas homoclinas en sistemas no simétricos y órbitas tanto heteroclinas como homoclinas en sistemas simétricos.

Las únicas evidencias que aparecían en la literatura sobre esta bifurcación en las ecuaciones de Lorenz eran los trabajos [30, 49]. Iniciamos este capítulo realizando un estudio teórico de la bifurcación de Takens–Bogdanov del equilibrio en el origen, encontrando los valores de los parámetros en los que ocurre. Mediante las técnicas analíticas correspondientes determinamos que el equilibrio trivial experimenta una bifurcación de Takens–Bogdanov degenerada de codimensión infinita.

A partir de los resultados teóricos obtenidos, detectamos numéricamente varios tipos de conexiones homoclinas y heteroclinas degeneradas, así como bifurcaciones de Takens–Bogdanov de órbitas periódicas. Mostramos la existencia de bifurcaciones de duplicación de periodo, silla-nodo y bifurcaciones a toros que son experimentadas por las correspondientes órbitas periódicas, y encontramos regiones del espacio de parámetros con atractores extraños. Se evidencia asimismo la existencia de conexiones homoclinas de codimensión tres que, junto con la degeneración triple-cero detectada en el paso de la bifurcación de Takens–Bogdanov de tipo homoclino a tipo heteroclino, actúan como principales centros organizadores en el espacio de parámetros del comportamiento extremadamente complejo del sistema de Lorenz.

Con las herramientas de continuación numérica también llegamos a mostrar la existencia del caos de Shilnikov (ver [22, 47]) que implica la presencia de una dinámica muy rica en el sistema de Lorenz; su detección llega a ser muy efectiva, pues las conexiones globales (tanto órbitas homoclinas como heteroclinas) constituyen importantes centros organizadores de la dinámica del sistema estudiado.

Por último, y al igual que en el capítulo 1, mediante cálculo simbólico y continuación numérica proporcionamos información sobre la bifurcación de Takens–Bogdanov tanto en el sistema de Chen como en el sistema de Lü.

En el capítulo 3 proponemos el siguiente sistema tridimensional

$$\dot{x} = y, \quad \dot{y} = a_1 x + a_2 y + Axz + Byz, \quad \dot{z} = a_3 z + Cx^2 + Dz^2, \tag{2}$$

que corresponde a un despliegue triparamétrico, próximo a la forma normal de la bi-

furcación triple cero exhibida por el sistema de Lorenz. Estas ecuaciones incluyen una amplia familia de sistemas tridimensionales similares al modelo de Lorenz que han sido estudiados en la literatura, entre los que cabe destacar el sistema de Shimizu-Morioka [80] y el analizado por Kobuku y Roussarie [50].

Entre las bifurcaciones que exhibe el equilibrio del origen en el sistema (2), hay una bifurcación doble-cero (autovalor cero doble con multiplicidad geométrica dos) que es el objeto de estudio de este capítulo. Mediante el uso de herramientas analíticas hemos demostrado la existencia de varias curvas de bifurcaciones de codimensión uno (transcrítica, pitchfork, Hopf y heteroclina) que emergen de esta singularidad. Por su interés, nos centramos en la bifurcación de Hopf y en la conexión heteroclina, que nos llevan a un comportamiento dinámico más complejo. También detectamos y estudiamos una degeneración en la bifurcación doble-cero. En este caso, usando el método de las transformaciones no lineales en el tiempo proporcionamos, a tercer orden, la expresión de la curva heteroclina que surge de este punto de codimensión tres. Además, mostramos que las degeneraciones de esta conexión heteroclina están relacionadas con la singularidad triple-cero que exhibe el equilibrio del origen. A partir de los resultados teóricos obtenidos, las técnicas de continuación numérica nos han permitido detectar bifurcaciones globales de codimensión uno, dos y tres en la región considerada del espacio triparamétrico así como zonas donde existen atractores caóticos.

A lo largo de esta memoria también hemos analizado la dinámica de otros sistemas tridimensionales cuadráticos similares al modelo de Lorenz que han surgido durante los últimos sesenta años y que han hecho posible seguir investigando en esta temática tan interesante como es la teoría del caos. Por ejemplo, O.E. Rössler introdujo algunos sistemas cuadráticos que han sido objeto de numerosos estudios [9,15,37,73,74], o J.C. Sprott, quien trabajó en una búsqueda sistemática de sistemas caóticos tridimensionales simples con términos cuadráticos; de hecho encontró 19 modelos diferentes con solo cinco o seis términos, con uno o dos de ellos no lineales, en concreto cuadráticos. En el capítulo 4 hemos considerado la siguiente familia tridimensional biparamétrica,

$$\dot{x} = a + yz, \quad \dot{y} = -y + x^2, \quad \dot{z} = b - 4x, \tag{3}$$

donde $a, b \in \mathbb{R}$. Esta familia coincide con uno de los sistemas estudiados por Sprott cuando $a = 0$ y $b = 1$, y con el sistema estudiado en [85] cuando $a \in \mathbb{R}, b = 1$.

En este sistema encontramos una conexión homoclina que es generada por la órbita periódica que nace de la bifurcación de Hopf que experimenta el único equilibrio presente. Demostramos la existencia de una degeneración sobre esta curva homoclina de codimensión dos conocida como bifurcación homoclina flip, la cual puede ser de dos tipos, inclinación flip u órbita flip [45, 65, 66].

La bifurcación homoclina flip es una degeneración que aparece cuando la variedad estable del equilibrio cambia su orientación pasando de orientable a no-orientable, bajo ciertas condiciones para los autovalores de la linealización del equilibrio [47, 48, 78] y puede ser de tres tipos, conocidos como **A**, **B** y **C**. A su vez, este último tipo puede ser

$\mathbf{C_{in}}$ o $\mathbf{C_{out}}$. Sandstede propuso un modelo que exhibe los tres casos mencionados anteriormente, pero dicho modelo sólo presenta el caso $\mathbf{C_{out}}$ [75], por lo que se cuestionaba si habría algún modelo que presentara el caso $\mathbf{C_{in}}$. A partir de la información proporcionada por los autovalores del equilibrio se deduce que el sistema (3) experimenta el caso $\mathbf{C}$ que corresponde a un escenario de bifurcaciones donde aparecen atractores extraños y cuyo comportamiento aún sigue siendo objeto de estudio [28,39,45–47]. La determinación de la posición de las curvas de conexiones homoclinas que emergen de esta degeneración respecto a la conexión homoclina principal nos permite afirmar que estamos en el caso $\mathbf{C_{in}}$ (ver [46, Fig. 5]). Hasta lo que sabemos es el primer ejemplo de un sistema tridimensional explícito con una bifurcación flip de este tipo (respondiendo así a la pregunta de Sandstede). Además, se trata de un sistema simple pues sólo tiene seis términos y dos no linealidades, y un único punto de equilibrio. La combinación de herramientas analíticas y numéricas nos ha permitido estudiar su dinámica que tiene como centro organizador una bifurcación homoclina flip del tipo $\mathbf{C_{in}}$.

En el capítulo 5, para complementar los resultados obtenidos en el capítulo 3, nos interesamos por el análisis de la bifurcación doble-cero que experimenta el equilibrio del origen en el sistema de Lorenz. Como en este caso este equilibrio no es aislado, no podemos utilizar las técnicas analíticas usuales. Para solventar esta dificultad añadimos un nuevo término cuadrático en la tercera ecuación del sistema de Lorenz. El estudio teórico de esa singularidad en este sistema cuasi-Lorenz nos garantiza, para ciertos valores de los parámetros, la existencia de un ciclo heteroclino. A continuación, el análisis numérico en el espacio de parámetros de esta conexión heteroclina nos permite detectar ciertas degeneraciones de las conexiones globales que actúan como importantes centros organizadores de la compleja dinámica del sistema que aún no se conoce y cuyo estudio es una tarea de futuro. Si observamos la evolución de este conjunto de degeneraciones cuando el coeficiente del nuevo término introducido se aproxima a cero, podemos entender, en el sistema de Lorenz, el origen de una sucesión infinita de conexiones globales que sí se menciona en varios trabajos (ver [26] , [18], [5]) pero cuyo origen era desconocido. Mostramos que estas conexiones globales están relacionadas con lazos heteroclinos conocidos como puntos-T o ciclos de Bykov [2,31,42,71].

Bibliografía

[1] ALGABA, A. Formas hipernormales y bifurcaciones en sistemas planos y tridimensionales. *Tesis Doctoral, Universidad de Sevilla*, (1996).

[2] ALGABA, A., FERNÁNDEZ-SÁNCHEZ, F., MERINO, M., AND RODRÍGUEZ-LUIS, A. J. Structure of saddle-node and cusp bifurcations of periodic orbits near a non-transversal T-point. *Nonlinear Dyn.*, **63** (2011), 455–476.

[3] ALGABA, A., FERNÁNDEZ-SÁNCHEZ, F., MERINO, M., AND RODRÍGUEZ-LUIS, A. J. Chen's attractor exists if Lorenz repulsor exists: The Chen system is a special case of the Lorenz system. *Chaos*, **23** (2013), 033108.

[4] ALGABA, A., FERNÁNDEZ-SÁNCHEZ, F., MERINO, M., AND RODRÍGUEZ-LUIS, A. J. The Lü system is a particular case of the Lorenz system. *Phys. Lett. A*, **377** (2013), 2771–2776.

[5] ALGABA, A., FERNÁNDEZ-SÁNCHEZ, F., MERINO, M., AND RODRÍGUEZ-LUIS, A. J. Analysis of the T-point-Hopf bifurcation in the Lorenz system. *Commun. Nonlinear Sci. Numer. Simul.*, **22** (2015), 676–691.

[6] ALGABA, A., FREIRE, E., GAMERO, E., PONCE, E., AND RODRÍGUEZ-LUIS, A. J. Hypernormal form calculation for triple-zero degeneracies. *B. Belg. Math. Soc.-Sim.*, **6** (1999), 357–368.

[7] ALGABA, A., FREIRE, E., GAMERO, E., AND RODRÍGUEZ-LUIS, A. J. Analysis of Hopf and Takens-Bogdanov bifurcations in a modified van der Pol-Duffing oscillator. *Nonlinear Dyn.*, **16** (1998), 369–404.

[8] ALGABA, A., FREIRE, E., GAMERO, E., AND RODRÍGUEZ-LUIS, A. J. On the Takens–Bogdanov bifurcation in the Chua's equation. *IEICE T. Fund. Electr.*, **E82-A** (1999), 1722–1728.

[9] ALGABA, A., FREIRE, E., GAMERO, E., AND RODRÍGUEZ-LUIS, A. J. Resonances of periodic orbits in Rössler system in presence of a triple-zero bifurcation. *Int. J. Bif. Chaos*, **17** (2007), 1997–2008.

[10] ALGABA, A., GAMERO, E., AND RODRÍGUEZ-LUIS, A. J. A bifurcation analysis of a simple electronic circuit. *Commun. Nonlinear Sci. Numer. Simulat.*, **10** (2005), 169–178.

[11] ANDRONOV, A., AND PONTRIAGUIN, L. Systèmes grossiers. *Dokl. Akad. Nauk SSSR*, **14** (1937), 247–251.

[12] ARNOLD, V. I. Proof of a theorem of A. N. Kolmogórov on the preservation of conditionally periodic motions under a small perturbation of the hamiltonian. *Uspehi Mat. Nauk*, **18** (1963), 13 – 40.

[13] ARNOLD, V. I. Instability of dynamical systems with many degrees of freedom. *Dokl. Akad. Nauk SSSR*, **156** (1964), 9–12.

[14] AUBIN, D., AND DALMEDICO, A. D. Writing the history of dynamical systems and chaos: longue durée and revolution, disciplines and cultures. *Hist. Math.*, **29** (2002), 273–339.

[15] BARRIO, R., BLESA, F., DENA, A., AND SERRANO, S. Qualitative and numerical analysis of the Rössler model: Bifurcations of equilibria. *Comput. Math Appl*, **62** (2011), 4140–4150.

[16] BARRIO, R., AND SERRANO, S. A three-parametric study of the Lorenz model. *Phys. D*, **229** (2007), 43–51.

[17] BARRIO, R., AND SERRANO, S. Bounds for the chaotic region in the Lorenz model. *Phys. D*, **238** (2009), 1615–1624.

[18] BARRIO, R., SHILNIKOV, A., AND SHILNIKOV, L. Kneadings, symbolic dynamics and painting Lorenz chaos. *Int. J. Bif. Chaos*, **22** 1230016 (2012).

[19] BAZYKIN, A. D. Nonlinear Dynamics of Interacting Populations. *Singapore: World Scientific* (1998).

[20] BYKOV, V. V. The bifurcations of separatrix contours and chaos. *Phys. D*, **62** (1993), 290–299.

[21] CAO, J., AND ZHANG, X. Dynamics of the Lorenz system having an invariant algebraic surface. *J. Math. Phys.*, **48** (2007), 1–13.

[22] CHAMPNEYS, A. R., AND KUZNETSOV., Y. A. Numerical detection and continuation of codimension-two homoclinic bifurcations. *Int. J. Bif. Chaos*, **4** (1994), 795–822.

[23] CHEN, G., AND UETA, T. Yet another chaotic attractor. *Int. J. Bif. Chaos*, **9** (1999), 1465–1466.

[24] CHEN, X. Lorenz equations. Part I: Existence and nonexistence of homoclinic orbits. *SIAM J. Math. Anal.*, **27** (1996), 1057–1069.

[25] CHOW, S., LI, C., AND WANG, D. Normal Forms and Bifurcation of Planar Vector Fields. *Cambridge University Press, Cambridge*, (1994).

[26] DE WITTE, V., GOVAERTS, W., KUZNETSOV, Y. A., AND FRIEDMAN, M. Interactive initialization and continuation of homoclinic and heteroclinic orbits in MATLAB. *ACM T. Math. Software*, **38** (2012), art. no. 18.

[27] DELSHAMS, A. Poincaré, creador de los métodos todavía modernos en las ecuaciones diferenciales y en la mecánica celeste. *Arbor: Ciencia, pensamiento y cultura*, **704** (2004), 669–690.

[28] DENG, A. Homoclinic twisting bifurcations and cusp horseshoe maps. *J. Dyn. Differ. Equ.*, **5** (1993), 417–467.

[29] DOEDEL, E. J., KRAUSKOPF, B., AND OSINGA, H. M. Global invariant manifolds in the transition to preturbulence in the Lorenz system. *Indagat. Math.*, **22** (2011), 222–240.

[30] ELGIN, J. N., AND MOLINA-GARZA, J. B. Traveling wave solutions of the Maxuell-Bloch equations. *Phys. Rev. A*, **35** (1987), 3986–3988.

[31] FERNÁNDEZ-SÁNCHEZ, F., FREIRE, E., AND RODRÍGUEZ-LUIS, A. J. T-Points in a $\mathbb{Z}_2$-symmetric electronic oscillator. (I) Analysis. *Nonlinear Dyn.*, **28** (2002), 53–69.

[32] FERNÁNDEZ-SÁNCHEZ, F. Comportamiento dinámico y de bifurcaciones en algunas conexiones globales de equilibrios en sistemas tridimensionales. *Tesis Doctoral, Universidad de Sevilla*, (2002).

[33] FREIRE, E., GAMERO, E., AND RODRÍGUEZ-LUIS, A. J. Study of a degenerate Bogdanov-Takens bifurcation in a family of mechanical oscillators. *Mech. Res. Commun.*, **25** (1988), 287–297.

[34] FREIRE, E., RODRÍGUEZ-LUIS, A. J., GAMERO, E., AND PONCE, E. A case study for homoclinic chaos in an autonomous electronic circuit. A trip from Takens–Bogdanov to Hopf–Shilnikov. *Phys. D*, **62** (1993), 230–253.

[35] GAMERO, E. Computación simbólica y bifurcaciones de sistemas dinámicos. *Tesis Doctoral, Universidad de Sevilla*, (1990).

[36] GASPARD, P., KAPRAL, R., AND NICOLIS, G. Bifurcation phenomena near homoclinic systems: A two-parameter analysis. *J. Stat. Phys.*, **35** (1984), 697–727.

[37] GENESIO, R., INNOCENTI, G., AND GUALDANI, F. A global qualitative view of bifurcations and dynamics in the Rössler system. *Phys. Lett. A*, **372** (2008), 1799–1809.

[38] GIACOMINI, H., AND NEUKIRCH, S. Integrals of motion and the shape of the attractor for the lorenz model. *Phys. Lett. A*, **227** (1997), 309–318.

[39] GIRALDO, A., KRAUSKOPF, B., AND OSINGA, H. M. Cascades of global bifurcations and chaos near a homoclinic flip bifurcation: A case study. *SIAM J. Appl. Dyn. Syst.*, **17** (2018), 2784–2829.

[40] GLEICK, J. Chaos. *Ed. Penguin Books, New York*, (1987).

[41] GLENDINNING, P., AND SPARROW, C. Local and global behaviour near homoclinic orbits. *J. Stat. Phys.*, **35** (1984), 645–696.

[42] GLENDINNING, P., AND SPARROW, C. T-points: A codimension two heteroclinic bifurcation. *J. Stat. Phys.*, **43** (1986), 479–488.

[43] GUCKENHEIMER, J., AND HOLMES, P. J. Nonlinear Oscillations, Dynamical Systems, and Bifurcations of Vector Fields. *Springer, New York*, (1983).

[44] HOLMES, P. Ninety plus thirty years of nonlinear dynamics: less is more and more is different. *Int. J. Bif. Chaos*, **15** (2005), 2703–2716.

[45] HOMBURG, A. J., KOKUBU, H., AND KRUPA, M. The cusp horseshoe and its bifurcations in the unfolding of an inclination-flip homoclinic orbit. *Ergod. Theor. Dyn. Syst.*, **14** (1994), 667–693.

[46] HOMBURG, A. J., AND KRAUSKOPF, B. Resonant homoclinic flip bifurcations. *J. Dyn. Differ. Equ.*, **12** (2000), 807–850.

[47] HOMBURG, A. J., AND SANDSTEDE, B. Homoclinic and heteroclinic bifurcations in vector fields. *In: H. Broer, F. Takens, B. Hasselblatt (eds.). Elsevier Science: Handbook of Dynamical Systems, 3*, **4** (2010), 379–524.

[48] KISAKA, M., KOKUBU, H., AND OKA., H. Bifurcations to n-homoclinic orbits and N-periodic orbits in vector fields. *J. Dyn. Differ. Equ.*, **5** (1993), 305–357.

[49] KNOBLOCH, E., PROCTOR, M. R. E., AND WEISS, N. O. Heteroclinic bifurcations in a simple model of double-diffusive convection. *J. Fluid. Mech.*, **239** (1992), 273–292.

[50] KOKUBU, H., AND ROUSSARIE, R. Existence of a singularly degenerate heteroclinic cycle in the Lorenz system and its dynamical consequences: Part 1. *J. Dyn. Differ. Equ.*, **16** (2004), 513–557.

[51] KOLMOGOROV, A. On conservation of conditionally periodic motions for a small change in Hamilton's function. *Dokl. Akad. Nauk SSSR*, **98** (1954), 527–530.

[52] KOLMOGOROV, A. The general theory of dynamical systems and classical mechanics. *In: Foundations of Mechanics. Ed: Benjamin/Cummings, Reading, Mass.*, **Apéndice** (1978 (versión original en 1954)), 741–757.

[53] KUZNETSOV, Y. A. Elements of Applied Bifurcation Theory. *Springer-Verlag, New York*, (2004).

[54] KÚS, M. Integrals of motion for the lorenz system. *J. Phys. A*, **16** (1983), L689–L691.

[55] LEONOV, G. A. Bounds for attractors and the existence of homoclinic orbits in the Lorenz system. *J. Appl. Math. Mech.*, **65** (2001), 19–32.

[56] LLIBRE, J., MESSIAS, M., AND DA SILVA, P. R. Global dynamics of the Lorenz system with invariant algebraic surfaces. *Int. J. Bif. Chaos*, **20** (2010), 3137–3155.

[57] LLIBRE, J., AND ZHANG, X. Invariant algebraic surfaces of the Lorenz system. *J. Math. Phys.*, **43** (2002), 1622–1645.

[58] LORENZ, E. N. Deterministic nonperiodic flow. *J.Atmos.Sci.*, **20** (1963), 130–141.

[59] LÜ, J., AND CHEN, G. A new chaotic attractor coined. *Int. J. Bif. Chaos*, **12** (2002), 659–661.

[60] MELLIBOVSKY, F., AND ECKHARDT, B. Takens-Bogdanov bifurcation of travelling-wave solutions in pipe flow. *J. Fluid Mech.*, **670** (2011), 96–129.

[61] MELNIKOV, V. On the stability of the center for time periodic perturbations. *Trans. Moscow MAth. Soc.*, **12** (1963), 1–57.

[62] MERINO, M. Análisis de algunas degeneraciones y de bifurcaciones globales en campos vectoriales simétricos. *Tesis Doctoral, Universidad de Huelva*, (2010).

[63] MESSIAS, M. Dynamics at infinity and the existence of singularly degenerate heteroclinic cycles in the Lorenz system. *J. Phys. A*, **42**, 115101 (2009).

[64] MÖSER, J. On invariant curves of area-preserving mappings of an annulus. *Nachr. Akad. Wiss. Göttingen Math.-Phys. Kl.*, **2** (1962), 1–20.

[65] NAUDOT, V. Strange attractor in the unfolding of an inclination-flip homoclinic orbit. *Ergod. Theor. Dyn. Syst.*, **16** (1996), 1071–1086.

[66] NAUDOT, V. A strange attractor in the unfolding of an orbit-flip homoclinic orbit. *Dyn. Syst.*, **17** (2002), 45–63.

[67] PERKO, L. Differential Equations and Dynamical Systems. *Springer-Verlag, New York*, (2003).

[68] PIZARRO, L. Bifurcaciones múltiples en sistemas dinámicos planos. *Tesis Doctoral, Universidad de Sevilla*, (1996).

[69] POINCARÉ, H. Sur certaines solutions particuliéres du problème des trois corps. *Bull. astronom.*, **1** (1884), 65–74.

[70] PÉREZ-MOLINA, M., AND PÉREZ-POLO, M. F. Steady-state, self-oscillating and chaotic behavior of a PID controlled nonlinear servomechanism by using Bogdanov–Takens and Andronov–Poincaré–Hopf bifurcations. *Commun. Nonlinear Sci. Numer. Simulat.*, **19** (2014), 3694–3717.

[71] RODRIGUES, A. A. P. Repelling dynamics near a Bykov cycle. *J. Dyn. Diff. Equat.*, **25** (2013), 605–625.

[72] RODRÍGUEZ-LUIS, A. J. Bifurcaciones multiparamétricas en osciladores autónomos. *Tesis Doctoral, Universidad de Sevilla*, (1991).

[73] RÖSSLER, O. E. An equation for continuous chaos. *Phys. Lett. A*, **57** (1976), 397–398.

[74] RÖSSLER, O. E. Continuous chaos – four prototype equations. *Ann. NY Acad. Sci.*, **316** (1979), 376–392.

[75] SANDSTEDE, B. Constructing dynamical systems having homoclinic bifurcation points of codimension two. *J. Dyn. Differ. Equ.*, **9** (1997), 269–288.

[76] SHILNIKOV, L. P. A case of the existence of a denumerable set of periodic motions. *Sov. Math. Dokl.*, **6** (1965), 163–166.

[77] SHILNIKOV, L. P. The existence of a denumerable set of periodic motions in four-dimensional space in an extended neighborhood of a saddle-focus. *Sov. Math. Dokl.*, **8** (1) (1968), 54–58.

[78] SHILNIKOV, L. P. On the generation of a periodic motion from trajectories doubly asymptotic to an equilibrium state of saddle type. *ath. USSR Sb.*, **6** (1968), 427–438.

[79] SHILNIKOV, L. P. A contribution to the problem of the structure of an extended neighborhood of a rough equilibrium state of saddle- focus type. *Math. USSR Sb.*, **10** (1) (1970), 91–102.

[80] SHIMIZU, T., AND MORIOKA, N. On the bifurcation of a symmetric limit cycle to an asymmetric one in a simple model. *Phys. Lett. A*, **76** (1980), 201–204.

[81] SMALE, S. Diffeomorphisms with many periodic points. *In: Differential and Combinatorial Topology (A Symposium in Honor of Marston Morse). Ed.: Princeton Univ. Press, Princeton, N.J.*, (1965), 63–80.

[82] SPARROW, C. The Lorenz Equations. *Springer, New York* (1982).

[83] VERDUZCO, F., AND CARRILLO, F. A. Takens-Bogdanov bifurcation in IFOC systems. *Dynam. Cont. Dis. Ser. B*, **20** (2013), 305–311.

[84] VIANA, M. What's new on lorenz strange attractors? *Math. Intell*, **22** (2000), 6–19.

[85] WANG, X., AND CHEN, G. A chaotic system with only one stable equilibrium. *Commun. Nonlinear Sci. Numer. Simulat.*, **17** (2012), 1264–1272.

[86] WIGGINS, S. Introduction to Applied Dynamical Systems and Chaos. *Springer, New York*, (2003).

PUBLICACIONES

Algunos de los trabajos publicados, debido a restricciones relativas a derechos de autor, han sido retirados de la tesis. En sustitución de los documentos ofrecemos la siguiente información: referencia bibliográfica, enlace al texto completo y resumen.

- Algaba, A., Domínguez-Moreno, M.C., Merino, M. et al. Study of the Hopf bifurcation in the Lorenz, Chen and Lü systems. Nonlinear Dyn 79, 885–902 (2015). https://doi.org/10.1007/s11071-014-1709-2

Enlace al texto completo: https://doi.org/10.1007/s11071-014-1709-2

Resumen:

In this paper, we perform a complete study of the Hopf bifurcations in the three-parameter Lorenz system, $\dot{x}=\sigma(y-x), \dot{y}=\rho x-y-xz, \dot{z}=-bz+xy$, with $\sigma,\rho,b\in R$. On the one hand, we reobtain the results found in the literature for the Lorenz model when the three parameters are positive. On the other hand, we completely determine the loci of all the degeneracies exhibited by the Hopf bifurcation of the origin and of the nontrivial equilibria. In this last case, we demonstrate, among other things, that the first two Lyapunov coefficients simultaneously vanish in two codimension-three bifurcation points, giving rise in both cases to the coexistence of three periodic orbits involved in a cusp bifurcation. The analytical study that we carry out, where several complicated expressions have to be handled, successfully closes the problem of the Hopf bifurcations in the Lorenz system. Moreover, from our results, it is easy to obtain all the information on the Hopf bifurcations in the Chen and Lü systems, taking into account that they are, generically, particular cases of the Lorenz system, as can be seen by means of a linear scaling in time and state variables.

- Algaba, A., Domínguez-Moreno, M. C., Merino, M., & Rodríguez-Luis, A. J. (2016). Takens–Bogdanov bifurcations of equilibria and periodic orbits in the Lorenz system. In Communications in Nonlinear Science and Numerical Simulation (Vol. 30, Issues 1–3, pp. 328–343). Elsevier BV. https://doi.org/10.1016/j.cnsns.2015.06.034

Enlace al texto completo: https://doi.org/10.1016/j.cnsns.2015.06.034

Resumen:

In this work we study Takens–Bogdanov bifurcations of equilibria and periodic orbits in the classical Lorenz system, allowing the parameters to take any real value. First, by computing the corresponding normal form we determine where the Takens–Bogdanov bifurcation of equilibria is non-degenerate, namely of homoclinic or of heteroclinic type.

The transition between these two types occurs by means of a triple-zero singularity. Moreover, we demonstrate that a degenerate homoclinic-type Takens–Bogdanov bifurcation of infinite codimension occurs. Secondly, taking advantage of the above analytical results, we carry out a numerical study of the Lorenz system. In this way, we find several kinds of degenerate homoclinic and heteroclinic connections as well as Takens–Bogdanov bifurcations of periodic orbits. The existence of these codimension-two degeneracies, that organize the symmetry-breaking, period-doubling, saddle-node and torus bifurcations undergone by the corresponding periodic orbits, guarantees in some cases the presence of Shilnikov chaos. We also show the existence of a codimension-three homoclinic connection that together with the triple-zero degeneracy act as main organizing centers in the parameter space of the Lorenz system. Finally, we obtain interesting information on the bifurcation sets of the widely studied Chen and Lü systems, taking into account that they are, generically, particular cases of the Lorenz system, as can be proved with a linear scaling in time and state variables. We remark that the heteroclinic case of the Takens–Bogdanov bifurcation in the Lorenz system was found in the literature, in a region with negative parameters, in the study of a thermosolutal convection model and in the analysis of traveling-wave solutions of the Maxwell–Bloch equations.

- Algaba, A., Domínguez-Moreno, M. C., Merino, M., & Rodríguez-Luis, A. J. (2019). Study of a simple 3D quadratic system with homoclinic flip bifurcations of inward twist case C. In Communications in Nonlinear Science and Numerical Simulation (Vol. 77, pp. 324–337). Elsevier BV. https://doi.org/10.1016/j.cnsns.2019.05.005

Enlace al texto completo: https://doi.org/10.1016/j.cnsns.2019.05.005

Resumen:

In this paper we consider a two-parameter quadratic three-dimensional system with only six terms and two nonlinearities. First we analyze the Hopf bifurcation of its only equilibrium detecting several degeneracies. With this information we numerically obtain various bifurcation diagrams of periodic orbits in which saddle-node and period-doubling bifurcations as well as homoclinic connections appear. A careful study of the homoclinic orbits, in a region of the two-parameter plane where the equilibrium is a real saddle, shows the presence of a homoclinic flip bifurcation of case **C**. Here this orbit changes from orientable to non-orientable, being the lowest codimension for a homoclinic bifurcation to a real saddle equilibrium that results in chaotic behavior. More specifically, we determine that it corresponds to the case inward twist **Cin**, in such a way that, as far as we know, it is the first example of a 3D vector field exhibiting this case.

Capítulo 1

ESTUDIO DE LA BIFURCACIÓN DE HOPF EN EL SISTEMA DE LORENZ.

Capítulo 2

BIFURCACIONES DE TAKENS-BOGDANOV DE EQUILIBRIOS Y ÓRBITAS PERIÓDICAS EN EL SISTEMA DE LORENZ.

Capítulo 3

DEGENERACIÓN DOBLE-CERO Y CICLOS HETEROCLINOS EN UNA PERTURBACIÓN DEL SISTEMA DE LORENZ.

Communications in Nonlinear Science and Numerical Simulation 111 (2022) 106482

Contents lists available at ScienceDirect

Communications in Nonlinear Science and Numerical Simulation

journal homepage: www.elsevier.com/locate/cnsns

Research paper

Double-zero degeneracy and heteroclinic cycles in a perturbation of the Lorenz system

A. Algaba [a], M.C. Domínguez-Moreno [a], M. Merino [a], A.J. Rodríguez-Luis [b,*]

[a] Departamento de Ciencias Integradas, Centro de Estudios Avanzados en Física, Matemática y Computación, Universidad de Huelva, 21071 Huelva, Spain

[b] Departamento de Matemática Aplicada II, E.T.S. Ingeniería, Universidad de Sevilla, Camino de los Descubrimientos s/n, 41092 Sevilla, Spain

ARTICLE INFO

Article history:
Received 17 September 2021
Received in revised form 8 March 2022
Accepted 24 March 2022
Available online 30 March 2022

Keywords:
Lorenz system
Normal form
Double-zero bifurcation
Global connections

ABSTRACT

In this paper we consider a 3D three-parameter unfolding close to the normal form of the triple-zero bifurcation exhibited by the Lorenz system. First we study analytically the double-zero degeneracy (a double-zero eigenvalue with geometric multiplicity two) and two Hopf bifurcations. We focus on the more complex case in which the double-zero degeneracy organizes several codimension-one singularities, namely transcritical, pitchfork, Hopf and heteroclinic bifurcations. The analysis of the normal form of a Hopf-transcritical bifurcation allows to obtain the expressions for the corresponding bifurcation curves. A degenerate double-zero bifurcation is also considered. The theoretical information obtained is very helpful to start a numerical study of the 3D system. Thus, the presence of degenerate heteroclinic and homoclinic orbits, T-point heteroclinic loops and chaotic attractors is detected. We find numerical evidence that, at least, four curves of codimension-two global bifurcations are related to the triple-zero degeneracy in the system analyzed.

1. Introduction

It is familiar that the dynamics exhibited by a three-dimensional autonomous system can be extremely complicated. The best known example and one of the most studied is the Lorenz system [1,2]. Although it was derived from a simple model of convection in the atmosphere, it also appears in many other fields (see, for instance, [3–11]). Due to their physical meaning, in most cases, its three parameters take positive values. However, in some situations, it also makes sense for them to be negative (see, for example, [6,7]). Therefore, it is interesting to consider that the three parameters can take any real value.

Despite the many works dedicated to knowing and explaining its extraordinarily complex dynamical behavior (for instance, we cite some of them devoted to chaotic behavior [12–18], heteroclinic loops called T-points [19–21], manifolds study [22–24], invariant algebraic surfaces [25,26] and resonances and periodic orbits [27,28]; see also references therein) there are still many aspects to be understood. Although numerical tools are essential to be able to carry out its study, the analysis of the local bifurcations of the equilibria provides valuable initial information. In this way, the full analysis of the pitchfork, Hopf and Bogdanov–Takens bifurcation exhibited by the origin of Lorenz system has already been carried out (see, for instance, [29–32]).

* Corresponding author.
E-mail address: ajrluis@us.es (A.J. Rodríguez-Luis).

https://doi.org/10.1016/j.cnsns.2022.106482

However, the study of the Hopf-pitchfork and the triple-zero degeneracies presents an additional difficulty since the origin is not an isolated equilibrium. In this case, it would be necessary to adapt the standard techniques of normal forms of the reduced system on the center manifold. This complication has encouraged us to start the study of the triple-zero bifurcation for systems invariant to the change $(x, y, z) \to (-x, -y, z)$ (symmetry exhibited by the Lorenz system), considering the corresponding normal form [33].

The triple-zero bifurcation is of codimension three when the eigenvalue has geometric multiplicity two. The study of this case, both in systems without symmetry (such as Rössler's) and in $\mathbb{Z}_2$-symmetric systems (such as Chua's) illustrates the richness and complexity of the dynamics that appears as a consequence of this degeneracy (see [34–36] and references therein). However, if the triple-zero eigenvalue has geometric multiplicity one, then the bifurcation is of codimension five [33], which reduces to codimension three if the above symmetry condition is assumed. Given the enormous difficulty of this problem, as a first step, we propose an unfolding with three parameters (see Eq. (3)). This system is of interest to us not only for small values of the parameters (on which we can do a local analysis) but also for large values (which are reached by numerical continuation). In fact, this system represents a wide family of Lorenz-like systems studied in the literature [37–42] (some of them well known, such as the Shimizu–Morioka system), although not only for small values of the parameters. Concretely, Kokubu and Roussarie demonstrate in this system the existence of non-degenerate heteroclinic cycles, which give rise to complex dynamical behaviors, in a region of the parameter space where there are small, unity order, and large parameters [42, Theorem 2.3]. We are interested in finding heteroclinic cycles in other regions of the parameter space and, in particular, to see its possible relationship with the triple-zero degeneracy.

A starting point to study the existence of heteroclinic cycles is the analysis of codimension-two local bifurcations which are close to the triple-zero. In this way, we find in the unfolding three local bifurcations of codimension two, Bogdanov–Takens (double-zero eigenvalue with geometric multiplicity one), double-zero (eigenvalue with geometric multiplicity two) and Hopf-zero. The Bogdanov–Takens bifurcation has already been analyzed [43]. The first part of this work is devoted to studying the double-zero bifurcation.

The global connections found, whose existence is guaranteed by the local analysis (Bogdanov–Takens and double-zero bifurcations), can be numerically continued, with which it is possible to study their degeneracies and their relationship with the triple-zero degeneracy (see Fig. 10). The corresponding results appear in the second part of this paper.

The final objective that we intend to achieve in this long process is the study of the triple-zero bifurcation in Lorenz-like systems obtained by perturbations of the Lorenz system, in such a way that an isolated equilibrium undergoes the triple-zero degeneracy. Thus, the Lorenz system will appear as the limit of a certain family of Lorenz-like systems (we trust that this procedure will allow to obtain interesting information about its dynamics).

The paper is organized as follows. In Section 2 we introduce the system under study and determine the local bifurcations it can exhibit, namely pitchfork, transcritical, Hopf, Bogdanov–Takens, Hopf-pitchfork, double-zero and triple-zero. The study of the double-zero degeneracy (double-zero eigenvalue with geometric multiplicity two) is carried out in Section 3. The presence of a nonlinear degeneration in the double-zero bifurcation is also discussed (some useful lemmas appear in Appendix A). Moreover, Hopf bifurcations of the nontrivial equilibria are analyzed and expressions for the loci in the parameter space where the first Lyapunov coefficient vanishes are provided (all the details appear in Appendix B). In Section 4 we conduct a numerical study starting near the double-zero bifurcation, taking advantage of the analytical results previously obtained. In this way we detect a very complex bifurcation scenario where, among other things, degenerate homoclinic and heteroclinic connections, T-point heteroclinic loops and chaotic attractors are present. We also show numerical evidence that at least four curves of codimension-two global bifurcations are related to the triple-zero degeneracy present in the unfolding analyzed. Finally, a section with conclusions is included.

2. A normal form for the Lorenz system

The Lorenz system is given by (see [1,2])

$$\begin{cases} \dot{x} = \sigma(y - x), \\ \dot{y} = \rho x - y - xz, \\ \dot{z} = -bz + xy, \end{cases} \tag{1}$$

where σ, ρ and b are real parameters. These equations are invariant under the change $(x, y, z) \to (-x, -y, z)$; therefore, the z-axis is invariant. The equilibria are the origin $(0, 0, 0)$ and, when $b(\rho - 1) > 0$, a pair of symmetric nontrivial equilibria $\left(\pm\sqrt{b(\rho-1)}, \pm\sqrt{b(\rho-1)}, \rho - 1\right)$. The origin can exhibit the following linear degeneracies:

- a pitchfork bifurcation when $\rho = 1$, $\sigma \neq 0, -1$, $b \neq 0$ [32, Sect. 3];
- a Hopf bifurcation for $\sigma = -1$, $\rho > 1$, $b \neq 0$ [30];
- a Bogdanov–Takens bifurcation when $\sigma = -1$, $\rho = 1$, $b \neq 0$ [31];
- a Hopf-pitchfork bifurcation for $\sigma = -1$, $b = 0$, $\rho > 1$;
- a triple-zero bifurcation if $\sigma = -1$, $\rho = 1$, $b = 0$.

Unfortunately the above Hopf-pitchfork and triple-zero bifurcations cannot be analyzed by the usual techniques because the origin is a non-isolated equilibrium when $b = 0$. To circumvent this obstacle in the case of the triple-zero

bifurcation, in this paper we consider a three-parameter unfolding, that is close to the normal form of the triple-zero bifurcation exhibited by the Lorenz system [33], given by

$$\begin{cases} \dot{x} = y, \\ \dot{y} = \varepsilon_1 x + \varepsilon_2 y + Axz + Byz, \\ \dot{z} = \varepsilon_3 z + Cx^2 + Dz^2, \end{cases} \tag{2}$$

where $\varepsilon_1, \varepsilon_2, \varepsilon_3 \approx 0$ and A, B, C, D are real parameters. System (2) exhibits a triple-zero bifurcation when $\varepsilon_1 = \varepsilon_2 = \varepsilon_3 = 0$. These equations are also invariant under the change $(x, y, z) \to (-x, -y, z)$.

We remark that several systems studied in the literature appear as particular cases of (2) for certain parameter choices. Thus, if $A = -1$, $C = 1$, $B = D = 0$ we obtain the Shimizu–Morioka system [37,38] (for $\varepsilon_1 = 1$, $\varepsilon_2 = -\lambda$, $\varepsilon_3 = -\alpha$) and a low-order model of magnetoconvection [39] (for $\varepsilon_1 = -\lambda$, $\varepsilon_2 = k$, $\varepsilon_3 = -1$). If $A = -a\,k$, $C = h$, $B = D = 0$, by means of the change $x = \widetilde{x}$, $y = a(\widetilde{y} - \widetilde{x})$, $z = \widetilde{z}$, a Lorenz-like system is obtained [40,41] (for $\varepsilon_1 = a\,b$, $\varepsilon_2 = -a$, $\varepsilon_3 = -c$). Finally, if $A = -1$, $C = 1$, $B = -\gamma$, $D = \delta$, $\varepsilon_1 = \tilde{A}$, $\varepsilon_2 = -1$, $\varepsilon_3 = -\beta$, the resulting system [42, Eq. (2.7)] has non-degenerate heteroclinic cycles that connect the equilibria located on the z-axis, in certain regions where ε_1 is sufficiently large, $\varepsilon_2 = -1$ and ε_3, $B < 0$ and $D > 0$ are close to zero (see [42, Theorem 2.3]).

If $AC \neq 0$, since system (2) is invariant to the changes

$$(x, y, z, t, \varepsilon_1, \varepsilon_2, \varepsilon_3, A, B, C, D) \longrightarrow (-x, y, -z, -t, \varepsilon_1, -\varepsilon_2, -\varepsilon_3, -A, B, C, D),$$
$$(x, y, z, t, \varepsilon_1, \varepsilon_2, \varepsilon_3, A, B, C, D) \longrightarrow (-x, y, z, -t, \varepsilon_1, -\varepsilon_2, -\varepsilon_3, A, -B, -C, -D),$$

we can take without loss of generality $A = -1$, $C = 1$

$$\begin{cases} \dot{x} = y, \\ \dot{y} = \varepsilon_1 x + \varepsilon_2 y - xz + Byz, \\ \dot{z} = \varepsilon_3 z + x^2 + Dz^2. \end{cases} \tag{3}$$

System (3) can have up to four equilibria, namely $E_1 = (0, 0, 0)$, $E_2 = (0, 0, -\varepsilon_3/D)$ if $D \neq 0$ and $E_{3,4} = \left(\pm\sqrt{-\varepsilon_1(\varepsilon_3 + D\varepsilon_1)}, 0, \varepsilon_1\right)$ if $\varepsilon_1(\varepsilon_3 + D\varepsilon_1) < 0$. Note that E_1 and E_2 are placed on the z-axis, that is an invariant set.

The Jacobian matrix of system (3) at the trivial equilibrium E_1 is

$$\begin{pmatrix} 0 & 1 & 0 \\ \varepsilon_1 & \varepsilon_2 & 0 \\ 0 & 0 & \varepsilon_3 \end{pmatrix}, \tag{4}$$

and then, its characteristic polynomial is given by $P(\lambda) = \lambda^3 + p_1\lambda^2 + p_2\lambda + p_3$, where

$$p_1 = -(\varepsilon_2 + \varepsilon_3), \quad p_2 = \varepsilon_2\varepsilon_3 - \varepsilon_1, \quad p_3 = \varepsilon_1\varepsilon_3.$$

Therefore, the origin exhibits the following bifurcations:

- a pitchfork bifurcation when $\varepsilon_1 = 0$, $\varepsilon_2 \neq 0$, $\varepsilon_3 \neq 0$. The equilibria $E_{3,4}$ appear when $\varepsilon_1(\varepsilon_3 + D\varepsilon_1) < 0$.
- A transcritical bifurcation (involving also E_2) when $\varepsilon_3 = 0$, $\varepsilon_1 \neq 0$, $\varepsilon_2 \neq 0$, $D \neq 0$.
- A Hopf bifurcation when $\varepsilon_2 = 0$, $\varepsilon_1 < 0$, $\varepsilon_3 \neq 0$.
- A Bogdanov–Takens bifurcation (a double-zero eigenvalue with geometric multiplicity one) when $\varepsilon_1 = 0$, $\varepsilon_2 = 0$, $\varepsilon_3 \neq 0$. It is of homoclinic type when $\varepsilon_3 < 0$ and of heteroclinic type if $\varepsilon_3 > 0$.
- A Hopf-zero bifurcation when $\varepsilon_2 = 0$, $\varepsilon_3 = 0$, $\varepsilon_1 < 0$.
- A double-zero bifurcation (a double-zero eigenvalue with geometric multiplicity two) when $\varepsilon_1 = 0$, $\varepsilon_3 = 0$, $\varepsilon_2 \neq 0$.
- A triple-zero bifurcation (a triple-zero eigenvalue with geometric multiplicity two) when $\varepsilon_1 = \varepsilon_2 = \varepsilon_3 = 0$.

As a first step in the study of system (3), the Bogdanov–Takens bifurcation has been analyzed in [43] whereas the double-zero bifurcation is considered in this paper. The study of the Hopf-zero and the triple-zero bifurcations will be carried out in the future.

Before starting with the study of the double-zero bifurcation, we are going to see that all the bifurcations that the equilibrium E_2 exhibits can be easily deduced from those of E_1. Indeed, to study the equilibrium $E_2 = (0, 0, -\varepsilon_3/D)$, $D \neq 0$, we translate it to the origin by means of the change

$$x = \bar{x}, \ y = \bar{y}, \ z = \bar{z} - \frac{\varepsilon_3}{D},$$

that transforms system (3) into

$$\begin{cases} \dot{\bar{x}} = \bar{y}, \\ \dot{\bar{y}} = (\varepsilon_1 + \frac{1}{D}\varepsilon_3)\bar{x} + (\varepsilon_2 - \frac{B}{D}\varepsilon_3)\bar{y} - \bar{x}\bar{z} + B\bar{y}\bar{z}, \\ \dot{\bar{z}} = -\varepsilon_3\bar{z} + \bar{x}^2 + D\bar{z}^2, \end{cases} \tag{5}$$

with $D \neq 0$.

Since system (3) is symmetric to the change

$$(x, y, z, t, \varepsilon_1, \varepsilon_2, \varepsilon_3, B, D) \longrightarrow \left(x, y, z - \frac{\varepsilon_3}{D}, t, \varepsilon_1 + \frac{\varepsilon_3}{D}, \varepsilon_2 - \frac{B\,\varepsilon_3}{D}, -\varepsilon_3, B, D\right), \tag{6}$$

it is immediate to obtain the stability and bifurcations of E_2 from the stability and bifurcations of E_1.

3. A double-zero bifurcation of the origin

The double-zero bifurcation exhibited by the equilibrium E_1 occurs when $\varepsilon_1 = 0$, $\varepsilon_3 = 0$, $\varepsilon_2 \neq 0$. Consequently, to study this codimension-two bifurcation, we fix the value of $\varepsilon_2 = \Delta^{-1} \neq 0$ (we use Δ to facilitate the writing of the expressions that will appear later) and assume that ε_1 and ε_3 are close to zero.

The results obtained in this section are summarized in the following theorem and in Fig. 1.

Theorem 3.1. *In system (3) the equilibrium E_1 exhibits a double-zero bifurcation when $\varepsilon_1 = \varepsilon_3 = 0$, $\varepsilon_2 = \Delta^{-1} \neq 0$. In a neighborhood of this codimension-two degeneracy, there are only periodic solutions (arising from a Hopf bifurcation) when $D > 0$ and $\Delta < 0$. In this case, the local codimension-one bifurcations involved are (see Fig. 1):*

(1) A transcritical bifurcation $\mathtt{T}$*, of equilibria E_1 and E_2, when $\varepsilon_3 = 0$.*

(2) Two pitchfork bifurcations $\mathtt{P}^1$*, when $\varepsilon_1 = 0$, and* $\mathtt{P}^2$*, for $\varepsilon_3 = -D\varepsilon_1 + \mathcal{O}(\varepsilon_1^2)$. They involve E_1 or E_2 and $E_{3,4}$.*

(3) A Hopf bifurcation $\mathtt{h}$ *of the equilibria $E_{3,4}$, when $\varepsilon_3 = -2D\varepsilon_1 + \mathcal{O}(\varepsilon_1^2)$, if $B \neq 2\Delta$. It is supercritical when $B > 2\Delta$ and subcritical if $B < 2\Delta$.*

(4) A heteroclinic loop between E_1 and E_2, when

$$\varepsilon_1 = -\frac{1}{2D}\,\varepsilon_3 + \frac{\Delta(B - 2\Delta)(D - \Delta)}{2D^2(2D - 3\Delta)}\,\varepsilon_3^2 + \mathcal{O}(\varepsilon_3^3), \tag{7}$$

if $B \neq 2\Delta$. It is attractive when $B > 2\Delta$ and repulsive if $B < 2\Delta$. This loop is formed by two heteroclinic connections, one is structurally stable (since it goes from E_j to E_i on the invariant z-axis) and the other one (from E_i to E_j and placed outside this axis) is more relevant as it is structurally unstable: $\mathtt{He}^{ij}$ *indicates that the connection between E_i and E_j is outside the z-axis. Concretely,* $\mathtt{He}^{21}$ *exists when $\varepsilon_3 > 0$ and* $\mathtt{He}^{12}$ *if $\varepsilon_3 < 0$.*

To study the double-zero bifurcation exhibited by the equilibrium E_1 first we apply the change of variables

$$x = Y + Z, \quad y = \varepsilon_2 Z, \quad z = X, \tag{8}$$

that transforms system (3) into

$$\begin{cases} \dot{X} = \varepsilon_3 X + (Y + Z)^2 + DX^2, \\ \dot{Y} = -\Delta\varepsilon_1 Y - \Delta\varepsilon_1 Z + \Delta XY + (\Delta - B)XZ, \\ \dot{Z} = \Delta\varepsilon_1 Y + (\Delta\varepsilon_1 + \frac{1}{\Delta})Z - \Delta XY - (\Delta - B)XZ. \end{cases} \tag{9}$$

Remark that the hyperbolic manifold of equilibrium E_1 (which is semi-hyperbolic at the double-zero) is attractive if $\Delta < 0$ and repulsive if $\Delta > 0$ (since $\dot{Z} \approx (1/\Delta)Z$). Moreover, note that system (9) is symmetric to the change $(X, Y, Z) \to (X, -Y, -Z)$, so the center manifold inherits this symmetry, that is, it will be of the form $Z = Y\Psi(X, Y^2)$, where Ψ is a smooth function. Therefore, the reduced system on the center manifold is invariant to the transformation $(X, Y) \to (X, -Y)$, so $Y = 0$ is an invariant curve of the reduced system. Consequently, it is enough to analyze the reduced system for $Y \geq 0$.

To determine the bifurcations that arise from this singularity we begin by studying the reduced system up to second order on the center manifold $Z = \Delta^2 XY + \cdots$

$$\begin{cases} \dot{X} = \varepsilon_3 X + DX^2 + Y^2 + \cdots, \\ \dot{Y} = -\Delta\varepsilon_1 Y + \Delta(1 - \Delta^2\varepsilon_1)XY + \cdots. \end{cases} \tag{10}$$

The change of variables

$$X = \frac{-1}{D}\,z - \frac{\varepsilon_3}{2D}, \quad Y = \frac{1}{\sqrt{|D|}}\,r, \quad D \neq 0, \tag{11}$$

transforms (10) into

$$\begin{cases} \dot{r} = \mu_1 r + arz, \\ \dot{z} = \mu_2 - sgn(D)r^2 - z^2, \end{cases} \tag{12}$$

where

$$\mu_1 = \frac{-\Delta}{2D}(2D\varepsilon_1 + \varepsilon_3) + \mathcal{O}(|\varepsilon_1, \varepsilon_3|^2), \quad \mu_2 = \frac{\varepsilon_3^2}{4}, \quad a = \frac{-\Delta}{D} + \mathcal{O}(|\varepsilon_1, \varepsilon_3|). \tag{13}$$

Therefore, $sgn(a) = -sgn(\Delta)sgn(D)$, i.e., $a > 0$ if $\Delta D < 0$ and $a < 0$ if $\Delta D > 0$.

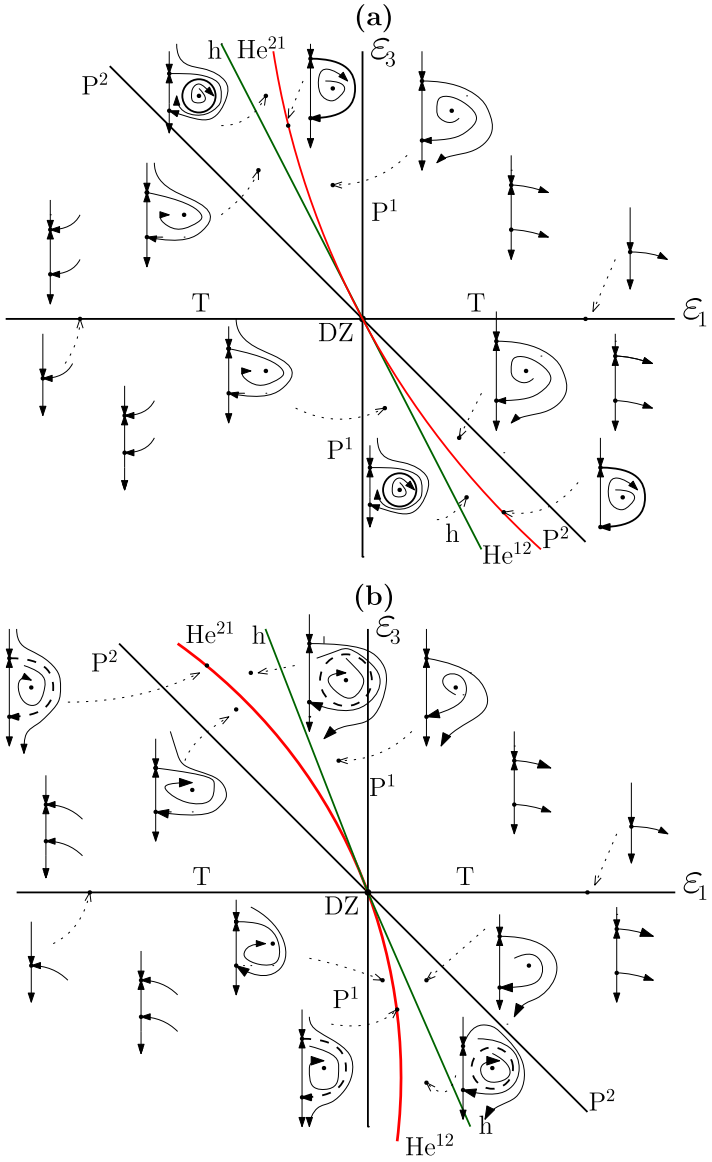

Fig. 1. Bifurcation set of system (3) in a neighborhood of the double-zero DZ exhibited by the equilibrium E_1, for $D > 0$ and $\Delta < 0$ when: (a) $B > 2\Delta$; (b) $B < 2\Delta$. The curves, according to Theorem 3.1, correspond to the following bifurcations: T, transcritical; P^1 and P^2, pitchfork; h, Hopf (supercritical when $B > 2\Delta$ and subcritical if $B < 2\Delta$); He^{12} and He^{21}, heteroclinic loop (attractive if $B > 2\Delta$ and repulsive when $B < 2\Delta$).

To study system (12) we can take advantage of the analysis of the Hopf-saddle–node degeneracy performed in [44] (we remark that (12) would correspond to a Hopf-transcritical bifurcation since $\mu_2 = \varepsilon_3^2/4$ is always positive), whose Eq. (7.4.9) is

$$\begin{cases} \dot{r} = \mu_1 r + arz, \\ \dot{z} = \mu_2 + br^2 - z^2, \end{cases} \tag{14}$$

with $b = \pm 1$. In this system there are six possible configurations (see [44, Sect.7.4] and [45, Sect.20.7]), labeled as I ($b = 1$, $a > 0$), IIa ($b = 1$, $-1 < a < 0$), IIb ($b = 1$, $a \leq -1$), III ($b = -1$, $a > 0$), IVa ($b = -1$, $-1 < a < 0$) and IVb ($b = -1$, $a < -1$). Between them, the cases of interest are IIa–IIb and III, due to the presence of periodic solutions. On the one hand, in case III, a Hopf bifurcation exists when $\mu_2 > 0$ and the periodic orbit disappears in a heteroclinic connection. On the other hand, in cases IIa–IIb, also a Hopf bifurcation exists when $\mu_2 < 0$.

Comparing (12) and (14) we see that $b = -sgn(D)$, that is, $b = +1$ if $D < 0$ and $b = -1$ if $D > 0$. Consequently, we deduce that system (12) is in case III when $D > 0$ and $\Delta < 0$. Conversely, system (12) is in cases IIa–IIb, when $D < 0$ and $\Delta < 0$. However, as $\mu_2 = \varepsilon_3^2/4 > 0$, there is no Hopf bifurcation (because, in cases IIa–IIb, it only exists when $\mu_2 < 0$). Note that the trivial cases I and IV (IVa–IVb), where only equilibria appear, occur when $D < 0$ and $\Delta > 0$ and when $D > 0$ and $\Delta > 0$, respectively.

Therefore, when $D < 0$ and $\Delta < 0$ (cases IIa–IIb), the following local bifurcations are present (see [44, Fig. 7.4.4]):

- A transcritical bifurcation when $\mu_2 = 0$, that is, when $\varepsilon_3 = 0$.
- A pitchfork bifurcation for $\mu_1^2 - a^2\mu_2 = 0$, that is, for $\varepsilon_1 = 0$ and for $\varepsilon_3 = -D\varepsilon_1 + \mathcal{O}(\varepsilon_1^2)$.

As stated above, in this case there is no Hopf bifurcation and, consequently, no heteroclinic connection.

In the rest of this section we will analyze system (12), when $D > 0$ and $\Delta < 0$ (case III), by following the steps given in [44, Sect. 7.4] for the Hopf-saddle–node bifurcation (recall that our case would correspond to a Hopf-transcritical bifurcation). The equilibria of system (12) are

$$\left(0, \pm\sqrt{\mu_2}\right) \quad \text{and} \quad \left(\pm\sqrt{\mu_2 - \frac{\mu_1^2}{a^2}}, \frac{-\mu_1}{a}\right) \quad \text{when} \quad a^2\mu_2 > \mu_1^2,$$

that in terms of the original parameters are given by

$$\left(0, \pm\frac{\varepsilon_3}{2}\right) \text{ and } \left(\pm\sqrt{\frac{-D\varepsilon_1(\varepsilon_3 + D\varepsilon_1)}{(\Delta^2\varepsilon_1 - 1)^2} + \mathcal{O}(|\varepsilon_1, \varepsilon_3|^3)}, \frac{-2D\varepsilon_1 - \varepsilon_3}{2(1 - \Delta^2\varepsilon_1)}\right), \quad \varepsilon_1(\varepsilon_3 + D\varepsilon_1) < 0.$$

Note that E_1 corresponds to the equilibrium $(0, -\varepsilon_3/2)$ and E_2 to $(0, \varepsilon_3/2)$.

From the study carried out in [44, Sect.7.4] we can deduce that the following local bifurcations are present (see Fig. 1):

- A transcritical bifurcation $\mathtt{T}$ of the equilibria placed on the z-axis when $\mu_2 = 0$, that is, when $\varepsilon_3 = 0$.
- A pitchfork bifurcation for $\mu_1^2 - a^2\mu_2 = 0$ that is, P^1 for $\varepsilon_1 = 0$ and P^2 for $\varepsilon_3 = -D\varepsilon_1 + \mathcal{O}(\varepsilon_1^2)$.
- A Hopf bifurcation $\mathtt{h}$ of the equilibria placed outside the z-axis when $\mu_1 = 0$, $\mu_2 > 0$, that is, when $\varepsilon_3 = -2D\varepsilon_1$.

However, the second-order terms are not enough to unfold neither the Hopf bifurcation nor the heteroclinic connection because, for the values of the parameter where both bifurcations appear, the system is integrable, i.e., it has an analytic first integral. In fact, for $a = 2$, it has a polynomial first integral (only case considered in [44]). Hence, it has a continuum of periodic orbits that ends in a degenerate heteroclinic connection (it corresponds to a Hopf bifurcation in which all the Lyapunov coefficients are zero, i.e., a center singular point) [44, Fig. 7.4.9]. Thus, to unfold and calculate the curves of Hopf bifurcation and heteroclinic connections (involving the two equilibria located on the z-axis), as well as their stabilities, we need the reduced system up to third order.

As the center manifold up to third order is $Z = Y(\Delta^2 X + \Delta^3 Y^2 + (D - B + 2\Delta)\Delta^3 X^2)$, we obtain the reduced system up to order three

$$\begin{cases} \dot{X} = \varepsilon_3 X + DX^2 + Y^2 + \Delta^2 XY^2, \\ \dot{Y} = -\Delta\varepsilon_1 Y + \Delta(1 - \Delta^2\varepsilon_1)XY - [\Delta - B + \Delta^2(D - B + 2\Delta)]\Delta^2 X^2 Y - \Delta^4\varepsilon_1 Y^3. \end{cases} \tag{15}$$

The change

$$X = \frac{-1}{D}z - \frac{\varepsilon_3}{2D}, \quad Y = \frac{1}{\sqrt{D - \Delta^2\varepsilon_3}}r, \tag{16}$$

transforms (15) into

$$\begin{cases} \dot{r} = \tilde{\mu}_1 r + \tilde{a}rz + \tilde{c}r^3 + \tilde{d}rz^2, \\ \dot{z} = \tilde{\mu}_2 - r^2 - z^2 + \tilde{e}r^2 z, \end{cases} \tag{17}$$

where

$$\begin{aligned} \tilde{\mu}_1 &= -\Delta\varepsilon_1 - \frac{\Delta}{2D}\varepsilon_3 + \frac{\Delta^3}{2D}\varepsilon_1\varepsilon_3 + \frac{\Delta^2(B - \Delta)}{4D^2}\varepsilon_3^2 + \mathcal{O}(|\varepsilon_1, \varepsilon_3|^3), \\ \tilde{\mu}_2 &= \frac{\varepsilon_3^2}{4} + \mathcal{O}(|\varepsilon_1, \varepsilon_3|^3), \quad \tilde{a} = \frac{-\Delta}{D} + \mathcal{O}(|\varepsilon_1, \varepsilon_3|), \quad \tilde{c} = \mathcal{O}(|\varepsilon_1, \varepsilon_3|), \\ \tilde{d} &= \frac{\Delta^2(B - \Delta)}{D^2} + \mathcal{O}(|\varepsilon_1, \varepsilon_3|), \quad \tilde{e} = \frac{2\Delta^2}{D} + \mathcal{O}(|\varepsilon_1, \varepsilon_3|). \end{aligned} \tag{18}$$

Applying Lemma A.1 of Appendix A, we obtain, modulo translation and scaling,

$$\begin{cases} \dfrac{ds}{d\tau} = \hat{\mu}_1 s + \hat{a}sw, \\ \dfrac{dw}{d\tau} = \hat{\mu}_2 - s^2 - w^2 + \hat{f}w^3, \end{cases} \tag{19}$$

where

$$\begin{aligned} \hat{\mu}_1 &= \tilde{\mu}_1 + \mathcal{O}(|\varepsilon_1, \varepsilon_3|^3), \quad \hat{\mu}_2 = \tilde{\mu}_2 + \mathcal{O}(|\varepsilon_1, \varepsilon_3|^3), \quad \hat{a} = \tilde{a} + \mathcal{O}(|\varepsilon_1, \varepsilon_3|), \\ \hat{f} &= \frac{2\Delta(B - 2\Delta)}{3D} + \mathcal{O}(|\varepsilon_1, \varepsilon_3|). \end{aligned} \tag{20}$$

Thus, in system (19), we can analyze both the Hopf bifurcation and the heteroclinic connection.

On the one hand, the Hopf bifurcation exhibits a first-order degeneracy when $B = 2\Delta$. To prove it, we obtain from system (19) the third-order reduced system

$$\begin{pmatrix} \dot{s} \\ \dot{w} \end{pmatrix} = \begin{pmatrix} 0 & -1 \\ 1 & 0 \end{pmatrix} \begin{pmatrix} s \\ w \end{pmatrix} + \begin{pmatrix} \frac{\hat{a}}{\sqrt{2\hat{a}}s_1} sw \\ -\frac{\hat{a}}{2\sqrt{2\hat{a}}s_1} s^2 - \frac{1}{\sqrt{2\hat{a}}s_1} w^2 + \frac{\tilde{f}}{\sqrt{2\hat{a}}s_1} w^3 \end{pmatrix}, \tag{21}$$

where $s_1 = \sqrt{(\hat{\mu}_2\hat{a}^3 - \hat{\mu}_1^2\hat{a} - \hat{f}\hat{\mu}_1^3)/\hat{a}^3}$. By using the recursive algorithm developed in Ref. [46], we compute the normal form of the Hopf bifurcation up to third order

$$\dot{r} = a_1 r^3 + \cdots, \quad \dot{\theta} = 1 + b_1 r^2 + \cdots, \tag{22}$$

where the first Lyapunov coefficient is given by $a_1 = 3\hat{f}/(8\sqrt{2\hat{a}}s_1)$. Therefore, the Hopf bifurcation is supercritical when $a_1 < 0$, i.e., if $\hat{f} < 0$, which occurs when $B > 2\Delta$, whereas it is subcritical if $a_1 > 0$, i.e., when $\hat{f} > 0$ or, equivalently, when $B < 2\Delta$. Consequently, a degenerate Hopf bifurcation appears when $a_1 = 0$, i.e., when $B = 2\Delta$.

On the other hand, when $\hat{f} \neq 0$, that is, if $B \neq 2\Delta$, Melnikov's method guarantees the existence of a heteroclinic connection whose curve is approximated by [47–49] (in [44] only the Hamiltonian case, $\hat{a} = 2$, is considered)

$$\mu_1 = -\frac{3\hat{a}^2\hat{f}}{2(3\hat{a}+2)}\mu_2 + \mathcal{O}(\mu_2^2),$$

that in terms of our parameters corresponds to

$$\varepsilon_1 = -\frac{1}{2D}\varepsilon_3 + \frac{\Delta(B-2\Delta)(D-\Delta)}{2D^2(2D-3\Delta)}\varepsilon_3^2 + \mathcal{O}(\varepsilon_3^3). \tag{23}$$

Concretely, $\mathtt{He}^{21}$ exists when $\varepsilon_3 > 0$ and $\mathtt{He}^{12}$ if $\varepsilon_3 < 0$. Note that very recently, using the nonlinear time transformation method (NTT) [50–53], the expression of the heteroclinic curve in system (19) has been computed at any order for all $\hat{a} \in \mathbb{R}$ [49, Eq.(3.20)].

With this we have completed the proof of the results stated in Theorem 3.1. Recall that all the curves mentioned in this theorem are drawn in Fig. 1.

3.1. Degenerate case $B = 2\Delta$

Next we show the steps that should be followed to study the degenerate case $B = 2\Delta$. In this situation, the Hopf bifurcation and the heteroclinic connection are not determined by system (19), and therefore we need the reduced system up to fifth order on the center manifold. Following the same steps as in the calculation up to order three, we obtain

$$\begin{cases} \dfrac{ds}{d\tau} = \hat{\mu}_1 s + \hat{a}sw + \mathcal{O}(|s,w|^4), \\ \dfrac{dw}{d\tau} = \hat{\mu}_2 - s^2 - w^2 + \mathcal{O}(|s,w|^4), \end{cases} \tag{24}$$

where $\hat{\mu}_1$, $\hat{\mu}_2$ and $\hat{a}$ are given in (20). Applying Lemmas A.2 and A.3 of Appendix A, we obtain, modulo translation and scaling,

$$\begin{cases} \dfrac{d\bar{s}}{d\tau} = \bar{\mu}_1\bar{s} + \bar{a}\bar{s}\bar{w}, \\ \dfrac{d\bar{w}}{d\tau} = \bar{\mu}_2 - \bar{s}^2 - \bar{w}^2 + \bar{h}\bar{w}^5, \end{cases} \tag{25}$$

where

$$\bar{\mu}_1 = \hat{\mu}_1 + \mathcal{O}(|\varepsilon_1,\varepsilon_3|^3), \quad \bar{\mu}_2 = \hat{\mu}_2 + \mathcal{O}(|\varepsilon_1,\varepsilon_3|^3), \quad \bar{a} = \hat{a} + \mathcal{O}(|\varepsilon_1,\varepsilon_3|), \tag{26}$$

and the expression for $\bar{h}$ is not included because it is too long.

When $\bar{h} \neq 0$, the application of the NTT method provides the following expression for the heteroclinic curve [54]

$$\bar{\mu}_1 = -\frac{15\bar{a}^3\bar{h}}{2(3\bar{a}+2)(5\bar{a}+2)}\bar{\mu}_2 + \mathcal{O}(\bar{\mu}_2^2),$$

that in terms of the original parameters corresponds to

$$\varepsilon_1 = -\frac{1}{2D}\varepsilon_3 - \frac{15\Delta^2\bar{h}}{8D(2D-3\Delta)(2D-5\Delta)}\varepsilon_3^2 + \mathcal{O}(\varepsilon_3^3).$$

3.2. Hopf bifurcations of $E_{3,4}$ and E_2 in the whole $(\varepsilon_1, \varepsilon_2, \varepsilon_3)$-space

The study made so far for the Hopf bifurcation of the equilibria $E_{3,4}$ is valid when ε_1 and ε_3 are small, close to the double-zero bifurcation. In Appendix B.1 we have completed the analysis of this Hopf bifurcation for any value of ε_1 and ε_3. Specifically, we provide the value of the first Lyapunov coefficient in Eq. (B.4) and give an expression for the Hopf surface in the $(\varepsilon_1, \varepsilon_2, \varepsilon_3)$-parameter space in Eq. (B.5). These results will be useful in the numerical study of system (3) carried out in Section 4.

On the other hand, in Appendix B.2 we consider the Hopf bifurcation of the equilibrium E_2 which is related to a Bogdanov–Takens bifurcation of E_2, as we will see in Section 4. In Eq. (B.6) the value of the first Lyapunov coefficient is given.

4. Numerical study

We have seen in the previous section that the presence of a double-zero bifurcation in system (3) guarantees the existence of a heteroclinic loop which initially emerges as a planar phenomenon (in the same way that a Bogdanov–Takens bifurcation ensures the presence of homoclinic or heteroclinic connections). However, as soon as we move away from the point DZ, the heteroclinic connection will start to develop a three-dimensional structure. Thus, the numerical continuation of the heteroclinic curve away from the double-zero will make possible to determine if any point of degeneracy appears. This situation, in most cases, will imply a greater richness in the dynamics of the system.

The objective of this section is twofold. On the one hand, in Section 4.1 we are going to study the bifurcations that appear from the degenerate double-zero bifurcation ($B = 2\Delta$, where $\Delta = 1/\varepsilon_2$), completing the local information provided in Theorem 3.1 and shown in Fig. 1. On the other hand, in Section 4.2, we will find regions of the parameter space in which the system (3) exhibits a very complex dynamics.

4.1. Degenerate DZ when $B = -1$ and $D = 1$

Taking advantage of the theoretical information obtained in Section 3, we are going to carry out a numerical study of system (3) by means of the continuation software AUTO [55]. Our goal is to obtain bifurcation sets in the vicinity of the double-zero bifurcation DZ exhibited by the equilibrium $E_1 = (0, 0, 0)$ when $(\varepsilon_1, \varepsilon_3) = (0, 0)$ and $\varepsilon_2 \neq 0$. Specifically, we will take slices $\varepsilon_2 = constant$ in the $(\varepsilon_1, \varepsilon_2, \varepsilon_3)$-parameter space, fixing $B = -1$ and $D = 1$.

We know from Section 3 that the double-zero bifurcation DZ is degenerate when $\varepsilon_2 = 2/B = -2$. Then we will consider values on both sides of this singularity, for instance, $\varepsilon_2 = -1.5$ and $\varepsilon_2 = -2.5$, that correspond, respectively, to the cases $B > 2\Delta$ and $B < 2\Delta$.

4.1.1. $\varepsilon_2 = -1.5$ (case $B > 2\Delta$)

Initially, we are going to obtain the bifurcation set for $\varepsilon_2 = -1.5$. Thus, as it is usual, in order to continue numerically the bifurcation curves in a parameter plane we previously draw some bifurcation diagrams. Then, we also fix $\varepsilon_3 = -0.5$ and study the evolution of the nontrivial equilibrium $E_3 = \left(\sqrt{\varepsilon_1(0.5 - \varepsilon_1)}, 0, \varepsilon_1\right)$ versus ε_1. It exhibits a Hopf bifurcation h when $\varepsilon_1 \approx 0.2297234$. The bifurcation diagram corresponding to the asymmetric stable periodic orbit emerged from h is drawn in Fig. 2(a). This periodic orbit disappears, when $\varepsilon_1 \approx 0.2304689$, in a heteroclinic cycle He^{12} between the saddle equilibria $E_1 = (0, 0, 0)$ and $E_2 = (0, 0, 0.5)$. Recall that this loop is formed by two heteroclinic connections, one is structurally stable (since it goes from E_2 to E_1 on the invariant z-axis) and the other one is more relevant as it is structurally unstable, of codimension one (the connection from E_1 to E_2 is placed outside this axis). For this reason this heteroclinic cycle is labeled with the superscript 12, that is, He^{ij} indicates that the connection between E_i and E_j is outside the z-axis. The projection of He^{12} onto the (x, z)-plane appears in Fig. 2(c). Remark that throughout this work, with the aim of simplifying the notation, we will label the heteroclinic cycle (in fact, due to the symmetry, a pair of heteroclinic cycles exists) and the heteroclinic bifurcation with the same symbol, although they are two different objects. In addition, when necessary, we will use superscripts to indicate the equilibria that are involved in a certain bifurcation, or in a degeneration of it.

If we fix $\varepsilon_3 = -0.9$, we obtain the bifurcation diagram shown in Fig. 2(b). The periodic orbit emerged from h is of saddle type, later it becomes stable in the saddle–node bifurcation sn ($\varepsilon_1 \approx 0.397233$) and, finally, it disappears in a heteroclinic cycle He^{12} ($\varepsilon_1 \approx 0.397237$) similar to the previous case. Note that the heteroclinic loop is attractive for both values of ε_3.

Now we can numerically compute for $\varepsilon_2 = -1.5$ the loci where the bifurcations detected in Fig. 2 occur in the $(\varepsilon_1, \varepsilon_3)$-plane. Thus, in the partial bifurcation set drawn in Fig. 3(a), we can observe the curves h (Hopf bifurcation of the equilibria $E_{3,4}$), He^{12} (heteroclinic cycle between the equilibria E_1 and E_2) and sn (saddle–node bifurcation of periodic orbits). Moreover, three straight lines intersect at the double-zero point DZ, namely P^1 (pitchfork bifurcation of the origin, $\varepsilon_1 = 0$), P^2 (pitchfork bifurcation of E_2, $\varepsilon_1 = -\varepsilon_3$) and T (transcritical bifurcation between E_1 and E_2, $\varepsilon_3 = 0$). Note that in these pitchfork bifurcations the equilibria $E_{3,4}$ emerge.

Going into more detail, near the origin in the fourth quadrant the equilibria $E_{3,4}$ arise from the curve P^1 as attractive nodes (their three real eigenvalues are negative). By increasing the value of ε_1 they become attractive foci until they

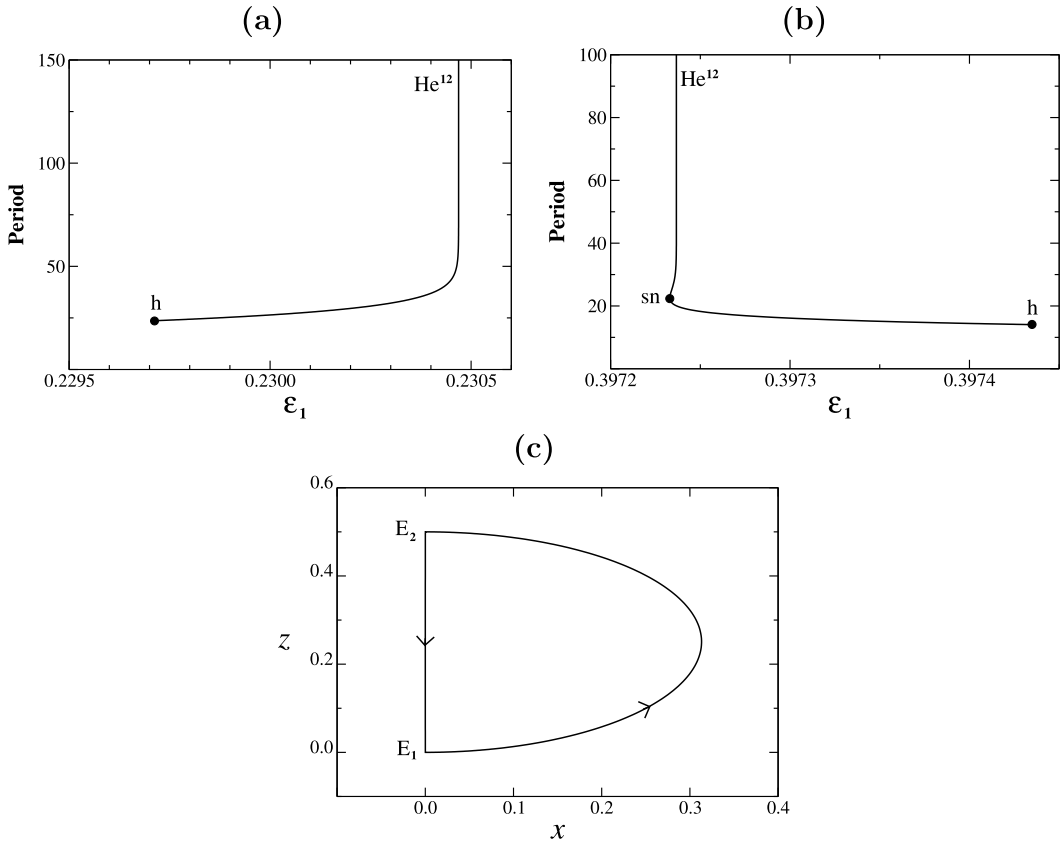

Fig. 2. For $\varepsilon_2 = -1.5, B = -1, D = 1$, bifurcation diagram of the asymmetric periodic orbit emerged from the Hopf bifurcation h, exhibited by the equilibrium E_3, when: (a) $\varepsilon_3 = -0.5$; (b) $\varepsilon_3 = -0.9$. (c) Projection onto the (x, z)-plane of the heteroclinic cycle He^{12} of panel (a) that exists when $\varepsilon_1 \approx 0.2304689$.

undergo a Hopf bifurcation h. On the other hand, in this quadrant the equilibrium E_1 is always a saddle–node ($\lambda_{1,3} < 0, \lambda_2 > 0$). This implies that, at any point in this region there exists, apart from the heteroclinic connection between E_1 and E_2, another structurally stable (codimension-zero) heteroclinic connection between the equilibria E_1 and E_3 (see Fig. 3(b) for $(\varepsilon_1, \varepsilon_3) = (0.15, -0.5)$). When the Hopf curve h is crossed, E_3 becomes a repulsive saddle-focus and then the unstable manifold of E_1 connects with the attractive periodic orbit arising from this Hopf bifurcation (see Fig. 3(c) for $(\varepsilon_1, \varepsilon_3) = (0.2304, -0.5)$). If ε_1 continues to increase, the periodic orbit grows and approaches the z-axis until the heteroclinic connection between E_1 and E_2 is formed (see Fig. 2(c)) for $(\varepsilon_1, \varepsilon_3) \approx (0.2304689, -0.5)$.

According to Eq. (B.5) of Appendix B.1, for a fixed value $\varepsilon_2 = constant$, the Hopf bifurcation curve h that emerges from the point DZ is given by the equation

$$\varepsilon_3 = \frac{3\varepsilon_1^2 - \varepsilon_2^2 + 2\varepsilon_1(1-\varepsilon_2) + \sqrt{(\varepsilon_1-\varepsilon_2)^4 + 4\varepsilon_1(\varepsilon_1^2+\varepsilon_1-\varepsilon_2^2)}}{2(-\varepsilon_1+\varepsilon_2)}.$$

In the fourth quadrant this curve is unbounded and the following inequalities hold $-2(\varepsilon_1 + 1) < \varepsilon_3 < -2\varepsilon_1$. The first one corresponds to the condition $p_2 > 0$ (a necessary condition for the existence of the Hopf bifurcation). The second inequality is due to the fact that the line $\varepsilon_3 = -2\varepsilon_1$ is an asymptote of the Hopf curve when $\varepsilon_1 \to +\infty$ and $\varepsilon_2 = constant$. Moreover, in accordance with the bifurcation diagrams of Fig. 2(a)–(b), a degenerate point Dh appears on h, when $(\varepsilon_1, \varepsilon_3) \approx (0.373821, -0.842653)$, since the first Lyapunov coefficient a_1 of the normal form vanishes (see Fig. 3(a)).

On the other hand, the curve of heteroclinic connections He^{12} is also unbounded. It emerges from the point DZ to the right of the Hopf curve h since $B > 2/\varepsilon_2$ (this agrees with the bifurcation diagram of Fig. 2(a)). However, when $(\varepsilon_1, \varepsilon_3) \approx (0.38281, -0.86445)$, both curves intersect and then, they change their relative position. Moreover, the curve He^{12} exhibits a degeneracy DHe^{12} at $(\varepsilon_1, \varepsilon_3) = (7/16, -1)$. To analyze it in the fourth quadrant of the parameter plane, we denote the eigenvalues of the Jacobian matrix at the origin E_1 as $\lambda_1, \lambda_3 < 0 < \lambda_2$, where

$$\lambda_3 = \varepsilon_3, \quad \lambda_{2,1} = \frac{\varepsilon_2 \pm \sqrt{\varepsilon_2^2 + 4\varepsilon_1}}{2},$$

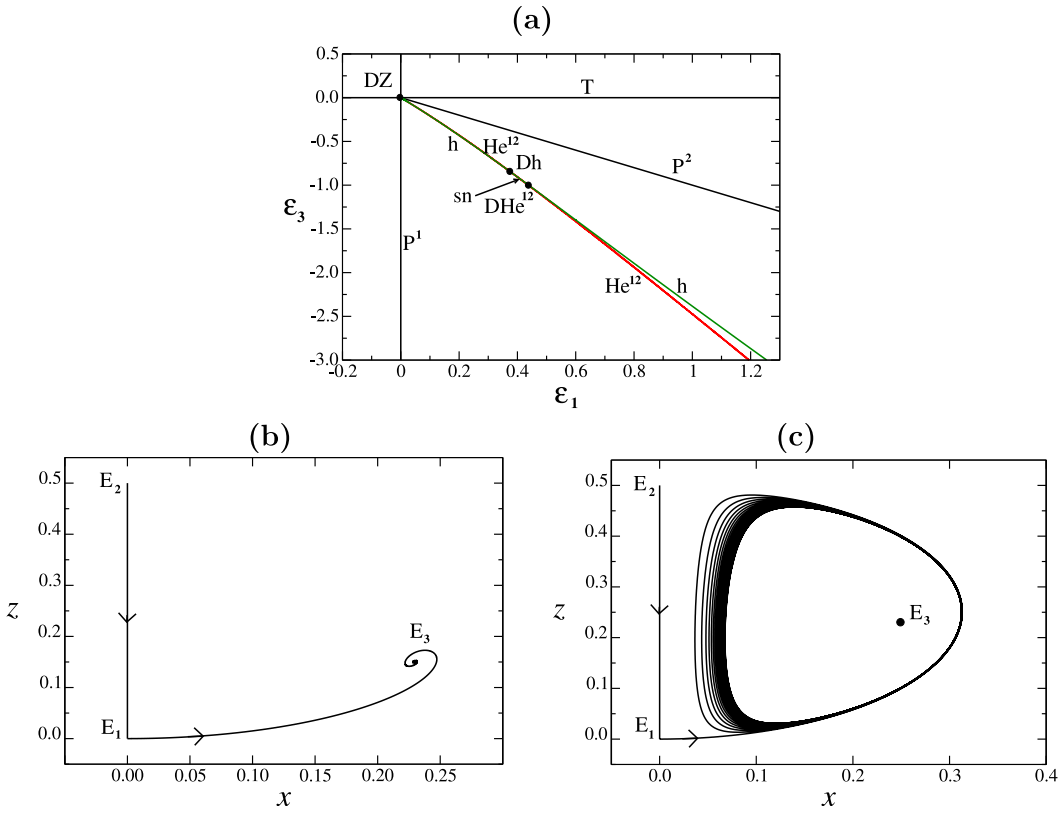

Fig. 3. For $\varepsilon_2 = -1.5, B = -1, D = 1$: (a) Partial bifurcation set in the vicinity of the double-zero point DZ, in the fourth quadrant. For $\varepsilon_3 = -0.5$, heteroclinic connections: (b) between E_2 and E_1 on the z-axis, and between E_1 and the attractive equilibrium E_3, when $\varepsilon_1 = 0.15$; (c) between E_2 and E_1 on the z-axis, and between E_1 and the stable limit cycle arising from h, when $\varepsilon_1 = 0.2304$.

and the eigenvalues of the Jacobian matrix at $E_2 = (0, 0, -\varepsilon_3)$ as $\lambda_1^* < \lambda_2^* < 0 < \lambda_3^*$, where

$$\lambda_3^* = -\varepsilon_3, \quad \lambda_{2,1}^* = \frac{\varepsilon_2 + \varepsilon_3 \pm \sqrt{(\varepsilon_2 + \varepsilon_3)^2 + 4(\varepsilon_1 + \varepsilon_3)}}{2}.$$

Now, we consider the saddle quantities $\delta_{E_1} = \left|\frac{max(\lambda_1,\lambda_3)}{\lambda_2}\right|$ and $\delta_{E_2} = \left|\frac{\lambda_2^*}{\lambda_3^*}\right|$.

Fixed a value $\varepsilon_2 = constant < 0$, in a neighborhood of the point DZ in the fourth quadrant, $\delta_{E_1} = \left|\frac{\lambda_3}{\lambda_2}\right|$, and consequently the locus where $\delta_{E_1}\delta_{E_2} = 1$ satisfies

$$\varepsilon_3 = \varepsilon_2 \frac{2\varepsilon_1 + \varepsilon_2 + \sqrt{4\varepsilon_1 + \varepsilon_2^2}}{1 - \varepsilon_1 - \varepsilon_2}.$$

Along the curve He^{12} of Fig. 3(a), and in general throughout this quadrant, both equilibria E_1 and E_2 are always real saddle.

At the degenerate point DHe^{12}, at $(\varepsilon_1, \varepsilon_3) = (7/16, -1)$,

$$\delta_{E_1}\delta_{E_2} = \left|\frac{\lambda_3\lambda_2^*}{\lambda_2\lambda_3^*}\right| = \left|\frac{-1 \cdot (-0.25)}{0.25 \cdot 1}\right| = 1,$$

in such a way that $\delta_{E_1}\delta_{E_2} > 1$ in the portion of the curve between the points DZ and DHe^{12} and, consequently, the periodic orbit involved in the heteroclinic cycle is stable (see [56,57]). On the other hand, this periodic orbit is of saddle type below DHe^{12} since $\delta_{E_1}\delta_{E_2} < 1$. We remark that the equilibrium E_1 has a double eigenvalue ($\lambda_1 = \lambda_3 = \varepsilon_3$) when $(\varepsilon_1, \varepsilon_3) \approx (0.790525, -1.913196)$. From this point $\delta_{E_1} = \left|\frac{\lambda_1}{\lambda_2}\right|$, but it is still true that $\delta_{E_1}\delta_{E_2} < 1$. Finally, as can be seen in Fig. 3(a), the degenerate points Dh and DHe^{12} are joined by the curve sn, where a saddle–node bifurcation of asymmetric periodic orbits occurs.

As the value of ε_2 increases (approaching the value $\varepsilon_2 = -2$ where the degeneration we are analyzing occurs), it is observed that the degenerate points Dh and DHe^{12}, as well as the intersection point between the curves h and

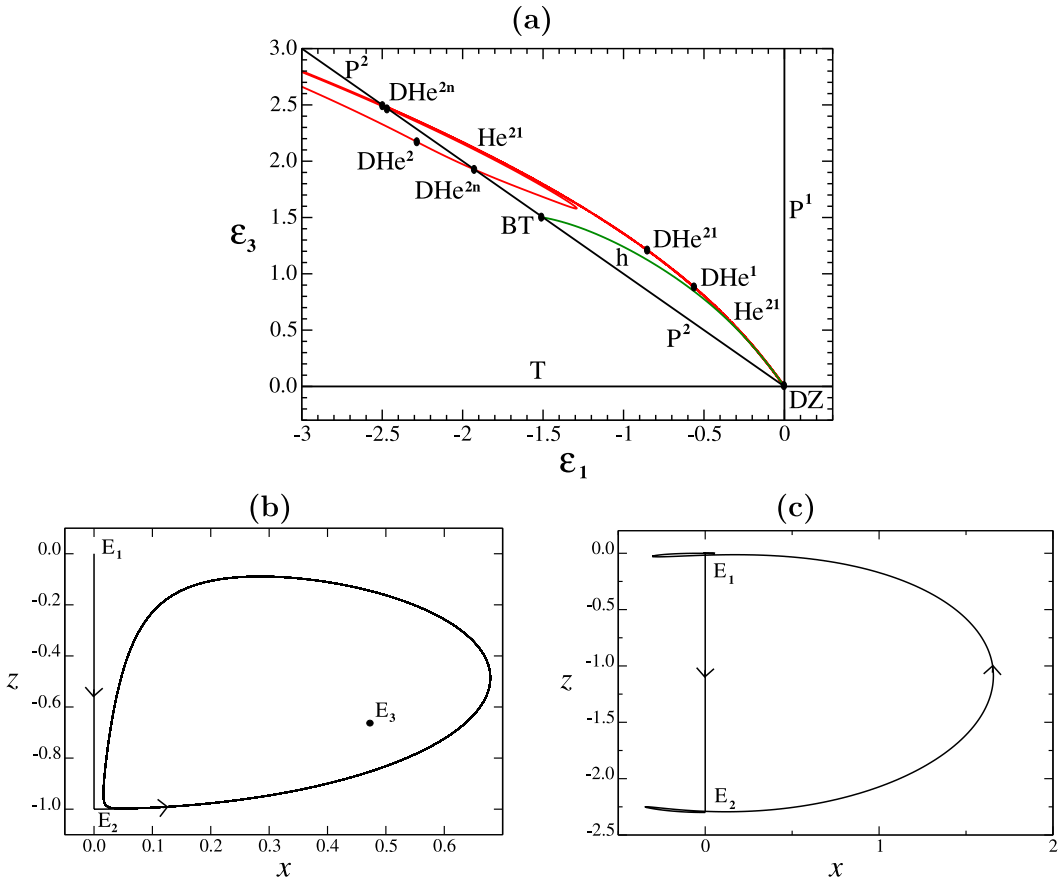

Fig. 4. For $\varepsilon_2 = -1.5, B = -1, D = 1$: (a) Partial bifurcation set, in the second quadrant, in a neighborhood of the point DZ. (b) For $\varepsilon_3 = 1$, $\varepsilon_1 = -0.663$, orbit joining the equilibrium E_2 and the periodic orbit emerged from the Hopf bifurcation h. (c) Projection onto the (x, z)-plane of the heteroclinic cycle He^{21} of panel (a) that exists when $(\varepsilon_1, \varepsilon_3) \approx (-2.4604356, 2.3)$.

He^{12}, are approaching the double-zero point DZ. Thus, for $\varepsilon_2 = -1.9$, the curve sn joins the points Dh which occurs at $(\varepsilon_1, \varepsilon_3) \approx (0.092275, -0.189040)$, and DHe^{12}, placed at $(\varepsilon_1, \varepsilon_3) = (39/400, -0.2)$. Moreover, the intersection between h and He^{12} occurs when $(\varepsilon_1, \varepsilon_3) \approx (0.09369, -0.19201)$.

According to the theoretical study done in Section 3, we know that the curves corresponding to the Hopf bifurcation of the nontrivial equilibria $E_{3,4}$ and to the heteroclinic connections between E_1 and E_2 also exist in the second quadrant of the $(\varepsilon_1, \varepsilon_3)$-plane, as can be seen in the bifurcation set for $\varepsilon_2 = -1.5$ drawn in Fig. 4(a). The Hopf bifurcation curve h is now bounded, as it ends at the point BT, which occurs at $(\varepsilon_1, \varepsilon_3) = (-1.5, 1.5)$, where the equilibrium E_2 undergoes a Bogdanov–Takens bifurcation [43]. Moreover, the curve h exists in the region $-\varepsilon_1 < \varepsilon_3 < -2\varepsilon_1$. In this case, the Hopf bifurcation is always supercritical and the attractive asymmetric periodic orbit arises to the right of the curve h. We note that the equilibria $E_{3,4}$ are attractive node when they arise from P^2. As the value of ε_1 is increased, their evolution is similar to the one mentioned above for the fourth quadrant, but exchanging the roles of E_1 and E_2 (now the unstable manifold of E_2 connects with E_3). Consequently we would have phase portraits of the same type than those of Fig. 3(b)–(c). However, the attractive periodic orbit arising from h, which in a neighborhood of the origin gives rise to the heteroclinic cycle He^{21} (the relevant heteroclinic connection, placed outside the z-axis, goes from E_2 to E_1), for other values of the parameters (for example $\varepsilon_3 = 1$), it goes approaching the equilibrium E_2 (see Fig. 4(b)) ending in a homoclinic connection to E_2 for $\varepsilon_1 \approx -0.6610023$ which will be analyzed later. We note that, in the region between the curves P^2 and He^{21} in Fig. 4(a), the eigenvalues of E_1 are $\lambda_3 = \varepsilon_3 > 0$ (whose associated eigenvector is found on the invariant axis) and $\lambda_2, \lambda_1 < 0$ (since $\varepsilon_1 < 0$), so homoclinic connections to this equilibrium cannot exist in that region.

The curve of heteroclinic cycles He^{21} also emerges from DZ and it is placed to the right of the Hopf curve h. In this case, as $\delta_{E_1}\delta_{E_2} = \left|\frac{\lambda_2\lambda_3^*}{\lambda_3\lambda_2^*}\right| > 1$, the periodic orbit involved in the heteroclinic cycle is stable.

On the curve He^{21} a first degeneracy DHe^1, placed at $(\varepsilon_1, \varepsilon_3) \approx (-0.5625, 0.8834547)$, appears when the equilibrium E_1 changes from saddle–node to saddle-focus. In the second part of this numerical study we will see the relation that exists between this degeneracy and the homoclinic connection to E_2 (originated by the periodic orbit drawn in Fig. 4(b)).

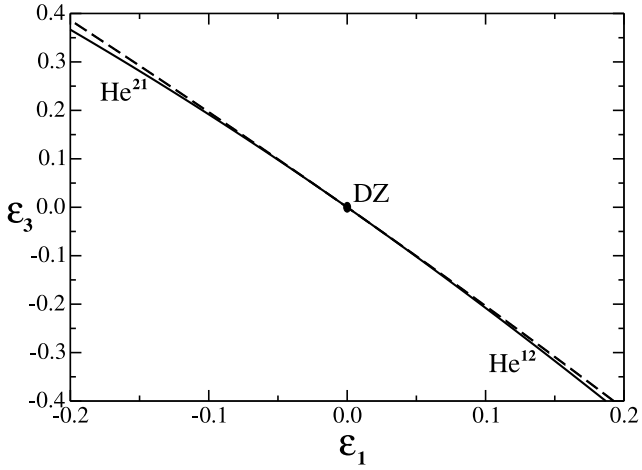

Fig. 5. For $B = -1$, $D = 1$ and $\varepsilon_2 = -1.5$, comparison between numerical continuation (solid) and analytical first-order approximation given by (23) (dashed) for the heteroclinic bifurcation curves He^{12} and He^{21}.

There is also a degenerate point DHe^{21}, located at $(\varepsilon_1, \varepsilon_3) \approx (-0.853422, 1.210866)$, similar to that found in the fourth quadrant, where $\delta_{E_1}\delta_{E_2} = 1$, condition that occurs when

$$\varepsilon_1 = -\varepsilon_3 \left(1 + 2\varepsilon_2 \left(\frac{\varepsilon_2 + \varepsilon_3}{\varepsilon_2 + 2\varepsilon_3}\right)^2\right),$$

since now $\delta_{E_1}\delta_{E_2} = \left|\frac{Re(\lambda_2)\lambda_1^*}{\lambda_3\lambda_2^*}\right|$. From this point DHe^{21}, $\delta_{E_1}\delta_{E_2} < 1$.

Unlike what happens with the degeneracy of the same type located in the fourth quadrant, the point DHe^{21} that exists in the second quadrant is not related to the degeneration exhibited by the double-zero bifurcation DZ at the point DDZ, which occurs at $(\varepsilon_1, \varepsilon_2, \varepsilon_3) = (0, -2, 0)$. Indeed, when we vary the parameter ε_2 approaching the value where the degeneration DDZ occurs, the point DHe^{21} moves away from the point DZ, and specifically, for $\varepsilon_2 = -2$, we obtain DHe^{21}, located at $(\varepsilon_1, \varepsilon_3) \approx (-1.15082, 1.64582)$.

Subsequently the curve of heteroclinic connections He^{21} intersects with the line P^2 at the point DHe^{2n}, which occurs at $(\varepsilon_1, \varepsilon_3) \approx (-2.5007629, 2.5007629)$, where the equilibrium E_2 has a zero eigenvalue $\lambda_1^* = 0$ and, as a consequence, E_2 has a two-dimensional unstable manifold when crossing the line P^2. Later, the curve He^{21} has a turning point outside the range of Fig. 4(a), for $(-10.761538, 5.917409)$, and cuts again P^2 at DHe^{2n}, placed at $(\varepsilon_1, \varepsilon_3) \approx (-2.4692096, -2.4692096)$. As He^{21} approaches the Bogdanov–Takens point BT, it experiences a new turning point and thus it intersects a third time with P^2 at DHe^{2n}, which occurs at $(\varepsilon_1, \varepsilon_3) \approx (-1.9246322, -1.9246322)$. In the region of the parameter plane where E_2 has a two-dimensional unstable manifold, a new degeneration DHe^2 appears on the heteroclinic cycle, for $(\varepsilon_1, \varepsilon_3) \approx (-2.285538, 2.1724805)$, because E_2 goes from real saddle to saddle focus when crossing this point. As can be seen in Fig. 4(c), for $(\varepsilon_1, \varepsilon_3) \approx (-2.4604356, 2.3)$, the equilibrium E_1 is a saddle-focus (with a two-dimensional stable manifold). We remark that bifurcations of generic heteroclinic loops (between a saddle–node hyperbolic equilibrium and a non-hyperbolic equilibrium which undergoes a pitchfork bifurcation) are considered in [58] for a four-dimensional system. In our case the hyperbolic equilibrium E_1 is a saddle-focus at the points DHe^{2n}.

We conclude our study for $\varepsilon_2 = -1.5$ showing, for the heteroclinic curves He^{12} and He^{21}, the good agreement between the theoretical prediction given by Eq. (23) and the numerical results, in the vicinity of the double-zero degeneracy (see Fig. 5).

4.1.2. $\varepsilon_2 = -2.5$ (case $B < 2\Delta$)

Next we set $\varepsilon_2 = -2.5$, on the other side of the value where the degeneracy DDZ occurs, and we find partial bifurcation sets in the fourth and second quadrants of the $(\varepsilon_1, \varepsilon_3)$-parameter plane. In this way we see in Fig. 6(a) the same bifurcation curves, related to double-zero bifurcation DZ, which are present in Fig. 3(a) except the curve of saddle–node bifurcation of periodic orbits sn. This is because no point of degeneration appears on the curves h (Hopf of the nontrivial equilibria $E_{3,4}$) and He^{12} (heteroclinic cycle) and then, the saddle periodic orbit arisen from h ends at the heteroclinic loop He^{12} (it holds $\delta_{E_1}\delta_{E_2} = \left|\frac{\lambda_3\lambda_2^*}{\lambda_2\lambda_3^*}\right| < 1$). We remark that the relative position between the curves h and He^{12} have changed in the vicinity of the point DZ, with respect to what they had in Fig. 3(a) when $\varepsilon_2 = -1.5$ (now we are in the case $B < 2/\varepsilon_2$). In the entire fourth quadrant, as was the case for $\varepsilon_2 = -1.5$, both equilibria E_1 and E_2 are always real saddle.

In Fig. 6(b), for $\varepsilon_2 = -2.5$, we see a partial bifurcation set in the second quadrant, with the curves related to the double-zero bifurcation DZ. As in the case of $\varepsilon_2 = -1.5$, the curve of Hopf bifurcation h ends at a Bogdanov–Takens bifurcation BT exhibited by the equilibrium E_2, which occurs at $(\varepsilon_1, \varepsilon_3) = (-2.5, 2.5)$. Initially, in accordance with the theoretical analysis

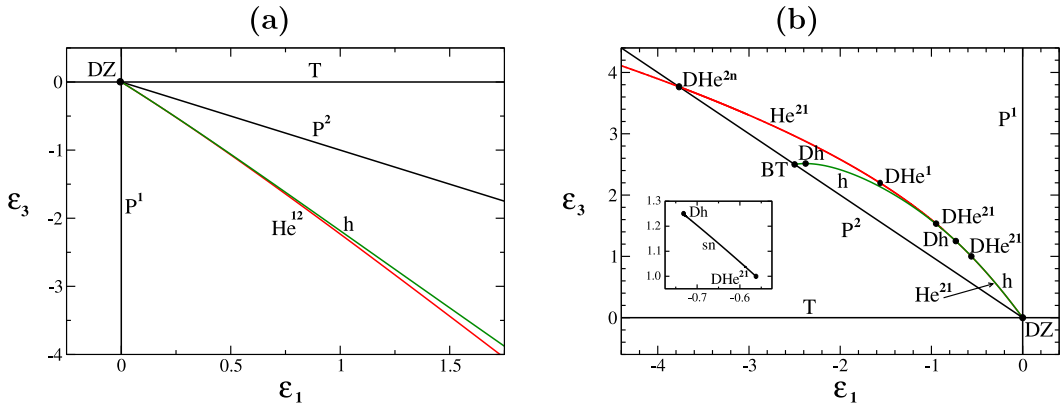

Fig. 6. For $\varepsilon_2 = -2.5, B = -1, D = 1$, partial bifurcation set in a neighborhood of the point DZ: (a) in the fourth quadrant; (b) in the second quadrant.

of Section 3, h arises from the point DZ to the right of the curve He^{21} (both curves are related by a non-stable periodic orbit). Subsequently h and He^{21} intersect and moreover at the point Dh, located at $(\varepsilon_1, \varepsilon_3) \approx (-0.732961, 1.24975)$, the first Lyapunov coefficient vanishes, in such a way that a stable periodic orbit emerges above this point. The curve of saddle–node bifurcations of periodic orbits sn, arisen from this degeneracy, is drawn in the inset of Fig. 6(b).

As in the fourth quadrant, in a neighborhood of the point DZ, it holds $\delta_{E_1}\delta_{E_2} = \left|\frac{\lambda_2\lambda_3^*}{\lambda_3\lambda_2^*}\right| < 1$ on the heteroclinic curve He^{21}. Later, a degeneracy DHe^{21}, where $\delta_{E_1}\delta_{E_2} = \left|\frac{-0.25\cdot(-1)}{1\cdot 0.25}\right| = 1$, occurs at $(\varepsilon_1, \varepsilon_3) = (-9/16, 1)$. This point is the end of the curve sn drawn in Fig. 6(b). We note that the existence in the second quadrant of the degeneration points Dh and DHe^{21} is due to the symmetry exhibited by system (3). Indeed, starting from the values of the degeneracy DHe^{12} for $\varepsilon_2 = -1.5$ in the fourth quadrant, and using the Eqs. (6), the values of the first degeneracy DHe^{21} in the second quadrant are obtained for $\varepsilon_2 = -2.5$. In particular, the eigenvalues of the equilibrium E_1 become those of the equilibrium E_2 and vice versa. On the other hand, the symmetrical point to Dh in the fourth quadrant for $\varepsilon_2 = -1.5$ appears in the plane $\varepsilon_2 \approx -2.342652$ for $(\varepsilon_1, \varepsilon_3) \approx (-0.468831, 0.842652)$. Logically the points on the line T, for $\varepsilon_3 = 0$, remain invariant under this symmetry, in particular the point DZ and its degeneracies.

On the Hopf curve h, near the point BT, there is a second degeneration point Dh, located at $(\varepsilon_1, \varepsilon_3) \approx (-2.37898, 2.51397)$, where the first Lyapunov coefficient vanishes. This new point arises from the bifurcation BT when $\varepsilon_2 = -2$, and it is related with a codimension-three Bogdanov–Takens bifurcation [43]. Analogously, on the curve of heteroclinic connections He^{21} there is a second degeneration point DHe^{21}, which occurs at $(\varepsilon_1, \varepsilon_3) \approx (-0.94877, 1.53434)$, where $\delta_{E_1}\delta_{E_2} = \left|\frac{\lambda_2\lambda_1^*}{\lambda_3\lambda_2^*}\right| = 1$. Once that point is passed, it holds $\delta_{E_1}\delta_{E_2} < 1$.

In this area is now located the degeneration DHe^{1} at $(\varepsilon_1, \varepsilon_3) \approx (-1.5625, 2.1968639)$ (see Fig. 6(b)) unlike what happened for $\varepsilon_2 = -1.5$, since at that point $\delta_{E_1}\delta_{E_2} > 1$ (see Fig. 4(a)). Subsequently the curve He^{21} intersects with the line P^2 at the point DHe^{2n}, situated at $(\varepsilon_1, \varepsilon_3) \approx (-3.7663574, -3.7663574)$, where E_2 has a zero eigenvalue, so that E_2 has a two-dimensional unstable manifold when crossing P^2.

4.1.3. Codimension-two bifurcations around the degenerate DZ

Next, we are going to study in the three-parameter space the loci where the detected codimension-two bifurcations occur. In Fig. 7(a) and (b) we represent, in a neighborhood of the point DDZ, which occurs at $(\varepsilon_1, \varepsilon_2, \varepsilon_3) = (0, -2, 0)$, the projections of the curves Dh, DHe^{12} and DHe^{21} onto the planes $(\varepsilon_2, \varepsilon_1)$ and $(\varepsilon_2, \varepsilon_3)$, respectively. We have also included the curve $\mathrm{He}^{\mathrm{DE1}}$ ($\mathrm{He}^{\mathrm{DE2}}$), where the equilibrium E_1 (E_2) has a non-leading double eigenvalue at the heteroclinic cycle He^{12} (He^{21}).

As can be seen, the curve DHe^{12} (as is the case with curve Dh) arises from the degeneracy DDZ, exhibited by the double-zero bifurcation DZ and analyzed in this paper for system (3). Moreover, DHe^{12} intersects with the curve $\mathrm{He}^{\mathrm{DE1}}$ when $(\varepsilon_1, \varepsilon_2, \varepsilon_3) = (0.64, -1.2, -1.6)$. At this point, the eigenvalues of E_1 are $\lambda_1 = \lambda_3 = -1.6$, $\lambda_2 = 0.4$ and those of E_2 are $\lambda_1^* = -2.4$, $\lambda_2^* = -0.4$, $\lambda_3^* = 1.6$, so that $\delta_{E_1}\delta_{E_2} = 1$. Because of the symmetry exhibited by system (3), the same situation appears for $(\varepsilon_1, \varepsilon_2, \varepsilon_3) = (-0.96, -2.8, 1.6)$, interchanging the roles of the equilibria E_1 and E_2. We note that there is no degeneration DHe^{21} on the surface He^{21} for $\varepsilon_2 < -2.8$, but there is degeneration DHe^{12} for $\varepsilon_2 > -1.2$ to the right of the curve $\mathrm{He}^{\mathrm{DE1}}$.

4.2. Looking for more complex behavior ($B = -0.1, D = 0.01, \varepsilon_2 = -1$)

Our next objective is to analyze some of the degenerations detected on the curves He^{12} and He^{21}, although now we will take $\varepsilon_2 = -1$, $B = -0.1$ and $D = 0.01$. Thus, for the same value of ε_2, we will find degenerations of the type DHe^{2}

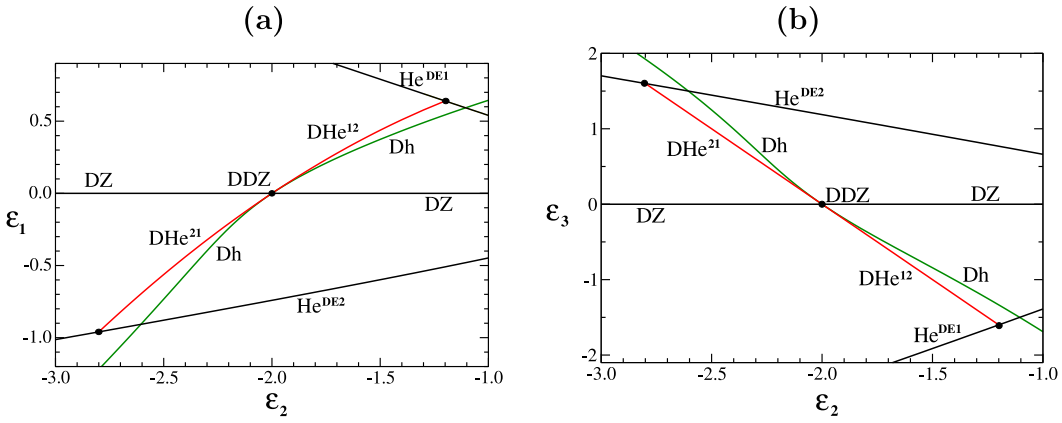

Fig. 7. For $B = -1, D = 1$, projection in the vicinity of the codimension-three bifurcation DDZ of the curves Dh (degenerate Hopf bifurcation of the equilibria $E_{3,4}$), DHe^{12} and DHe^{21} (degeneracy condition $\delta_{E_1}\delta_{E_2} = 1$ on the curves of heteroclinic connections He^{12} and He^{21}, respectively), $\mathrm{He}^{\mathrm{DE1}}$ and $\mathrm{He}^{\mathrm{DE2}}$ (non-leading double eigenvalue of E_1 on He^{12} and of E_2 on He^{21}, respectively) onto: (a) the $(\varepsilon_2, \varepsilon_1)$-plane. (b) the $(\varepsilon_2, \varepsilon_3)$-plane.

and DHe^1 in the fourth and second quadrants, respectively. This situation was not possible with the previous values of the parameters. These degeneracies will allow us to find regions in which there are complex dynamical behaviors.

On the one hand, in the partial bifurcation set of Fig. 8(a)–(b) we see that the curve of nondegenerate heteroclinic cycles He^{12} arises from the double-zero degeneracy DZ. Initially, these heteroclinic cycles are attractive ($\delta_{E_1}\delta_{E_2} > 1$) but their stability changes when crossing the points DHe^{12}. In the fourth quadrant we have found two of these points DHe^{12}, placed at $(\varepsilon_1, \varepsilon_3) \approx (1.057329, -0.028677)$ and $(\varepsilon_1, \varepsilon_3) \approx (17.952116, -0.653279)$, where $\delta_{E_1}\delta_{E_2} = \left|\frac{\lambda_3 Re(\lambda_2^*)}{\lambda_2\lambda_3^*}\right| = 1$ (in fact, $\delta_{E_1}\delta_{E_2} < 1$ at the points on the curve He^{12} between both of them). Specifically, the eigenvalues of E_2, in terms of the parameters B and D, are given by

$$\lambda_3^* = -\varepsilon_3, \qquad \lambda_{2,1}^* = \frac{\varepsilon_2 - \frac{B}{D}\varepsilon_3 \pm \sqrt{\left(\varepsilon_2 - \frac{B}{D}\varepsilon_3\right)^2 + 4\left(\varepsilon_1 + \frac{\varepsilon_3}{D}\right)}}{2}.$$

Thus, the curve where the equilibrium E_2 changes from real saddle to saddle-focus intersects the curve He^{12} in two points. Indeed, when $\varepsilon_1 > 0$, the equilibrium E_1 is always a real saddle along the curve He^{12}. For its part, E_2 is also a real saddle when it arises from DZ, but it becomes a saddle-focus from the point DHe^2, which occurs at $(\varepsilon_1, \varepsilon_3) \approx (0.2328879, -0.00508985)$, placed between DZ and the first degeneracy DHe^{12} (see Fig. 8(b)). Below the second degeneration DHe^{12} there is another similar point DHe^2, situated at $(\varepsilon_1, \varepsilon_3) \approx (72.3710927, -2.7397356)$, where E_2 goes from saddle-focus to real saddle (see Fig. 8(a)).

Several bifurcation curves emerge from the first of these degenerate points DHe^2. Specifically, in Fig. 8(b) we have drawn two curves of homoclinic connections to the origin, H_1^1 and H_2^1, fulfilling that $\delta_{E1} < 1$ when they arise from DHe^2. These curves H_1^1 and H_2^1 end in other degenerations that exist on He^{12} for the values $(\varepsilon_1, \varepsilon_3) \approx (90, -3.4225563)$ and $(\varepsilon_1, \varepsilon_3) \approx (75.0355, -2.8429)$, respectively.

On the homoclinic curve H_1^1 there is a degenerate point DH_1^1, which occurs at $(\varepsilon_1, \varepsilon_3) \approx (1.1370815, -0.6777442)$, where $\delta_{E_1} = 1$, because its eigenvalues fulfill $\lambda_1 < \lambda_3 = -\lambda_2$. In Fig. 8(b) we also find two curves sn and SN of saddle–node bifurcations of (asymmetric and symmetric, respectively) periodic orbits. Whereas sn exists between this point and the degeneration DHe^2 closest to DZ, the curve SN connects this DHe^2 point with $(\varepsilon_1, \varepsilon_3) \approx (75.0355, -2.8429)$, point where the curve H_2^1 ends on He^{12}.

These curves (H_1^1, sn, SN, H_2^1, …) are the first of an infinite sequence of curves of the same type (homoclinic connections to E_1, saddle–node bifurcations of asymmetric and symmetric periodic orbits, …) that all arise from the degeneracy DHe^2. Curves of period-doubling bifurcations (exhibited by the asymmetric periodic orbits involved in sn) and of symmetry-breaking bifurcations (exhibited by the symmetric periodic orbits involved in SN) are also present. As a consequence of the above, in the region between the aforementioned bifurcation curves and He^{12}, we can find attractors of various types as shown in Fig. 8(c)–(f).

On the other hand, in the second quadrant (see Fig. 9(a)) there is a single point DHe^{21} (similar to that found in the second quadrant in Fig. 4(a)), which occurs at $(\varepsilon_1, \varepsilon_3) \approx (-1.11049, 0.01772)$, where $\delta_{E_1}\delta_{E_2} = \left|\frac{Re(\lambda_2)\lambda_3^*}{\lambda_3\lambda_2^*}\right| = 1$. In the rest of the curve He^{21} (starting from the point DHe^{21}), it is true that $\delta_{E_1}\delta_{E_2} < 1$. Remark that these degeneracies DHe^{21}, in which one of the two equilibria E_1 and E_2 involved in the heteroclinic cycle is saddle-focus, are not related to the codimension-three degeneracy DDZ previously analyzed. In this quadrant, the Hopf bifurcation of the equilibria $E_{3,4}$ is always supercritical and the curve h is bounded as it joins the points DZ and BT, placed at $(\varepsilon_1, \varepsilon_3) = (-10, 0.1)$ (where E_2 exhibits a Bogdanov–Takens bifurcation). Since $\varepsilon_3 > 0$, this Bogdanov–Takens bifurcation is of homoclinic type [43]. Consequently, apart from other bifurcation curves, a curve H_1^2 of homoclinic connections to E_2 emerges from BT (see Fig. 9(b)–(c)).

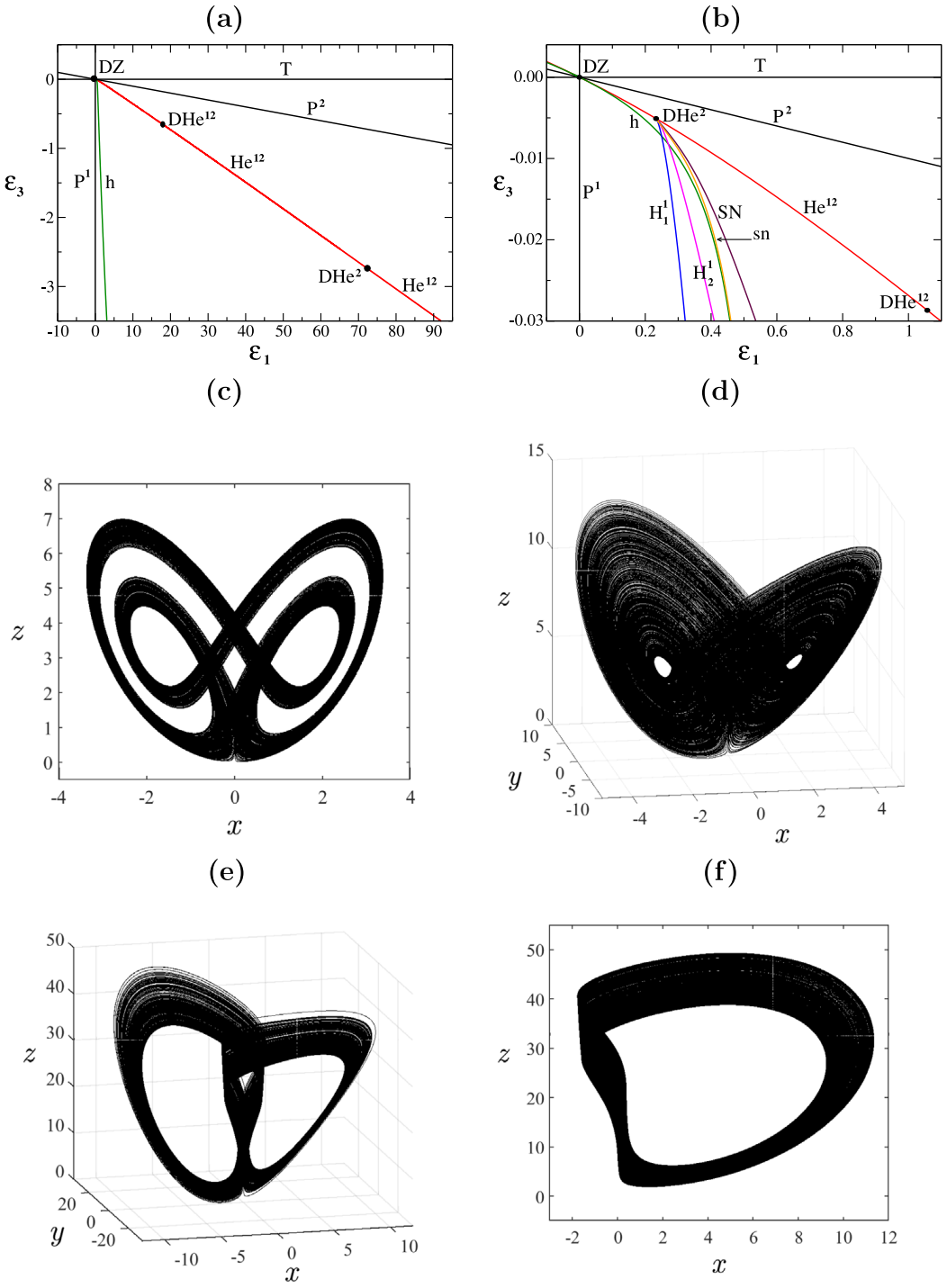

Fig. 8. For $\varepsilon_2 = -1, B = -0.1, D = 0.01$: (a) partial bifurcation set in the fourth quadrant; (b) zoom of panel (a) in a neighborhood of the point DZ. For $\varepsilon_3 = -1$ geometric Lorenz attractor when: (c) $\varepsilon_1 = 3$ with initial conditions $(x_0, y_0, z_0) = (3, -2, 6.5)$. (d) $\varepsilon_1 = 5$ with initial conditions $(x_0, y_0, z_0) = (2.8, 1, 5)$. (e) $\varepsilon_1 = 15$ with initial conditions $(x_0, y_0, z_0) = (0.2, 0.3, 20)$. (f) $\varepsilon_1 = 16.3$ with initial conditions $(x_0, y_0, z_0) = (-0.2, 1.2, 17)$.

When $\varepsilon_1 < 0$, the equilibrium E_2 is always a real saddle along the curve He^{21}. However, although the equilibrium E_1 is also a real saddle when it arises from DZ, it becomes a saddle-focus from the point DHe^{1}, which occurs at $(\varepsilon_1, \varepsilon_3) \approx (-0.25, 0.004611)$, placed between the points DHe^{21} and DZ. Precisely, the homoclinic curve H^2_1, which emerges from the Bogdanov–Takens bifurcation, ends at the point DHe^{1}. As we commented previously, an infinite sequence of homoclinic connections to E_2 arises from DHe^{1}. In Fig. 9(b)–(c) we have drawn the following two homoclinic connections, H^2_2 and H^2_3, of the mentioned sequence. Unlike what happened with the bifurcation curves of the fourth quadrant (which were organized by the degeneracies DHe^{2} and DHe^{12}), in the second quadrant the following two curves of the sequence of homoclinic connections (as well as the first curve H^2_1), now organized by the degeneracy DHe^{1}, do not end on the heteroclinic curve He^{21} (that is, they are not related to the principal heteroclinic loop).

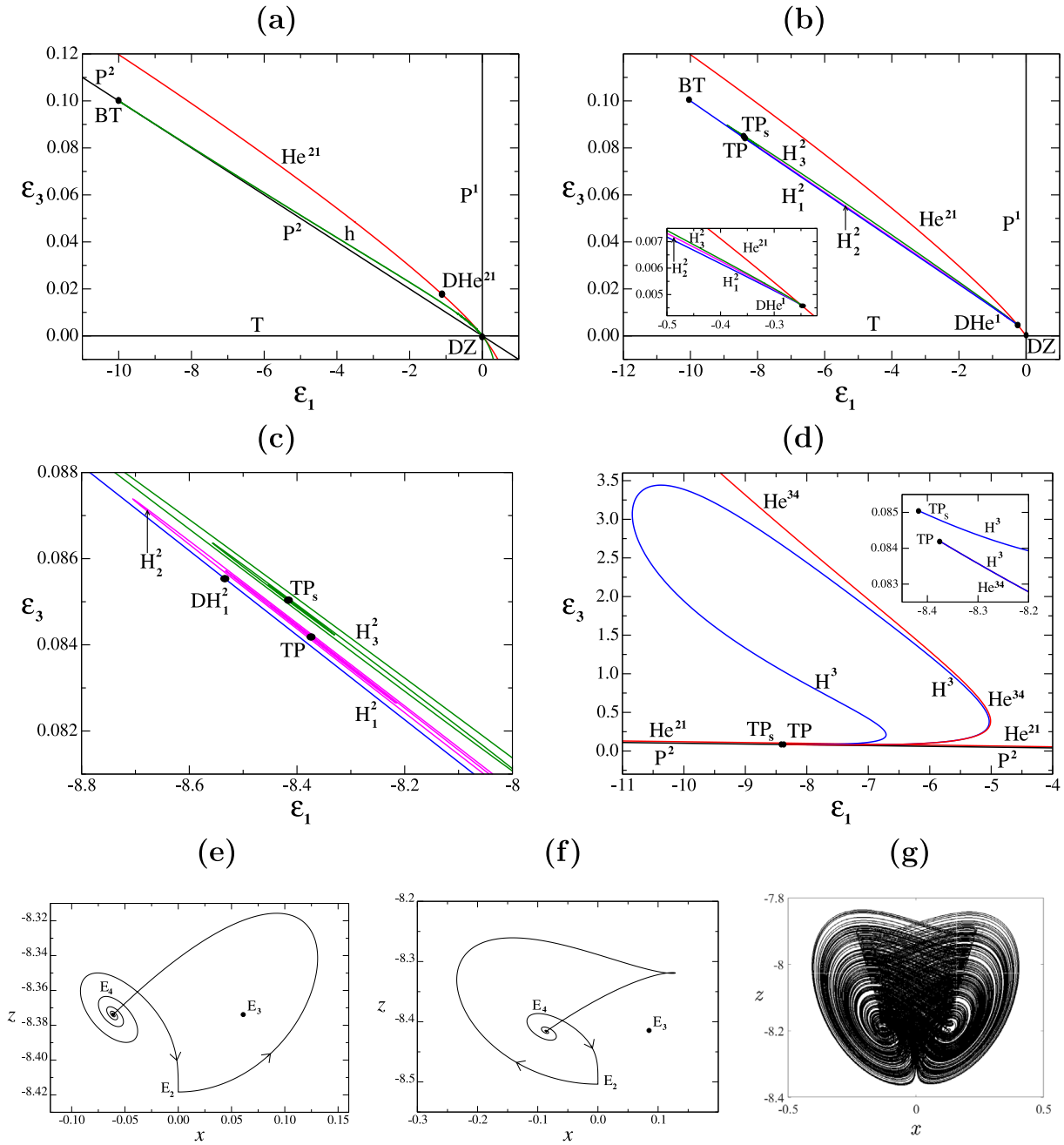

Fig. 9. For $\varepsilon_2 = -1, B = -0.1, D = 0.01$: (a)–(d) partial bifurcation set in the second quadrant of the $(\varepsilon_1, \varepsilon_3)$-plane. Projection onto the (x, z)-plane of the T-point heteroclinic loop between E_2 and the equilibria $E_{3,4}$ (note that because of the symmetry a pair of the corresponding orbits exists): (e) principal T-point when $(\varepsilon_1, \varepsilon_3) \approx (-8.3738877, 0.08418346)$; (f) secondary T-point when $(\varepsilon_1, \varepsilon_3) \approx (-8.4159326, 0.08503685)$. (g) For $(\varepsilon_1, \varepsilon_3) = (-8.2, 0.084)$, geometric Lorenz attractor with initial conditions $(x_0, y_0, z_0) = (0.2, 0, -8.2)$.

On the curve H_1^2 there exists a degenerate point DH_1^2, which occurs at $(\varepsilon_1, \varepsilon_3) \approx (-8.533961, 0.085536)$, where the condition $\delta_{E2} = 1$ (resonant eigenvalues) is fulfilled (see Fig. 9(c)). Moreover, as we can see in Fig. 9(b)–(c), the curve H_2^2 ends at the point TP, which occurs at $(\varepsilon_1, \varepsilon_3) \approx (-8.37388775, 0.08418346)$, where there exists a (principal) heteroclinic T-point loop between E_2 and $E_{3,4}$ [19,59]. Its projection on the (x, z)-plane is drawn in Fig. 9(e). As can be seen in Fig. 9(b)–(d), three curves of global connections emerge from the point TP: He^{34} (heteroclinic connections between E_3 and E_4), H^3 (homoclinic connections to E_3 and E_4) and a spiral shaped curve H_2^2 of homoclinic connections to E_2. Remark that the curves H^3 and H_3^2 end at a secondary T-point heteroclinic loop $\mathrm{TP_s}$ between E_2 and $E_{3,4}$, which occurs at $(\varepsilon_1, \varepsilon_3) \approx (-8.4159326, 0.08503685)$, whose projection on the (x, z)-plane is drawn in Fig. 9(f). In this scenario of global bifurcations the presence of chaotic motions is guaranteed [16,17]. For instance, when $(\varepsilon_1, \varepsilon_3) = (-8.2, 0.084)$ (a point placed in the range of Fig. 9(c)), the attractor obtained with initial conditions $(x_0, y_0, z_0) = (0.2, 0, -8.2)$ is represented in Fig. 9(g). Note that its shape is different from that of the other attractors drawn in Fig. 8(c)–(f).

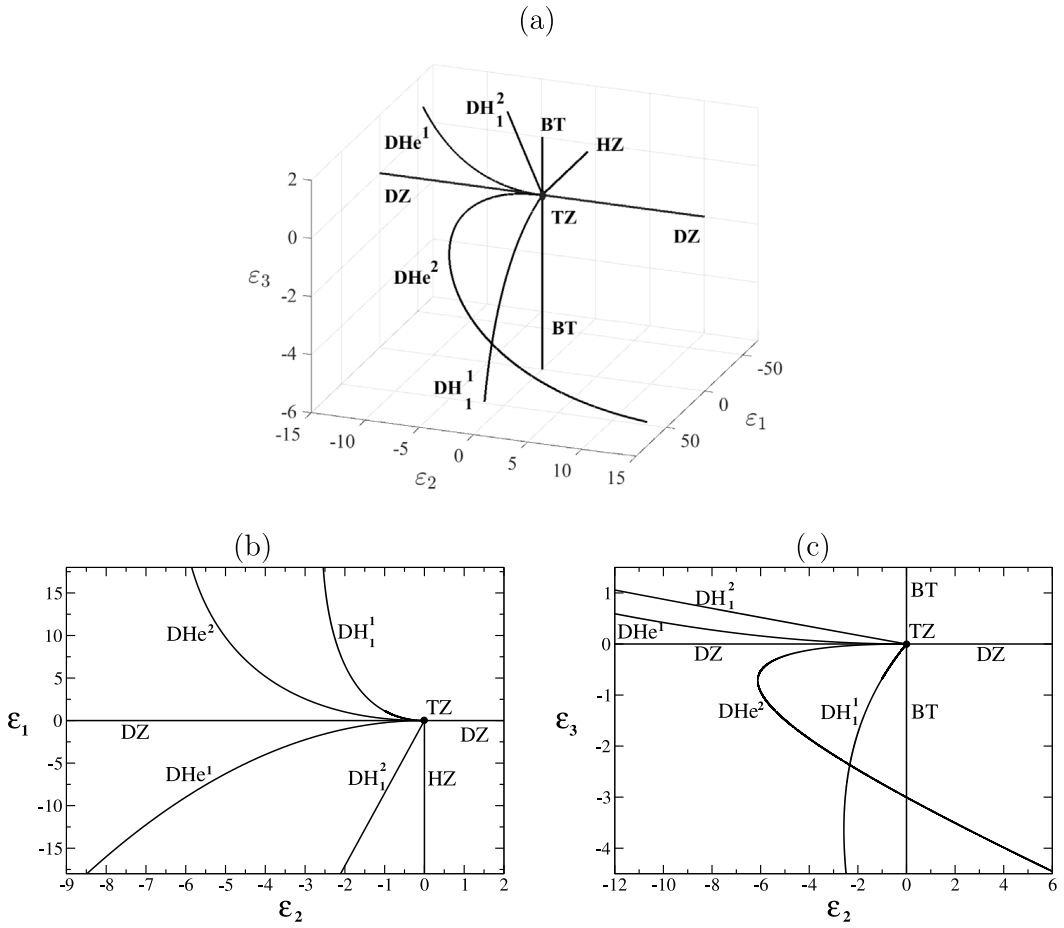

Fig. 10. Partial bifurcation set in a neighborhood of the triple-zero bifurcation TZ, for $B = -0.1$ and $D = 0.01$: (a) in the $(\varepsilon_1, \varepsilon_2, \varepsilon_3)$-space; (b) projection onto the $(\varepsilon_2, \varepsilon_1)$-plane; (c) projection onto the $(\varepsilon_2, \varepsilon_3)$-plane. Seven curves of codimension-two bifurcations appear: three are local (BT, HZ, DZ) and four are global (DHe^1, DHe^2, DH_1^1 and DH_1^2).

4.2.1. Triple-zero bifurcation

Finally, to have a global idea of the bifurcation scenario and the main organizing centers in this region of the parameter space of system (3), we have drawn in Fig. 10 a partial bifurcation set in a neighborhood of the triple-zero degeneracy TZ, when $B = -0.1$ and $D = 0.01$. The curves in the $(\varepsilon_1, \varepsilon_2, \varepsilon_3)$-space appear in Fig. 10(a), their projection onto the $(\varepsilon_2, \varepsilon_1)$-plane in Fig. 10(b) and onto the $(\varepsilon_2, \varepsilon_3)$-plane in Fig. 10(c). Specifically, we draw the loci where the following codimension-two bifurcations occur:

- BT, Bogdanov–Takens bifurcation of equilibrium E_1.
- HZ, Hopf-zero bifurcation of E_1.
- DZ, double-zero bifurcation (a double-zero eigenvalue with geometric multiplicity two) of E_1.
- DHe^1 and DHe^2, degenerate heteroclinic connections because the equilibria E_1 and E_2, respectively, change from saddle–node to saddle-focus.
- DH_1^1 and DH_1^2, degenerate homoclinic connections of E_1 and E_2 due to the existence of resonant eigenvalues $\delta_{E_1} = 1$ and $\delta_{E_2} = 1$, respectively.

Finally we emphasize that similar configurations of curves of codimension-two global bifurcations around a triple-zero degeneracy TZ have been found in previous works, both in the study of some $\mathbb{Z}_2$-symmetric control systems particularized in the Chua's equation [35] as well as in the analysis of non-symmetric electronic circuits [60].

5. Conclusions

In order to continue advancing in the analysis of the Lorenz system (and of so many other quadratic systems called Lorenz-like systems) it is necessary to combine analytical and numerical tools. Given the impossibility of studying by standard methods the triple-zero bifurcation that the equilibrium at the origin of the Lorenz system exhibits when $\sigma = -1$, $\rho = 1$, $b = 0$, in this work we carry out a partial study of system (3), an unfolding of the normal form of

the triple-zero bifurcation. We remark that several systems studied in the literature appear as particular cases for certain parameter choices [37–42].

The theoretical analysis of the double-zero bifurcation (a double-zero eigenvalue with geometric multiplicity two) has allowed to determine the different cases that may appear. For this we have established a connection between the reduced system on the corresponding two-dimensional center manifold and the planar normal form of the Hopf-zero bifurcation [44, Sect. 7.4]. For its greater interest, we have focused on the case that leads to a more complex dynamical behavior (existence of Hopf bifurcation and heteroclinic connection), and we have provided the expressions of the bifurcation curves organized by the double-zero degeneracy.

Taking as a starting point the theoretical results obtained, we have carried out a numerical study that has allowed to find bifurcations of codimension one (Hopf, transcritical, pitchfork, saddle–node of periodic orbits, heteroclinic, homoclinic), two (double-zero, Bogdanov–Takens, degenerate Hopf, degenerate heteroclinic, degenerate homoclinic, T-point) and three (degenerate double-zero, triple-zero) in the region considered of the parameter space. On the other hand, we have also found zones of existence of chaotic attractors. Various aspects of the bifurcation set of system (3) are worth studying in the future. For example, to complete the study of degeneracies that appear on the bifurcation curves and to determine the new curves that emerge from those degenerate points.

The double-zero bifurcation has allowed to find a heteroclinic connection. The degeneracies of this heteroclinic cycle are connected with the triple-zero bifurcation TZ (see Fig. 10). This codimension-three linear degeneracy deserves further study whose results can be applied to the Lorenz system.

Declaration of competing interest

The authors declare that they have no known competing financial interests or personal relationships that could have appeared to influence the work reported in this paper.

Acknowledgments

We thank the reviewers for their careful reading of the manuscript and their very constructive remarks which have helped a lot to improve the presentation of the results. This work has been partially supported by the *Ministerio de Economía y Competitividad*, Spain (project MTM2017-87915-C2-1-P, co-financed with FEDER funds), by the *Ministerio de Ciencia, Innovación y Universidades*, Spain (project PGC2018-096265-B-I00, co-financed with FEDER funds) and by the *Consejería de Economía, Innovación, Ciencia y Empleo de la Junta de Andalucía*, Spain (FQM-276, TIC-0130, UHU-1260150 and P20_01160).

Appendix A. Some useful changes of variables

The first lemma is obtained directly from the results shown in [44, Sect. 7.4]. We state it here for clarity and completeness.

Lemma A.1. *System*

$$\begin{cases} \dot{r} = arz + cr^3 + drz^2, \\ \dot{z} = -r^2 - z^2 + er^2z + fz^3, \end{cases} \tag{A.1}$$

for $a \neq 0$, by means of the change of variables

$$s = r, \quad w = z + hr^2 + iz^2, \quad d\tau = (1 + jz)^{-1}dt, \tag{A.2}$$

where

$$h = \frac{c}{a}, \quad i = \frac{d + ae + 2(a+1)c}{3a}, \quad j = \frac{ae - 2d + 2(a+1)c}{3a}, \tag{A.3}$$

is transformed into

$$\begin{cases} \dfrac{ds}{d\tau} = asw + \mathcal{O}(|s, w|^4), \\ \dfrac{dw}{d\tau} = -s^2 - w^2 + \hat{f}w^3 + \mathcal{O}(|s, w|^4), \end{cases} \tag{A.4}$$

where $\hat{f} = f - j$.

Lemma A.2. *System*

$$\begin{cases} \dot{r} = arz + cr^3z + drz^3, \\ \dot{z} = -r^2 - z^2 + er^4 + fr^2z^2 + mz^4, \end{cases} \tag{A.5}$$

for $a \neq 0, -1/2$, is orbitally equivalent to

$$\begin{cases} \dfrac{ds}{d\tau} = asw + \mathcal{O}(|s, w|^5), \\ \dfrac{dw}{d\tau} = -s^2 - w^2 + \mathcal{O}(|s, w|^5), \end{cases} \tag{A.6}$$

by means of the change of variables

$$s = r(1 + gr^2 + hz^2), \quad w = z(1 + irz + jz^2), \quad d\tau = (1 + kr^2)^{-1}dt, \tag{A.7}$$

where

$$\begin{aligned} g &= -\frac{a^2e + (a+1)c + af - 2am - d}{2a(2a+1)}, \quad h = \frac{d - am}{2}, \quad j = m, \\ i &= \frac{a(2a+5)m + (1-2a)d + ae - 2af - c}{2(2a+1)}, \quad k = \frac{ae - am - c + d}{2a}, \end{aligned} \tag{A.8}$$

Lemma A.3. *System*

$$\begin{cases} \dot{r} = arz + cr^5 + dr^3z^2 + erz^4, \\ \dot{z} = -r^2 - z^2 + fr^4z + gr^2z^3 + hz^5, \end{cases} \tag{A.9}$$

for $a \neq 0$, is orbitally equivalent to

$$\begin{cases} \dfrac{ds}{d\tau} = asw + \mathcal{O}(|s, w|^6), \\ \dfrac{dw}{d\tau} = -s^2 - w^2 + \hat{h}w^5 + \mathcal{O}(|s, w|^6), \end{cases} \tag{A.10}$$

where

$$\hat{h} = h + \frac{2(1-4a^2)c - 2(a+1)d + 2e - 3ag + a(1-2a)f}{5a}.$$

Appendix B. Hopf bifurcations of the nontrivial equilibria

In this appendix we analyze the Hopf bifurcations of the nontrivial equilibria $E_{3,4}$ and E_2 of system (3). The results obtained, valid for any value of ε_1, ε_2 and ε_3, will be useful in the numerical study carried out in Section 4.

B.1. Hopf bifurcation of the equilibria $E_{3,4}$

Due to the symmetry, we will only consider in our study one of these equilibria, namely $E_3 = (\sqrt{-\varepsilon_1(\varepsilon_3 + D\varepsilon_1)}, 0, \varepsilon_1)$, that exists when $\varepsilon_1(\varepsilon_3 + D\varepsilon_1) < 0$.

Firstly, we translate the nontrivial equilibria E_3 to the origin by means of the change

$$X = x - \sqrt{-\varepsilon_1(\varepsilon_3 + D\varepsilon_1)}, \quad Y = y, \quad Z = z - \varepsilon_1,$$

that transforms system (3) into

$$\begin{cases} \dot{X} &= Y, \\ \dot{Y} &= \xi_2 Y - \xi_1 Z - XZ + BYZ, \\ \dot{Z} &= 2\xi_1 X + \xi_3 Z + X^2 + DZ^2, \end{cases} \tag{B.1}$$

with

$$\xi_1 = \sqrt{-\varepsilon_1(\varepsilon_3 + D\varepsilon_1)}, \quad \xi_2 = \varepsilon_2 + B\varepsilon_1, \quad \xi_3 = \varepsilon_3 + 2D\varepsilon_1. \tag{B.2}$$

Therefore, the characteristic polynomial of the linearization matrix of system (B.1) at the origin is given by

$$p = \lambda^3 + p_1\lambda^2 + p_2\lambda + p_3,$$

where

$$p_1 = -(\xi_2 + \xi_3), \quad p_2 = \xi_2\xi_3, \quad p_3 = 2\xi_1^2.$$

Thus, a Hopf bifurcation of E_3 occurs when $p_1p_2 = p_3$, $p_2 > 0$, $p_1 \neq 0$, that is, when

$$\xi_1^2 = -\frac{1}{2}\xi_2\xi_3(\xi_2 + \xi_3), \quad \xi_2\xi_3 > 0, \quad \xi_2 + \xi_3 < 0, \quad \xi_2 < 0, \quad \xi_3 < 0.$$

Considering system (B.1) at the critical values where the Hopf bifurcation occurs, we perform the following linear change to put the matrix of the linear part into the corresponding canonical form

$$\begin{pmatrix} X \\ Y \\ Z \end{pmatrix} = \begin{pmatrix} 0 & 1 & 1 \\ \omega_0 & 0 & -K_1^2 \\ K_2 & K_3 & K_4 \end{pmatrix} \begin{pmatrix} u \\ v \\ w \end{pmatrix},$$

where

$$\omega_0 = \sqrt{\xi_2 \xi_3}, \quad K_1 = \sqrt{-(\xi_2 + \xi_3)}, \quad K_2 = \frac{\sqrt{2}\xi_2}{K_1}, \quad K_3 = \frac{\sqrt{2}\omega_0}{K_1}, \quad K_4 = \frac{\sqrt{2}\omega_0 K_1}{\xi_2}.$$

Thus, with this change, system (B.1) becomes

$$\begin{pmatrix} \dot{u} \\ \dot{v} \\ \dot{w} \end{pmatrix} = \begin{pmatrix} 0 & -\omega_0 & 0 \\ \omega_0 & 0 & 0 \\ 0 & 0 & -K_1^2 \end{pmatrix} \begin{pmatrix} u \\ v \\ w \end{pmatrix} + \frac{1}{C} \begin{pmatrix} A_1 u^2 + A_2 v^2 + A_3 w^2 + A_4 uv + A_5 uw + A_6 vw \\ A_7 u^2 + A_8 v^2 + A_9 w^2 + A_{10} uv + A_{11} uw + A_{12} vw \\ -A_7 u^2 - A_8 v^2 - A_9 w^2 - A_{10} uv - A_{11} uw - A_{12} vw \end{pmatrix}, \tag{B.3}$$

where

$$\begin{aligned}
C &= \xi_2 K_2 + \xi_3 K_2 + K_3 \omega_0 - K_4 \omega_0 \neq 0, \\
A_1 &= K_2 \, (K_3 \, \omega_0 - K_4 \, \omega_0 - \xi_2 \, K_2 - \xi_3 \, K_2) \, , \\
A_2 &= {K_3}^2 E_2 + {K_3}^2 E_3 - {K_3}^2 + K_3 \, K_4 + E_2 + E_3, \\
A_3 &= -K_3 \, K_4 \, E_2 + 2 \, {K_4}^2 E_2 - K_3 \, K_4 \, E_3 + 2 \, {K_4}^2 E_3 - K_3 \, K_4 + {K_4}^2 + E_2 + E_3, \\
A_4 &= 2 \, K_2 \, K_3 \, E_2 + 2 \, K_2 \, K_3 \, E_3 - {K_3}^2 \omega_0 + K_3 \, K_4 \, \omega_0 - K_2 \, K_3 + K_2 \, K_4, \\
A_5 &= -K_2 \, K_3 \, E_2 + 3 \, K_2 \, K_4 \, E_2 - K_2 \, K_3 \, E_3 + 3 \, K_2 \, K_4 \, E_3 - K_3 \, K_4 \, \omega_0 \\
&\quad + {K_4}^2 \omega_0 - K_2 \, K_3 + K_2 \, K_4, \\
A_6 &= -{K_3}^2 E_2 + 3 \, K_3 \, K_4 \, E_2 - {K_3}^2 E_3 + 3 \, K_3 \, K_4 \, E_3 - {K_3}^2 + {K_4}^2 + 2 \, E_2 + 2 \, E_3, \\
A_7 &= 2 \, \omega_0 {K_2}^2, \\
A_8 &= \omega_0 {K_3}^2 + K_3 \, K_2 + \omega_0, \\
A_9 &= K_4 \, \xi_2 \, K_2 + K_4 \, \xi_3 \, K_2 + {K_4}^2 \omega_0 + K_4 \, K_2 + \omega_0, \\
A_{10} &= K_2 \, (3 \, K_3 \, \omega_0 + K_2) \, , \\
A_{11} &= K_2 \, (\xi_2 \, K_2 + \xi_3 \, K_2 + 3 \, K_4 \, \omega_0 + K_2) \, , \\
A_{12} &= K_3 \, \xi_2 \, K_2 + K_3 \, \xi_3 \, K_2 + 2 \, K_4 \, \omega_0 K_3 + K_3 \, K_2 + K_4 \, K_2 + 2 \, \omega_0.
\end{aligned}$$

Now, considering the second-order approximation to the center manifold

$$w = \alpha_1 u^2 + \alpha_2 uv + \alpha_3 v^2 + \cdots,$$

we obtain the reduced system up to third order on the center manifold. And, by using the recursive algorithm developed in [46], we obtain the normal form for the Hopf bifurcation to third-order (22), where the first Lyapunov coefficient is given by

$$a_1 = \frac{\sqrt{\xi_2 \, \xi_3} N_1}{4 \xi_2 \xi_3 \, (\xi_2 + \xi_3) \left({\xi_2}^2 + 6 \, \xi_2 \, \xi_3 + {\xi_3}^2 \right) \left({\xi_2}^2 + 3 \, \xi_2 \, \xi_3 + {\xi_3}^2 \right)}, \tag{B.4}$$

with

$$\begin{aligned}
N_1 &= 2 \, {\xi_2}^5 + 31 \, {\xi_2}^4 \xi_3 + 39 \, {\xi_2}^3 {\xi_3}^2 + {\xi_2}^2 {\xi_3}^3 - \xi_2 \, {\xi_3}^4 + 4 \, {\xi_2}^4 + 56 \, {\xi_2}^3 \xi_3 \\
&\quad + 25 \, {\xi_2}^2 {\xi_3}^2 - 12 \, \xi_2 \, {\xi_3}^3 - {\xi_3}^4 + 2 \, {\xi_2}^2 \xi_3 - 24 \, \xi_2 \, {\xi_3}^2 - 2 \, {\xi_3}^3.
\end{aligned}$$

Since $\xi_2 \xi_3 > 0$, we obtain that $a_1 = 0$ if, and only if, $N_1 = 0$.

In Fig. B.1 we have drawn the curve $N_1 = 0$ in the (ξ_2, ξ_3)-plane near the origin. It is a bounded curve connecting the points $(-2, 0)$ and $(0, -2)$.

In terms of the original parameters of the system, the Hopf surface of the equilibria $E_{3,4}$ is given by

$$\begin{aligned}
\varepsilon_3 &= \frac{2\varepsilon_1 - 2(B + 2D)\varepsilon_1 \varepsilon_2 - B(B + 4D)\varepsilon_1^2 - \varepsilon_2^2}{2(B\varepsilon_1 + \varepsilon_2)} \\
&\quad + \frac{\sqrt{(B\varepsilon_1 + \varepsilon_2)^4 + 4\varepsilon_1(\varepsilon_1 - 2D(B\varepsilon_1 + \varepsilon_2)\varepsilon_1 - (B\varepsilon_1 + \varepsilon_2)^2)}}{2(B\varepsilon_1 + \varepsilon_2)},
\end{aligned} \tag{B.5}$$

in the zones where the above inequalities are fulfilled.

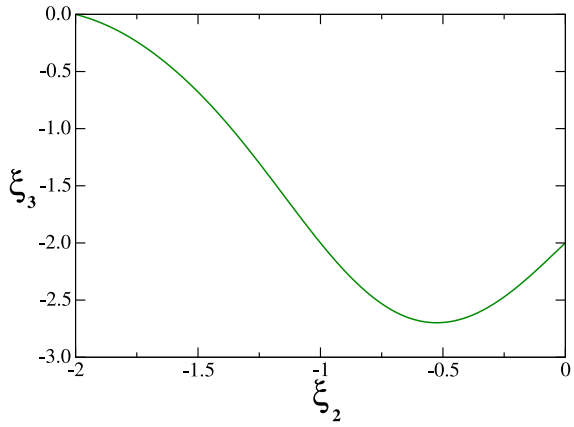

Fig. B.1. Curve $N_1 = 0$ in the (ξ_2, ξ_3)-plane in the vicinity of the origin. It corresponds to the degeneracy $a_1 = 0$ in the Hopf bifurcation of the equilibria $E_{3,4}$.

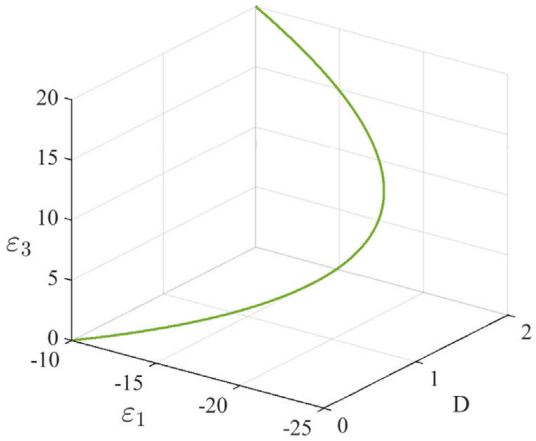

Fig. B.2. For $\varepsilon_2 = -1$, $B = -0.1$, curve on the Hopf surface where $M_1 = 0$ in the $(D, \varepsilon_1, \varepsilon_3)$-space. It corresponds to the degeneracy $a_1 = 0$ in the Hopf bifurcation of equilibrium E_2.

B.2. Hopf bifurcation of the equilibrium E_2

Now we consider the equilibrium $E_2 = (0, 0, -\varepsilon_3/D)$. According to Section 2, it exhibits a Hopf bifurcation when $B\varepsilon_3 = D\varepsilon_2$, if $\varepsilon_1 + \varepsilon_3/D < 0$ and $\varepsilon_3 \neq 0$. Repeating the previous calculations we obtain that the first Lyapunov coefficient, in terms of the original parameters of the system, is given by

$$a_1 = \frac{B^2 M_1}{8\sqrt{-\frac{B\varepsilon_1+\varepsilon_2}{B}}\, D\,\varepsilon_2 \left(4B^2\varepsilon_1 + 4B\varepsilon_2 - D^2{\varepsilon_2}^2\right)}, \tag{B.6}$$

with

$$M_1 = 8B^2\varepsilon_1 + 8B\varepsilon_2 - D^2{\varepsilon_2}^2 - 2D\varepsilon_2.$$

If $B \neq 0$, we obtain that $a_1 = 0$ if, and only if, $M_1 = 0$.

For $\varepsilon_2 = -1$ and $B = -0.1 < 0$, in Fig. B.2 we have drawn, in the $(D, \varepsilon_1, \varepsilon_3)$-space, the curve on the Hopf surface where $M_1 = 0$. This curve exists between the points $(0, -10, 0)$ (where a triple-zero bifurcation in a continuum of equilibria occurs) and $(2, -10, 20)$ (that corresponds to a degenerate Bogdanov–Takens bifurcation) [43]. Also, if we set a value $D \in (0, 2)$, there is a unique degeneracy $a_1 = 0$ on the Hopf curve of E_2 when $\varepsilon_1 < -10$, and there are no degenerations if $D < 0$.

References

[1] Lorenz EN. Deterministic non-periodic flows. J Atmospheric Sci 1963;20:130–41. http://dx.doi.org/10.1175/1520-0469(1963)020<0130:DNF>2.0.CO;2.

[2] Sparrow C. The Lorenz equation: bifurcations, chaos and strange attractors. New York: Springer; 1982, http://dx.doi.org/10.1007/978-1-4612-5767-7.

[3] Haken H. Analogy between higher instabilities in fluids and lasers. Phys Lett A 1975;53:77–8. http://dx.doi.org/10.1016/0375-9601(75)90353-9.
[4] Knobloch E. Chaos in the segmented disc dynamo. Phys Lett A 1981;82:439–40. http://dx.doi.org/10.1016/0375-9601(81)90274-7.
[5] Gorman M, Widmann PJ, Robbins KA. Nonlinear dynamics of a convection loop: a quantitative comparison of experiment with theory. Physica D 1986;19:255–67. http://dx.doi.org/10.1016/0167-2789(86)90022-9.
[6] Elgin JN, Molina-Garza JB. Traveling wave solutions of the Maxwell–Bloch equations. Phys Rev A 1987;35:3986–8. http://dx.doi.org/10.1103/PhysRevA.35.3986.
[7] Knobloch E, Proctor MRE, Weiss NO. Heteroclinic bifurcations in a simple model of double-diffusive convection. J Fluid Mech 1992;239:273–92. http://dx.doi.org/10.1017/S0022112092004403.
[8] Cuomo KM, Oppenheim AV. Circuit implementation of synchronized chaos with applications to communications. Phys Rev Lett 1993;71:65–8. http://dx.doi.org/10.1103/PhysRevLett.71.65.
[9] Poland D. Cooperative catalysis and chemical chaos: a chemical model for the Lorenz equations. Physica D 1993;65:86–99. http://dx.doi.org/10.1016/0167-2789(93)90006-M.
[10] Hemati N. Strange attractors in brushless DC motors. IEEE T Circuits-I 1994;41:40–5. http://dx.doi.org/10.1109/81.260218.
[11] Alexeev I. Lorenz system in the thermodynamic modelling of leukaemia malignancy. Med Hypotheses 2017;102:150–5. http://dx.doi.org/10.1016/j.mehy.2017.03.027.
[12] Tucker W. The Lorenz attractor exists. C R Acad Sci 1999;328:1197–202. http://dx.doi.org/10.1016/S0764-4442(99)80439-X.
[13] Osinga HM, Krauskopf B. Visualizing the structure of chaos in the Lorenz system. Comput Graph 2002;26:815–23. http://dx.doi.org/10.1016/S0097-8493(02)00136-X.
[14] Barrio R, Serrano S. Bounds for the chaotic region in the Lorenz model. Physica D 2009;238:1615–24. http://dx.doi.org/10.1016/j.physd.2009.04.019.
[15] Yajima T, Nagahama H. Tangent bundle viewpoint of the Lorenz system and its chaotic behavior. Phys Lett A 2010;374:1315–9. http://dx.doi.org/10.1016/j.physleta.2010.01.025.
[16] Barrio R, Blesa F, Serrano S. Global organization of spiral structures in biparameter space of dissipative systems with Shilnikov saddle-foci. Phys Rev E 2011;84:035201. http://dx.doi.org/10.1103/PhysRevE.84.035201.
[17] Barrio R, Shilnikov AL, Shilnikov LP. Kneadings, symbolic dynamics and painting Lorenz chaos. Int J Bifurcation Chaos 2012;22:1230016. http://dx.doi.org/10.1142/S0218127412300169.
[18] Leonov GA, Kuznetsov NV, Korzhemanova NA, Kusakin DV. Lyapunov dimension formula for the global attractor of the Lorenz system. Commun Nonlinear Sci Numer Simul 2016;41:84–103. http://dx.doi.org/10.1016/j.cnsns.2016.04.032.
[19] Glendinning P, Sparrow C. T-points: a codimension two heteroclinic bifurcation. J Stat Phys 1986;43:479–88. http://dx.doi.org/10.1007/BF01020649.
[20] Algaba A, Fernández-Sánchez F, Merino M, Rodríguez-Luis AJ. Analysis of the T-point-Hopf bifurcation in the Lorenz system. Commun Nonlinear Sci Numer Simul 2015;22:676–91. http://dx.doi.org/10.1016/j.cnsns.2014.09.025.
[21] Creaser JL, Krauskopf B, Osinga HM. α-Flips and T-points in the Lorenz system. Nonlinearity 2015;28:R39–65. http://dx.doi.org/10.1088/0951-7715/28/3/R39.
[22] Doedel EJ, Krauskopf B, Osinga HM. Global bifurcations of the Lorenz manifold. Nonlinearity 2006;19:2947–72. http://dx.doi.org/10.1088/0951-7715/19/12/013.
[23] Doedel EJ, Krauskopf B, Osinga HM. Global invariant manifolds in the transition to preturbulence in the Lorenz system. Indag Math 2011;22:222–40. http://dx.doi.org/10.1016/j.indag.2011.10.007.
[24] Doedel EJ, Krauskopf B, Osinga HM. Global organization of phase space in the transition to chaos in the Lorenz system. Nonlinearity 2015;28:R113–39. http://dx.doi.org/10.1088/0951-7715/28/11/R113.
[25] Llibre J, Zhang X. Invariant algebraic surfaces of the Lorenz system. J Math Phys 2002;43:1622–45. http://dx.doi.org/10.1063/1.1435078.
[26] Llibre J, Messias M, da Silva PR. Global dynamics of the Lorenz system with invariant algebraic surfaces. Int J Bifurcation Chaos 2010;20:3137–55. http://dx.doi.org/10.1142/S0218127410027593.
[27] Algaba A, Gamero E, Merino M, Rodríguez-Luis AJ. Resonances of periodic orbits in the Lorenz system. Nonlinear Dyn 2016;84:2111–36. http://dx.doi.org/10.1007/s11071-016-2632-5.
[28] Algaba A, Merino M, Rodríguez-Luis AJ. Superluminal periodic orbits in the Lorenz system. Commun Nonlinear Sci Numer Simul 2016;39:220–32. http://dx.doi.org/10.1016/j.cnsns.2016.03.004.
[29] Algaba A, Fernández-Sánchez F, Merino M, Rodríguez-Luis AJ. Centers on center manifolds in the Lorenz, Chen and Lü systems. Commun Nonlinear Sci Numer Simul 2014;19:772–5. http://dx.doi.org/10.1016/j.cnsns.2013.08.003.
[30] Algaba A, Domínguez-Moreno MC, Merino M, Rodríguez-Luis AJ. Study of the Hopf bifurcation in the Lorenz, Chen and Lü systems. Nonlinear Dyn 2015;79:885–902. http://dx.doi.org/10.1007/s11071-014-1709-2.
[31] Algaba A, Domínguez-Moreno MC, Merino M, Rodríguez-Luis AJ. Takens–Bogdanov bifurcations of equilibria and periodic orbits in the Lorenz system. Commun Nonlinear Sci Numer Simul 2016;30:328–43. http://dx.doi.org/10.1016/j.cnsns.2015.06.034.
[32] Algaba A, Domínguez-Moreno MC, Merino M, Rodríguez-Luis AJ. A review on some bifurcations in the Lorenz system. In: Carmona V, et al., editors. Nonlinear systems, vol. 1. Mathematical theory and computational methods. Cham: Springer; 2018, p. 3–36. http://dx.doi.org/10.1007/978-3-319-66766-9_1.
[33] Gamero E. On the normal form of the triple-zero degeneracy with geometric multiplicity two. Dynam Cont Dis Ser A 2001;8:531–50.
[34] Freire E, Gamero E, Rodríguez-Luis AJ, Algaba A. A note on the triple-zero linear degeneracy: Normal forms, dynamical and bifurcation behaviors of an unfolding. Int J Bifurcation Chaos 2002;12:2799–820. http://dx.doi.org/10.1142/S0218127402006175.
[35] Algaba A, Merino M, Freire E, Gamero E, Rodríguez-Luis AJ. Some results on Chua's equation near a triple-zero linear degeneracy. Int J Bifurcation Chaos 2003;13:583–608. http://dx.doi.org/10.1142/S0218127403006741.
[36] Gamero E, Freire E, Rodríguez-Luis AJ, Ponce E, Algaba A. Hypernormal form calculation for triple-zero degeneracies. Bull Belg Math Soc Simon Stevin 1999;6:357–68. http://dx.doi.org/10.36045/bbms/1103065855.
[37] Shimizu T, Morioka N. On the bifurcation of a symmetric limit cycle to an asymmetric one in a simple model. Phys Lett A 1980;76:201–4. http://dx.doi.org/10.1016/0375-9601(80)90466-1.
[38] Shil'nikov AL. On bifurcations of the Lorenz attractor in the Shimizu-Morioka model. Physica D 1993;62:338–46. http://dx.doi.org/10.1016/0167-2789(93)90292-9.
[39] Rucklidge AM. Chaos in a low-order model of magnetoconvection. Physica D 1993;62:323–37. http://dx.doi.org/10.1016/0167-2789(93)90291-8.
[40] Liu C, Liu T, Liu L, Liu K. A new chaotic attractor. Chaos Solitons Fractals 2004;22:1031–8. http://dx.doi.org/10.1016/j.chaos.2004.02.060.
[41] Mello LF, Messias M, Braga DC. Bifurcation analysis of a new Lorenz-like chaotic system. Chaos Solitons Fractals 2008;37:1224–55. http://dx.doi.org/10.1016/j.chaos.2007.11.008.
[42] Kokubu H, Roussarie R. Existence of a singulary degenerate heteroclinic cycle in the Lorenz system and its dynamical consequences: Part I. J Dyn Differ Equ 2004;16:513–57. http://dx.doi.org/10.1007/s10884-004-4290-4.

[43] Algaba A, Domínguez-Moreno MC, Merino M, Rodríguez-Luis AJ. A degenerate Takens–Bogdanov bifurcation in a normal form of Lorenz's equations. In: Lacarbonara W, et al., editors. Advances in Nonlinear Dynamics. Proceedings of the Second International Nonlinear Dynamics Conference (NODYCON 2021), vol. 1. Cham: Springer; 2022, p. 699–709. http://dx.doi.org/10.1007/978-3-030-81162-4_60.
[44] Guckenheimer J, Holmes PJ. Nonlinear oscillations, dynamical systems, and bifurcations of vector fields. New York: Springer; 1983, http://dx.doi.org/10.1007/978-1-4612-1140-2.
[45] Wiggins S. Introduction to applied dynamical systems and chaos. New York: Springer; 2003, http://dx.doi.org/10.1007/b97481.
[46] Gamero E, Freire E, Ponce E. Normal forms for planar systems with nilpotent linear part. In: Seydel R, et al., editors. Bifurcation and chaos: analysis, algorithms, applications. International Series of Numerical Mathematics, vol. 97, Basel: Birkhäuser; 1991, p. 123–7. http://dx.doi.org/10.1007/978-3-0348-7004-7_14.
[47] Keener JP. Infinite period bifurcation and global bifurcation branches. SIAM J Appl Math 1981;41:127–44. http://dx.doi.org/10.1137/0141010.
[48] Chow SN, Li C, Wang D. Normal forms and bifurcation of planar vector fields. Cambridge: Cambridge University Press; 1994, http://dx.doi.org/10.1017/CBO9780511665639.
[49] Qin BW, Chung KW, Algaba A, Rodríguez-Luis AJ. High-order approximation of heteroclinic bifurcations in truncated 2D-normal forms for the generic cases of Hopf-zero and non-resonant double Hopf singularities. SIAM J Appl Dynam Syst 2021;20:403–37. http://dx.doi.org/10.1137/0141010.
[50] Algaba A, Chung KW, Qin BW, Rodríguez-Luis AJ. A nonlinear time transformation method to compute all the coefficients for the homoclinic bifurcation in the quadratic Takens–Bogdanov normal form. Nonlinear Dyn 2019;97:979–90. http://dx.doi.org/10.1007/s11071-019-05025-2.
[51] Algaba A, Chung KW, Qin BW, Rodríguez-Luis AJ. Computation of all the coefficients for the global connections in the $\mathbb{Z}_2$-symmetric Takens–Bogdanov normal forms. Commun Nonlinear Sci Numer Simul 2020;81:105012. http://dx.doi.org/10.1016/j.cnsns.2019.105012.
[52] Qin BW, Chung KW, Algaba A, Rodríguez-Luis AJ. High-order analysis of global bifurcations in a codimension-three Takens–Bogdanov singularity in reversible systems. Int J Bifurcation Chaos 2020;30:2050017. http://dx.doi.org/10.1142/S0218127420500170.
[53] Qin BW, Chung KW, Algaba A, Rodríguez-Luis AJ. Analytical approximation of cuspidal loops using a nonlinear time transformation method. Appl Math Comput 2020;373:125042. http://dx.doi.org/10.1016/j.amc.2020.125042.
[54] Qin BW, Chung KW. Personal communication (2019).
[55] Doedel EJ, Champneys AR, Dercole F, Fairgrieve T, Kuznetsov Y, Oldeman BE, Paffenroth R, Sandstede B, Wang X, Zhang C. Auto07-P: Continuation and bifurcation software for ordinary differential equations (with HomCont). Technical report, Concordia University; 2012.
[56] Krupa M, Melbourne I. Asymptotic stability of heteroclinic cycles in systems with symmetry. Ergod Theor Dyn Syst 1995;15:121–47. http://dx.doi.org/10.1017/S0143385700008270.
[57] Krupa M, Melbourne I. Asymptotic stability of heteroclinic cycles in systems with symmetry, II. P Roy Soc Edinb A 2004;134:1177–97. http://dx.doi.org/10.1017/S0308210500003693.
[58] Geng F, Xu Y. Bifurcations of heteroclinic loop accompanied by pitchfork bifurcation. Nonlinear Dyn 2012;70:1645–55. http://dx.doi.org/10.1007/s11071-012-0563-3.
[59] Fernández-Sánchez F, Freire E, Rodríguez-Luis AJ. T-points in a $\mathbb{Z}_2$-symmetric electronic oscillator. (I) Analysis. Nonlinear Dynam 2002;28:53–69. http://dx.doi.org/10.1023/A:1014917324652.
[60] Algaba A, Merino M, García C, Reyes M. Degenerate global bifurcations in a simple circuit. Int J Pure Appl Math 2009;57:265–78.

Capítulo 4

ESTUDIO DE UN SISTEMA CUADRÁTICO 3D SIMPLE CON BIFURCACIONES HOMOCLINAS FLIP.

Capítulo 5

DINÁMICA COMPLEJA EN EL SISTEMA DE LORENZ.

A double-zero bifurcation in a Lorenz-like system

Antonio Algaba · M. Cinta Domínguez-Moreno · Manuel Merino · Alejandro J. Rodríguez-Luis

Abstract The Lorenz system presents a double-zero bifurcation (a double-zero eigenvalue with geometric multiplicity two). However, its study by means of standard techniques is not possible because it occurs for a non-isolated equilibrium. To circumvent this difficulty, we add in the third equation a new term, Dz^2. In this Lorenz-like system, the analysis of the double-zero bifurcation of the equilibrium at the origin guarantees, for certain values of the parameters, the existence of a heteroclinic cycle between the two equilibria located on the z-axis. The numerical continuation in parameter space of the locus of heteroclinic connections allows to detect various degeneracies of codimension two and three, some of which have not been previously studied in the literature. These bifurcations are organizing centers of the complicated dynamics exhibited by this system. Furthermore, studying how the bifurcation sets evolve when D tends to zero, we are able to explain, in the Lorenz system, the origin of several global connections which are related to T-point heteroclinic loops.

Keywords Lorenz-like system · double-zero bifurcation · global connections · Lorenz system

PACS 37C29 · 37G05 · 37G10 · 37G15

1 Introduction

Lorenz system, since its introduction sixty years ago [1], has become an icon in the world of dynamical systems. Although it was derived from a simplified model of convection in the atmosphere, this system appears in the study of a wide variety of problems (see, for instance, [2,3,4,5,6,7,8,9,10]). In spite of the hundreds of papers devoted to studying the complex dynamics that it exhibits (see, for example, [11,12,13,14,15,16, 17,18,19,20,21,22] and references therein) the origin of many of its intricate behaviors is still a long way off.

When a specific system is studied, the combination of analytical and numerical methods is usually useful to shed light on concrete aspects of its dynamics, in some region of the parameter space. For example, the application of this strategy to a 3D modified van der Pol–Duffing oscillator, starting with the study of local bifurcations of equilibria, provides very interesting information about its behavior (see, for instance, [23,24,25,26,27,28,29] and references therein). Regarding global bifurcations, from the pioneering works of

This work has been partially supported by the *Ministerio de Economía y Competitividad* (MTM2017-87915-C2-1-P), by the *Ministerio de Ciencia, Innovación y Universidades* (PGC2018-096265-B-I00, PID2021-123200NB-I00) and by the *Consejería de Economía, Innovación, Ciencia y Empleo de la Junta de Andalucía* (projects FQM-276, TIC-0130, P20_01160 and UHU-1260150).

A. Algaba
Departamento de Ciencias Integradas,
Centro Estudios Avanzados en Física, Matemática y Comp.,
Universidad de Huelva, 21071 Huelva, Spain.
E-mail: algaba@uhu.es, ORCID: 0000-0001-5872-7112

M.C. Domínguez-Moreno
Departamento de Ciencias Integradas,
Centro Estudios Avanzados en Física, Matemática y Comp.,
Universidad de Huelva, 21071 Huelva, Spain.
E-mail: mcinta.dominguez@dmat.uhu.es,
ORCID: 0000-0001-7949-934X

M. Merino
Departamento de Ciencias Integradas,
Centro Estudios Avanzados en Física, Matemática y Comp.,
Universidad de Huelva, 21071 Huelva, Spain.
E-mail: merino@uhu.es, ORCID: 0000-0002-4119-680X

A.J. Rodríguez-Luis (corresponding author)
Departamento de Matemática Aplicada II,
E.T.S. Ingenieros, Universidad de Sevilla,
Camino de los Descubrimientos s/n, 41092 Sevilla, Spain.
E-mail: ajrluis@us.es, ORCID: 0000-0002-9959-0789

Shilnikov it is well known that they can be at the origin of extremely complicated dynamical behavior [30,31]. A simple analytical way to detect global connections is from a Takens–Bogdanov bifurcation (the linearization matrix has a double-zero eigenvalue with geometric multiplicity one) (see, for example, [32,33,34,35,36, 37,38,39,40] and references therein). If the double-zero eigenvalue has geometric multiplicity two (the so-called double-zero bifurcation), a heteroclinic connection may also appear [41,42].

In the case of the Lorenz system, some local bifurcations can be studied by standard techniques (analysis of the linearization around an isolated equilibrium, computation of the reduced system on the center manifold, study of the unfolding of the normal form), as the Hopf and Takens–Bogdanov bifurcations [16,43,44,45]. However, other singularities (double-zero, Hopf-pitchfork and triple-zero) are exhibited by non-isolated equilibria, which makes their study more difficult [46].

To avoid this problem, we are going to introduce a Lorenz-like system, as simple as possible, that presents a double-zero bifurcation in an isolated equilibrium. Specifically, we will add a single term, Dz^2, to the third equation of the Lorenz system. In this way, after analyzing this Lorenz-like system, we will obtain valuable information for the Lorenz system by making D tend to zero (see Fig. 12). Specifically, we will explain how a degenerate heteroclinic connection organizes a family of infinitely many homoclinic orbits previously found in the literature [47, Fig.6], [48, Fig.8(B)], [17, Fig. 3], whose origin was unknown. This family is related to a kind of heteroclinic loop called T-point [11,31,49,50, 51].

This paper is organized as follows. In Sect. 2 we introduce the new Lorenz-like system. Sect. 3 is devoted to the analytical study of the double-zero bifurcation undergone by its equilibrium at the origin (the results obtained are summarized in Theorem 1). The most important outcome is that, in a region of parameter space, the existence of a heteroclinic connection is guaranteed. A detailed numerical analysis, the core of this paper, appears in Sect. 4. The continuation of the heteroclinic orbit emerged from the double-zero bifurcation allows to detect several global bifurcations (homoclinic and heteroclinic connections) of codimension two and three (see Fig. 7) which act as important organizing centers of the dynamics. As far as we know, the theoretical analysis of three of these degenerate global connections has not been performed so far in the literature. Moreover, we find that the curve of heteroclinic connections accumulates on a line segment of saddle-node bifurcations of periodic orbits (see Fig. 3(d)). Unlike similar cases known in the literature, this heteroclinic orbit accumulates on a non-hyperbolic periodic orbit. This is because the heteroclinic connection exists on the other side of the saddle-node curve, that is, in the zone where the periodic orbits do not exist. On the other hand, studying how the bifurcation sets evolve when D tends to zero, we are able to explain, in the Lorenz system, the origin of an infinite sequence of global connections which are related to T-points (see Fig. 12). In this scenario, the three new degenerate global connections mentioned above play a key role. Finally, some conclusions are included in Sect. 5.

2 A Lorenz-like system

The Lorenz system is given by (see [1,52])

$$\begin{aligned} \dot{x} &= \sigma(y-x),\\ \dot{y} &= \rho x - y - xz,\\ \dot{z} &= -bz + xy, \end{aligned} \tag{1}$$

where σ, ρ and b are real parameters. The equilibria are the origin $(0,0,0)$ and a pair of symmetric nontrivial equilibria $\left(\pm\sqrt{b(\rho-1)}, \pm\sqrt{b(\rho-1)}, \rho-1\right)$ when $b(\rho-1)>0$. The Lorenz equations are invariant under the change $(x,y,z)\to(-x,-y,z)$, which implies that the z-axis is invariant (and, therefore, there is a heteroclinic connection between the origin and the equilibria at infinity corresponding to this axis).

The characteristic polynomial of its linearization matrix at the origin is given by $p=\lambda^3+p_1\lambda^2+p_2\lambda+p_3$, with

$$p_1 = b+1+\sigma, \quad p_2 = \sigma(1+b-\rho)+b, \quad p_3 = -b\sigma(\rho-1).$$

The origin exhibits a triple-zero bifurcation when $\sigma=-1$, $\rho=1$ and $b=0$. In the (ρ,b,σ)-parameter space, three curves of codimension-two bifurcations emerge from this point corresponding to Takens–Bogdanov (when $\sigma=-1$, $\rho=1$ and $b\neq 0$), Hopf-pitchfork (if $\sigma=-1$, $b=0$ and $\rho>1$) and double-zero (for $b=0$, $\rho=1$ and $\sigma\neq-1$) singularities of the origin.

Specifically, when the double-zero bifurcation occurs, the linearization matrix has the eigenvalues $\lambda_1=\lambda_2=0$, $\lambda_3=-\sigma-1$. But, for these parameter values, the analysis of the origin cannot be performed because it is not an isolated equilibrium. Also, the corresponding normal form is degenerate (all coefficients of z^k are null). To avoid this, we introduce a new nonlinear term in the third equation,

$$\begin{aligned} \dot{x} &= \sigma(y-x),\\ \dot{y} &= \rho x - y - xz,\\ \dot{z} &= -bz + xy + Dz^2, \end{aligned} \tag{2}$$

where $D \in \mathbb{R}$, so that the Lorenz system (1) is embedded in this one. As we will see in Sect. 4, the use of numerical continuation methods will allow us, reaching $D = 0$, to obtain valuable information on the Lorenz system.

From now on, in our theoretical analysis we will assume that $D \neq 0$. Thus, system (2) can have up to four equilibria, namely

$$E_1 = (0,0,0), \quad E_2 = \left(0,0,\frac{b}{D}\right),$$
$$E_{3,4} = \left(\pm\sqrt{M}, \pm\sqrt{M}, \rho - 1\right),$$
$$\text{with } M = b(\rho-1) - D(\rho-1)^2.$$

Observe that E_2 exists if $D \neq 0$ and $E_{3,4}$ when $M > 0$. Note that, as in the Lorenz system, system (2) is also invariant to the change $(x, y, z) \to (-x, -y, z)$. In this way, the equilibria E_1 and E_2 are always connected by a heteroclinic orbit located on the z-axis.

The origin E_1 exhibits the following local bifurcations (when $D \neq 0$):

(i) A pitchfork bifurcation when $\rho = 1$, $\sigma \neq -1$, $b \neq 0$.
(ii) A transcritical bifurcation of equilibria, involving E_1 and E_2, when $b = 0$, $\rho \neq 1$, $\sigma \neq -1$.
(iii) A Hopf bifurcation if $\sigma = -1$, $\rho > 1$, $b \neq 0$.
(iv) A Takens–Bogdanov bifurcation (a double-zero eigenvalue with geometric multiplicity one) when $\rho = 1$, $\sigma = -1$, $b \neq 0$.
(v) A double-zero bifurcation (a double-zero eigenvalue with geometric multiplicity two) for $\rho = 1$, $b = 0$, $\sigma \neq -1$. In this work, we will analyze this bifurcation.
(vi) A Hopf-transcritical bifurcation when $\sigma = -1$, $b = 0$, $\rho > 1$.
(vii) A degenerate triple-zero bifurcation appears when $b = 0$, $\rho = 1$, $\sigma = -1$.

Remark that the linearization matrix at the origin is the same for systems (1) and (2). The only bifurcation of the origin that appears in system (2) and not in the Lorenz system is the transcritical bifurcation (ii). This causes system (2) to undergo a Hopf-transcritical bifurcation instead of a Hopf-pitchfork as in the Lorenz system.

As can be straightforwardly verified, when $D \neq 0$, system (2) is symmetric to the change

$$(x, y, z, t, \sigma, \rho, b, D) \to \left(x, y, z - \frac{b}{D}, t, \sigma, \rho - \frac{b}{D}, -b, D\right). \tag{3}$$

Consequently, all the results obtained for E_1 can be easily translated for E_2.

3 A double-zero bifurcation at the origin

In this section we analyze the double-zero bifurcation undergone by the origin, E_1. Since this degeneracy occurs when $\rho = 1$, $b = 0$, $\sigma \neq -1$, $D \neq 0$, our local study is valid for ρ and b close to one and zero, respectively.

The bifurcations that appear in system (2) as a consequence of the double-zero singularity are summarized in the following theorem, whose proof is the core of this section. We will focus on the most interesting case, which occurs when limit cycles appear from a Hopf bifurcation. These periodic orbits disappear in a heteroclinic connection. The corresponding bifurcation sets are drawn in Fig. 1.

Theorem 1 *The equilibrium E_1 of system (2) undergoes a double-zero bifurcation* **DZ** *if $\rho = 1$, $b = 0$, $\sigma \neq -1$, $D \neq 0$. In a vicinity of this singularity, there are only limit cycles when $D > 0$ and $\sigma \in (-\infty, -1) \cup (0, +\infty)$. In this situation, the following bifurcations appear (see Fig. 1):*

1. *A transcritical bifurcation* **T**, *when $b = 0$. It involves the equilibria E_1 and E_2.*
2. *Two pitchfork bifurcations,* $\mathbf{P^1}$ *for $\rho = 1$ (concerning E_1 and $E_{3,4}$) and* $\mathbf{P^2}$ *when $b = D(\rho-1)+\mathcal{O}(\rho^2)$ (involving E_2 and $E_{3,4}$).*
3. *A Hopf bifurcation* **h** *of the equilibria $E_{3,4}$, when $b = 2D(\rho-1)$, $\sigma \neq 1/3$. This bifurcation is supercritical if $\sigma > 1/3$ whereas it is subcritical when $\sigma < 1/3$.*
4. *A heteroclinic cycle connecting E_1 and E_2, for*

$$\rho - 1 = \frac{1}{2D}\, b + \frac{\sigma(3\sigma-1)}{8D^2(\sigma+1)^2(3\sigma+2D(\sigma+1))}\, b^2 + \mathcal{O}(b^3), \tag{4}$$

when $\sigma \neq 1/3$. The global connection is attractive if $\sigma > 1/3$ and repulsive when $\sigma < 1/3$. The loop is formed by two heteroclinic connections: one is placed on the invariant z-axis (which exists for any value of the parameters and is therefore of zero codimension) and the other one is placed outside this axis (it is structurally unstable).

When the conditions $D > 0$ and $\sigma \in (-\infty, -1) \cup (0, +\infty)$ are not fulfilled, only local bifurcations of equilibria (transcritical and pitchfork) are present.

In the analysis of the double-zero bifurcation undergone by E_1 in system (2) (this codimension-two bifurcation occurs when $\rho = 1$, $b = 0$, $\sigma \neq -1$, $D \neq 0$), we first perform the change

$$x = Y - \sigma Z, \quad y = Y + Z, \quad z = X,$$

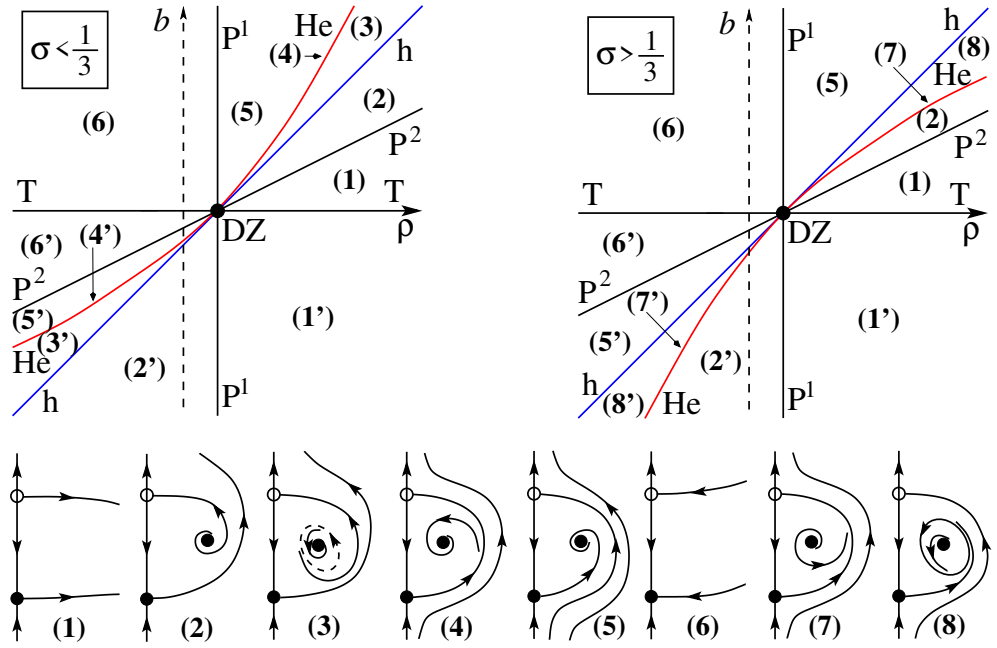

Fig. 1 Bifurcation set of system (2) in a neighborhood of the double-zero bifurcation **DZ** exhibited by the equilibrium E_1, for $D > 0$, when $\sigma < 1/3$ (left) and $\sigma > 1/3$ (right). The curves, according to Theorem 1, correspond to the following bifurcations: **T**, transcritical; **P1** and **P2**, pitchfork; **h**, Hopf of $E_{3,4}$ (supercritical when $\sigma > 1/3$ and subcritical if $\sigma < 1/3$); **He**, heteroclinic loop between E_1 and E_2 (attractive if $\sigma > 1/3$ and repulsive when $\sigma < 1/3$). The phase portraits, in the $(r, \bar{z})$-plane, are for system (11). On the $\bar{z}$-axis, the filled circle represents the equilibrium of (11) that corresponds to equilibrium E_1 in system (2) and the empty circle is used for the equilibrium that corresponds to E_2. For $b < 0$, to obtain the phase portrait in region (i'), it is enough to interchange the two equilibria on the z-axis in the phase portrait of region (i).

which converts system (2), for $b \approx 0$ and $\rho \approx 1$, to

$$\begin{aligned}
\dot{X} &= -bX + (1-\sigma)YZ + DX^2 + Y^2 - \sigma Z^2, \\
\dot{Y} &= \sigma^2(1-\rho)\Delta Z + \sigma(\rho-1)\Delta Y - \sigma\Delta XY + \sigma^2\Delta XZ, \\
\dot{Z} &= (\rho-1)\Delta Y - \big(1+\sigma(\sigma+\rho)\Delta\big)Z - \Delta XY + \sigma\Delta XZ,
\end{aligned} \tag{5}$$

with $\Delta = \dfrac{1}{\sigma+1}$, $\sigma \neq -1$. Next, considering the center manifold to second order, $Z = -\Delta^2 XY + \cdots$, we obtain the reduced system

$$\begin{aligned}
\dot{X} &= -bX + DX^2 + Y^2 + \cdots, \\
\dot{Y} &= \sigma(\rho-1)\Delta Y + \sigma\Delta\big(-1 + (\rho-1)\sigma\Delta^2\big)XY + \cdots.
\end{aligned} \tag{6}$$

If we truncate this system to second order, the change $x = Y$, $y = X$ leads to

$$\begin{aligned}
\dot{x} &= \sigma(\rho-1)\Delta x + \sigma\Delta\big(-1 + (\rho-1)\sigma\Delta^2\big)xy, \\
\dot{y} &= -by + x^2 + Dy^2.
\end{aligned} \tag{7}$$

Now, by means of the change

$$x \to \frac{1}{\sqrt{|D|}}\,x, \quad y \to \frac{-1}{D}\,y + \frac{b}{2D}, \quad D \neq 0,$$

we obtain

$$\begin{aligned}
\dot{x} &= \mu_1 x + axy, \\
\dot{y} &= \mu_2 - sgn(D)x^2 - y^2,
\end{aligned} \tag{8}$$

with

$$\begin{aligned}
\mu_1 &= \frac{\sigma\Delta}{2D}\big(2D(\rho-1) - b + b(\rho-1)\sigma\Delta^2\big), \\
\mu_2 &= \frac{b^2}{4}, \qquad a = \frac{\sigma\Delta}{D}\big(1 + (1-\rho)\sigma\Delta^2\big).
\end{aligned} \tag{9}$$

Due to its importance in determining the behavior of the system (8), we need to study the sign of a in the vicinity of $\rho = 1$ and $b = 0$. If $D > 0$ and $\sigma \in (-\infty, -1) \cup (0, +\infty)$ or if $D < 0$ and $\sigma \in (-1, 0)$, then $a > 0$. Alternatively, when $D > 0$ and $\sigma \in (-1, 0)$ or when $D < 0$ and $\sigma \in (-\infty, -1) \cup (0, +\infty)$, we have $a < 0$.

System (8) can be analyzed using the study of the Hopf-saddle-node bifurcation carried out in [32, Sect. 4]. Thus, comparing system (8) with [32, Eq. (7.4.9)], we can obtain the bifurcations exhibited by (8). Consequently, we deduce that system (8) is in case III [32, Sect. 4] when $D > 0$ and $\sigma \in (-\infty, -1) \cup (0, +\infty)$. It is in cases IIa-IIb, when $D < 0$ and $\sigma \in (-\infty, -1) \cup (0, +\infty)$. However, as $\mu_2 = b^2/4 > 0$, there is no Hopf bifurcation (because, in cases IIa-IIb, it only exists when $\mu_2 < 0$) and only transcritical and pitchfork bifurcations of equilibria appear. Note that the trivial cases I and IV (IVa-IVb), where only equilibria exist (as there are no periodic orbits, there are no global connections either), appear when $D < 0$ and $\sigma \in (-1, 0)$ and when $D > 0$ and $\sigma \in (-1, 0)$, respectively.

In what follows we will focus on the case where the most interesting dynamics appears, that is, when there are periodic orbits (if $D>0$ and $\sigma\in(-\infty,-1)\cup(0,+\infty)$). Thus, system (8) can have up to four equilibria,

$$\left(0,\pm\frac{b}{2}\right),\quad \left(\pm\sqrt{N+\mathcal{O}(|b,\rho-1|^3)},-D(\rho-1)+\frac{b}{2}\right),$$

where $N=D(\rho-1)\left(b-D(\rho-1)\right)$, which must be positive for these latter equilibria to exist.

Note that E_1 corresponds to the equilibrium $(0,-b/2)$ and E_2 to $(0,b/2)$.

From the study carried out in [32, Sect.7.4] we can deduce that the following local bifurcations are present (see Fig. 1):

- A transcritical bifurcation **T**, involving E_1 and E_2, for $b=0$.
- Two pitchfork bifurcations, $\mathbf{P^1}$ for $\rho=1$ and $\mathbf{P^2}$ if $b=D(\rho-1)+\mathcal{O}(\rho^2)$.
- A Hopf bifurcation **h** of the equilibria $E_{3,4}$ when $2D(\rho-1)=b$.

As explained in [32, Sect.7.4], the second-order terms included in system (8) allow neither the study of the Hopf bifurcation nor that of the heteroclinic connection. This is because the system is integrable for the values of the parameters where the two bifurcations occur: a continuum of periodic orbits bounded by a heteroclinic loop appears (see [32, Fig. 7.4.9] for the easiest case $a=2$). Therefore, to complete the analysis it is necessary to also include the third-order terms.

Hence, the reduced system of (5) on to the center manifold up to third order, $Z=\Delta^2 Y\left(-X+\Delta(D-2\sigma\Delta)X^2+\Delta Y^2\right)+\cdots$, is

$$\begin{aligned}\dot X &= -bX+DX^2+Y^2+(\sigma-1)\Delta^2XY^2,\\ \dot Y &= \sigma(\rho-1)\Delta Y+\sigma\Delta\big(-1+(\rho-1)\sigma\Delta^2\big)XY\\ &\quad -\sigma^2\Delta^3\big(\Delta(\rho-1)(-2\Delta\sigma+D)+1\big)X^2Y\\ &\quad -\sigma^2\Delta^4(\rho-1)Y^3.\end{aligned}\tag{10}$$

The change

$$X=\frac{-1}{D}\bar z+\frac{b}{2D},\quad Y=\frac{2}{\sqrt{2D+(\sigma-1)\Delta^2 b}}\,r,$$

transforms (10) into

$$\begin{aligned}\dot r &= \tilde\mu_1 r+\tilde a\, r\bar z+\tilde c\, r^3+\tilde d\, r\bar z^2,\\ \dot{\bar z} &= \tilde\mu_2-r^2-\bar z^2+\tilde e\, r^2\bar z,\end{aligned}\tag{11}$$

where

$$\begin{aligned}\tilde\mu_1 &= \sigma\Delta(\rho-1)-\frac{\sigma\Delta}{2D}b+\frac{\sigma^2\Delta^3}{2D}b(\rho-1)-\frac{\sigma^2\Delta^3}{4D^2}b^2\\ &\quad +\mathcal{O}(|b,\rho-1|^3),\\ \tilde\mu_2 &= \frac{b^2}{4}+\mathcal{O}(|b,\rho-1|^3),\quad \tilde a=\frac{\sigma\Delta}{D}+\mathcal{O}(|b,\rho-1|),\\ \tilde c &= \mathcal{O}(|b,\rho-1|),\quad \tilde d=\frac{-\sigma^2\Delta^3}{D^2}+\mathcal{O}(|b,\rho-1|),\\ \tilde e &= \frac{(\sigma-1)\Delta^2}{D}+\mathcal{O}(|b,\rho-1|).\end{aligned}$$

Finally, through the change of coordinates,

$$s=r(1+g\bar z),\quad w=\bar z+hr^2+i\bar z^2,\quad \tau=(1+j\bar z)^{-1}t,$$

where we choose

$$\begin{aligned}g &= \tilde c-\tilde a h,\quad i=\frac{\tilde a\tilde e+\tilde d-\tilde c+3\tilde a h+2\tilde a\tilde c}{3\tilde a},\\ j &= \frac{\tilde a\tilde e-2\tilde d+2\tilde c+2\tilde a\tilde c}{3\tilde a},\quad h\in\mathbb{R},\end{aligned}$$

system (11) becomes

$$\begin{aligned}\frac{ds}{d\tau} &= \hat\mu_1 s+\hat a sw,\\ \frac{dw}{d\tau} &= \hat\mu_2-s^2-w^2+\hat f w^3,\end{aligned}\tag{12}$$

where

$$\begin{aligned}\hat\mu_1 &= \tilde\mu_1+\mathcal{O}(|b,\rho-1|^3),\quad \hat\mu_2=\tilde\mu_2+\mathcal{O}(|b,\rho-1|^3),\\ \hat a &= \tilde a+(|b,\rho-1|),\quad \hat f=\frac{\Delta^2(1-3\sigma)}{3D}+\mathcal{O}(|b,\rho-1|).\end{aligned}$$

Thus, in system (12), we can analyze both the Hopf bifurcation and the heteroclinic connection.

Regarding the Hopf bifurcation, a standard analysis provides the first Lyapunov coefficient

$$a_1=\frac{3\hat f}{8\eta},\quad \text{where}\quad \eta=\frac{\sqrt{2(\hat\mu_2\hat a^3-\hat\mu_1^2\hat a-\hat f\hat\mu_1^3)}}{|\hat a|}.$$

If $a_1<0$ the Hopf bifurcation is supercritical whereas it is subcritical when $a_1>0$. Consequently, the bifurcation is supercritical if $\hat f<0$, i.e, if $\sigma>1/3$ and it is subcritical when $\sigma<1/3$. The Hopf bifurcation is degenerate when $\sigma=1/3$ (since $a_1=0$), this occurs at the point $(\rho,b,\sigma)=(\rho,2D(\rho-1),1/3)$.

As far as the heteroclinic connection is concerned, its existence is ensured by Melnikov's method if $\hat f\neq 0$, which occurs when $\sigma\neq 1/3$. The curve of these global connections is estimated by [53,54,55] (only if $\hat a=2$ a Hamiltonian case appears [32])

$$\hat\mu_1=\frac{-3\hat a^2\hat f}{2(3\hat a+2)}\hat\mu_2+\mathcal{O}(\hat\mu_2^2),$$

which according to the original parameters is

$$\rho - 1 = \frac{1}{2D}\, b + \frac{\sigma \Delta^3 (3\sigma - 1)}{8D^2(3\Delta\sigma + 2D)}\, b^2 + \mathcal{O}(b^3)$$
$$= \frac{1}{2D}\, b + \frac{\sigma(3\sigma - 1)}{8D^2(\sigma + 1)^2(3\sigma + 2D(\sigma + 1))}\, b^2 + \mathcal{O}(b^3).$$

In this way we have already proved all the statements of Theorem 1.

We end this section noting that, when $\rho = 1$, $b = 0$, $\sigma = 1/3$, $D \neq 0$, system (2) exhibits a degenerate double-zero bifurcation **DDZ** (because $\hat{f} = 0$ when $\sigma = 1/3$). Although its analysis is not complicated, we have not included it here for brevity. To perform it (i.e., to determine the character of the Hopf bifurcation and of the heteroclinic connection), it would be necessary to compute the reduced system of (5) up to fifth order on the center manifold (see similar computations in [41, Sect. 3.1]). From this point **DDZ** in the three-parameter space, two curves **Dh** and **DHe** emerge, corresponding to a degenerate Hopf bifurcation **Dh** and to degenerate heteroclinic connections **DHe** (see Fig. 7). Remark that, when $b = 0$ and $\sigma = 1/3$, Lorenz system has an invariant algebraic surface [15].

4 Numerical study

Based on the above theoretical analysis, we are going to perform a numerical study with the continuation code AUTO [56]. We will "extend" the bifurcation sets from the vicinity of the double-zero bifurcation **DZ** of the equilibrium $E_1 = (0, 0, 0)$, that occurs when $(\rho, b) = (1, 0)$ and $\sigma \neq -1$, $D \neq 0$. We are going to focus on the case of greatest dynamical richness, that is, when curves of Hopf bifurcation **h** and of heteroclinic connections **He** emerge from the point **DZ** (see Fig. 1). This happens if $D > 0$ and $\sigma \in (-\infty, -1) \cup (0, +\infty)$.

We divide this analysis in two parts. In Sect. 4.1, our objective will be to study the degeneracy of the double-zero bifurcation **DDZ** which, according to the previous analytical study of Sect. 3, appears when $\sigma = 1/3$. To do this we will fix $D = 0.1$ and then we will take slices $\sigma = constant$ in the (ρ, b, σ)-parameter space, in the vicinity of the point **DDZ** located at $(1, 0, 1/3)$. This will allow us to find several degenerate heteroclinic bifurcations, of codimension two and three (see Fig. 7).

In the second part, in Sect. 4.2, we are going to obtain information about the Lorenz system, by making D tend to zero (see Fig. 12). Specifically, we will explain how some degenerate global connections organize the family of homoclinic orbits previously found in the literature (see [47, Fig. 6], [48, Fig. 8(B)], [17, Fig. 3]), whose origin was unknown.

4.1 Degenerate double-zero

According to the previous analytical study of Sect. 3 there is a degeneracy of the double-zero bifurcation **DZ** when $\sigma = 1/3$. So first we fix $\sigma = 0.3$ and, in order to numerically obtain the bifurcation curves arising from the **DZ** bifurcation point, we are going to draw several bifurcation diagrams (note that, for $\sigma = 0.3$, we must obtain the left bifurcation set of Fig. 1).

First, we set $b = 0.2$ and continue in the parameter ρ the equilibrium E_3. It undergoes a Hopf bifurcation that we will denote by **h**, for $\rho \approx 2.1940452$. The bifurcation diagram corresponding to the saddle periodic orbit, which arises to the left of **h** for $b = 0.2$, appears in Fig. 2(a). As can be seen, this periodic orbit does not experience any bifurcation before ending, for $\rho \approx 2.1907764$, in a heteroclinic cycle between the equilibria $E_1 = (0, 0, 0)$ and $E_2 = (0, 0, 2)$, which we denote by **He**. This cycle is formed by two heteroclinic connections (see Fig. 2(a)), the one located on the z-axis (which exists for any value of the parameters) and the other one is structurally unstable (and it is located outside the z-axis).

We point out that, in order not to overcomplicate the notation of this work, although a heteroclinic bifurcation (in parameter space) and a heteroclinic cycle (in phase space) are two different objects, we are going to denote them with the same label, **He**. Furthermore, if we have to indicate which equilibrium is involved in a particular bifurcation, we will do so by using a superscript (as we did, for example, with the pitchfork bifurcations $\mathbf{P^1}$ and $\mathbf{P^2}$ in Theorem 1).

When $b = 0.3$ (see Fig. 2(b)), a stable periodic orbit arises from the Hopf bifurcation **h** ($\rho \approx 2.9069632$) to the right. Subsequently, for $\rho \approx 2.9072735$, it undergoes a saddle-node bifurcation of periodic orbits **sn** when it collapses with a saddle periodic orbit which finally disappears in a heteroclinic cycle for $\rho \approx 2.9068041$. Finally, in Fig. 2(c), for $b = -0.2$, we show the bifurcation diagram corresponding to the saddle periodic orbit, which arises to the left of **h**. As in the case $b = 0.2$ this periodic orbit does not experience any bifurcation before ending in a heteroclinic cycle between $E_2 = (0, 0, -2)$ and $E_1 = (0, 0, 0)$, for $\rho \approx 0.1907764$. Its projection onto the (x, z)-plane also appears in Fig. 2(c). We note that the results obtained for $b = -0.2$ were expected due to the symmetry that system (2) has: when passing through $b = 0$ the equilibria E_1 and E_2 undergo the transcritical bifurcation T, and consequently the above diagram can be easily obtained by applying the change of variables (3).

Now we can numerically compute in the (ρ, b)-plane the bifurcation curves detected in the diagrams of Fig.

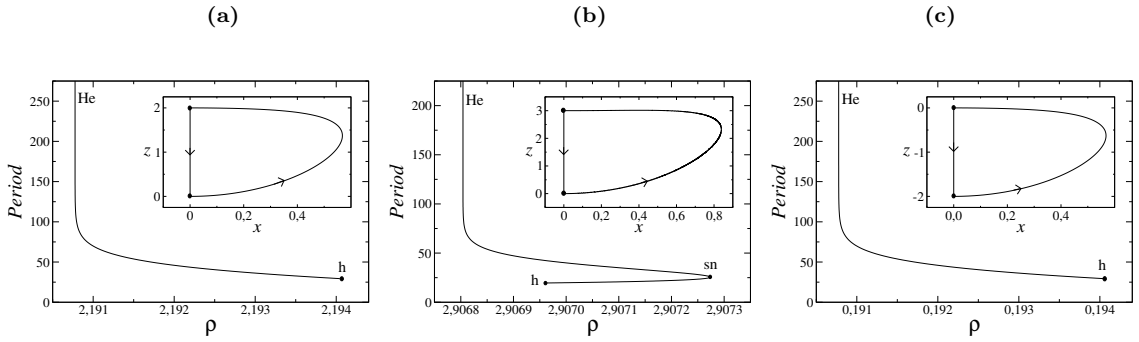

Fig. 2 For $\sigma = 0.3$ and $D = 0.1$, bifurcation diagram of the asymmetric periodic orbit born in the bifurcation Hopf **h** of the equilibrium E_3 for: (a) $b = 0.2$. (b) $b = 0.3$. (c) $b = -0.2$. In the inset of panels (a), (b) and (c), projection onto the (x, z)-plane of the heteroclinic cycle **He** connecting the origin E_1 and E_2, that exist for $\rho \approx 2.1907764$, $\rho \approx 2.9068041$ and $\rho \approx 0.1907764$ respectively.

2 for $\sigma = 0.3$. Thus, in Fig. 3(a) we have drawn the three straight lines that intersect at the double-zero bifurcation point **DZ**, namely $\mathbf{P^1}$, pitchfork bifurcation of E_1 for $\rho = 1$, $\mathbf{P^2}$, pitchfork bifurcation of E_2 for $b = 0.1(\rho - 1)$ and **T**, transcritical bifurcation between E_1 and E_2 for $b = 0$. We also see the curves **h** and **He** corresponding, respectively, to Hopf bifurcations of the equilibria $E_{3,4}$ and to heteroclinic connections between the equilibria E_1 and E_2. In particular, the Hopf bifurcation curve **h** is given by:

$$\begin{aligned}
&[2D(\rho-1) - b - \sigma - 1]\,[b(\rho+\sigma) - 2D(\rho-1)\sigma \\
&\qquad + D(1-\rho^2)] + 2(b - D(\rho-1))\,(\rho-1)\sigma = 0, \\
&2D(\rho-1) - b - \sigma - 1 \neq 0, \\
&b(\rho+\sigma) - 2D(\rho-1)\sigma + D(1-\rho^2) > 0. \qquad (13)
\end{aligned}$$

Note that when $D = 0$, (13) coincides with the expression for the curve of the Hopf bifurcation of the nontrivial equilibria in the Lorenz system [44, Sect. 3.1].

Let us remember that due to the symmetry that system (2) presents, we can easily obtain the third quadrant of the bifurcation set by applying the change of variables (3) to each of the curves of the first quadrant. For this reason, in what follows, we will only focus on the first quadrant.

To analyze some of the degeneracies that may exist on the curve **He** in the first quadrant of the parameter plane (ρ, b), we will denote by λ_1, λ_2, λ_3 the eigenvalues of the Jacobian matrix at $E_1 = (0, 0, 0)$ and λ_1^*, λ_2^*, λ_3^* the eigenvalues of the Jacobian matrix at $E_2 = (0, 0, b/D)$, where

$$\lambda_{1,2} = \frac{-(1+\sigma) \pm \sqrt{(1-\sigma)^2 + 4\sigma\rho}}{2}, \qquad \lambda_3 = -b,$$

and

$$\lambda_{1,2}^* = \frac{-(1+\sigma) \pm \sqrt{(1-\sigma)^2 + 4\sigma(\rho - b/D)}}{2}, \quad \lambda_3^* = b.$$

Note that in the first quadrant of the parameter plane $\lambda_2 < \lambda_3 < 0 < \lambda_1$ and $Re(\lambda_2^*) \leq Re(\lambda_1^*) < 0 < \lambda_3^*$. In this case, the saddle quantities are given by $\delta_1 = \left|\frac{\lambda_3}{\lambda_1}\right|$ and $\delta_2 = \left|\frac{Re(\lambda_1^*)}{\lambda_3^*}\right|$. The saddle quantity corresponding to the heteroclinic cycle is given by the product $\delta_1\delta_2 \equiv \delta_{12}$ (when $\delta_{12} = 1$ the heteroclinic cycle is degenerate [32]). Moreover, in a neighborhood of the point $\mathbf{DZ} = (1, 0)$ in the first quadrant, the eigenvalues of E_2 are real, consequently $\delta_2 = \left|\frac{\lambda_1^*}{\lambda_3^*}\right|$. Therefore, the curve where the product $\delta_1\delta_2 \equiv \delta_{12} = 1$ satisfies the equation

$$b = \frac{(1+\sigma)D\left[-(1+\sigma) + \sqrt{(1+\sigma)^2 - 4\sigma(1-\rho)}\right]}{\sigma}. \qquad (14)$$

Initially the Hopf bifurcation curve **h** arises from the point **DZ** to the right of the heteroclinic connection curve **He**, being subcritical (see Theorem 1). As can be seen in Fig. 3(a), on the curve **h** there is a degeneracy of codimension two at the point **Dh**, that occurs when $(\rho, b) \approx (2.7093960, 0.2730477)$, where the first Lyapunov coefficient a_1 vanishes. From this point **Dh** a saddle-node bifurcation curve of periodic orbits **sn** arises (this curve is drawn in the inset of Fig. 3(a)). It ends in another degeneracy **DHe**, for $(\rho, b) \approx (3.1169844, 0.3279419)$, located on the curve of heteroclinic connections **He**, where it is verified that $\delta_{12} = 1$. We remark that the curves **h** and **He** intersect at the point $(\rho, b) \approx (2.925824, 0.302549)$ and they change their relative position (this change can be seen better in Fig. 3(c)). At the points of the curve **He** between the degeneracies **DZ** and **DHe** it is true that $\delta_{12} < 1$ and, in accordance with the bifurcation diagrams in Fig. 2, a saddle periodic orbit arises from the heteroclinic cycle. Next, on the curve **He** a new degeneracy $\mathbf{DHe^2}$ appears for $(\rho, b) \approx (3.9754280, 0.43837613)$, where $\lambda_1^* = \lambda_2^* = -0.65$ and, as a consequence, in the remaining points the equilibrium E_2 changes its configuration, becoming a saddle-focus since both eigenvalues are now complex.

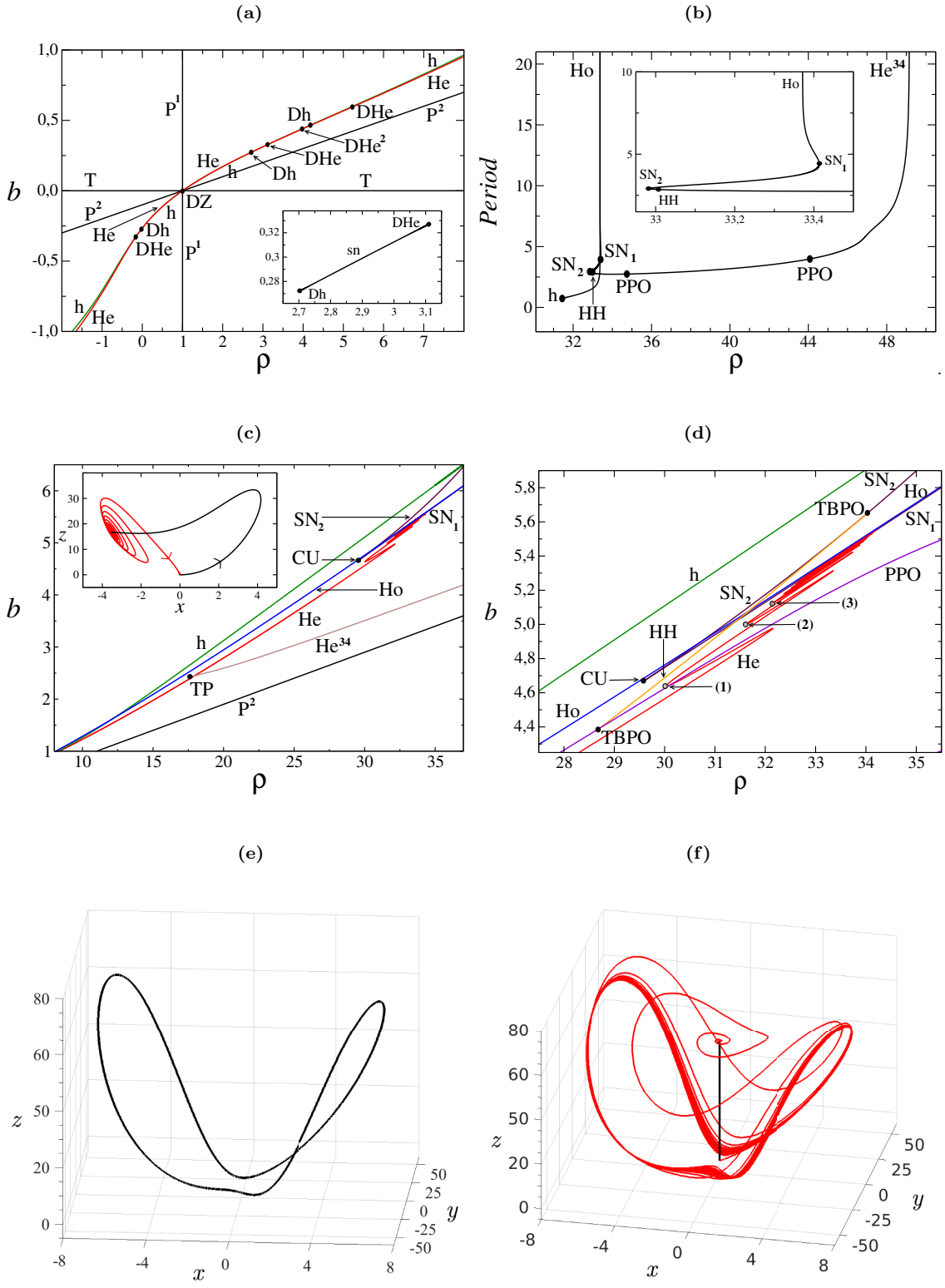

Fig. 3 For $\sigma = 0.3$, $D = 0.1$: (a) Partial bifurcation set in a neighborhood of the double-zero point **DZ**. (b) Bifurcation diagram for $b = 5.4$. (c) Partial bifurcation set in the first quadrant, in a range outside the panel (a). The projection on the (x, z)-plane of the T-point **TP** is drawn in the inset. (d) Zoom of panel (c) near the accumulation process of **He**. For $b = 5.4$ phase portrait in panel (d) corresponding to: (e) a degenerate symmetric periodic orbit, placed on the curve $\mathbf{SN_1}$, for $\rho \approx 33.413688$; (f) the heteroclinic cycle on **He**, for $\rho \approx 33.414582$ (the black line corresponds to the connection placed on the invariant z-axis).

Note that we use superscripts to indicate on the curve **He** which of the two equilibria (E_1 or E_2) experiences a certain degeneration. The previous change implies that, in the range of Fig. 3(a) in the first quadrant, the expression of the curve where $\delta_{12} = 1$ is now

$$\rho = \frac{3 + 10\sigma + 3\sigma^2}{4\sigma}, \tag{15}$$

instead of Eq. (14). As we can see, this expression does not depend on b, since now $\delta_2 = \left|\frac{Re(\lambda_1^*)}{\lambda_3^*}\right|$. Note that in the range of Fig. 3(a), on the curve **h** there is another degenerate point **Dh**, for $(\rho, b) \approx (4.17986, 0.466067)$, where $a_1 = 0$. As we will see later in Fig. 7, this second **Dh** point is not involved in the degeneracy **DDZ** of the double-zero bifurcation. The fold of the curve **Dh** with respect to σ explains its existence when $\sigma = 0.3$.

From our numerical study we deduce that the dynamics around the point $\mathbf{DHe^2}$ is very complex (this bifurcation will be considered in more detail in Sect. 4.2). Thus, we conjecture the existence of an infinite sequence of bifurcation curves of various types that emanate from this point: saddle-nodes of asymmetric and symmetric periodic orbits, period-doublings of the asymmetric periodic orbits, symmetry-breakings of the symmetric periodic orbits, homoclinic connections of the origin..., which implies the existence of diverse types of attractors in a neighborhood of the origin (see [41, Fig. 8]). In Fig. 3(c) we have included one of them, **Ho** (blue color), the first curve of the sequence of homoclinic connections of the origin that arise from the point $\mathbf{DHe^2}$. This interesting point that, as far as we know, has not been studied in the literature, will deserve to be analyzed theoretically in the future. In this work we restrict ourselves to studying some of the bifurcations that it organizes in system (2) and that will give us information about the Lorenz system (see Sect. 4.2).

Once we have numerically found all the bifurcation curves whose existence is guaranteed by the analysis of the double-zero degeneracy, we are going to study in more depth the behavior of the heteroclinic curve **He** as we move away from the point **DZ**. For this task we are going to detect new bifurcations by considering the diagram of Fig. 3(b), for $b = 5.4$. We see that now the pair of asymmetric attractive periodic orbits, that arises from the Hopf bifurcation **h**, ends at a homoclinic connection of the origin, **Ho**. Moreover, the symmetric attractive periodic orbit that also arises from **Ho** ends in a heteroclinic connection between the equilibria $E_{3,4}$, $\mathbf{He^{34}}$. As observed in the bifurcation diagram, the symmetric periodic orbit exhibits several bifurcations, namely: two saddle-node bifurcations, $\mathbf{SN_1}$ and $\mathbf{SN_2}$, a torus bifurcation **HH** and two symmetry-breaking bifurcations, **PPO**.

We are now in a position to see that the heteroclinic curve **He** ends in an interesting accumulation process. In Fig. 3(c) we have drawn a partial bifurcation set, in the first quadrant, at another range of values furthest from **DZ**. In addition to the curves $\mathbf{P^2}$, **h** and **He**, we can see two curves of saddle-node bifurcation of symmetric periodic orbits, $\mathbf{SN_1}$ and $\mathbf{SN_2}$. Both curves collapse at the cusp point **CU**, when $(\rho, b) \approx (29.57655304, 4.6665097)$. The curve **Ho** (of homoclinic connections of the origin) is located to the left of $\mathbf{SN_1}$ in the range of this figure. We observe that the curve **He** experiences a sequence of oscillations, each time closer to each other, which accumulates to the curve $\mathbf{SN_1}$. In this figure we have also included the curve of heteroclinic connections $\mathbf{He^{34}}$ between the equilibria $E_{3,4}$ (brown color), which arises from the point **TP**, for $(\rho, b) \approx (17.7017834, 2.4215793)$, where a heteroclinic cycle, called (principal) T-point, exists. The projection onto the (x, z)-plane of the T-point **TP** heteroclinic loop is drawn in the inset of Fig. 3(c), where the black line corresponds to the intersection between the one-dimensional manifolds of the equilibria E_1 and E_4 and the red one to the intersection between the two-dimensional manifolds. This codimension-two bifurcation organizes three curves of global connections corresponding to homoclinic orbits of the origin and to homoclinic and heteroclinic orbits of the equilibria $E_{3,4}$ [11,17,31]. We note that the curve $\mathbf{SN_1}$ is related to a degeneracy that appears, outside the range of Fig. 3(c), on the curve $\mathbf{He^{34}}$.

In the zoom shown in Fig. 3(d) we can observe better that the curve **He** accumulates on a line segment on $\mathbf{SN_1}$. As a consequence, the heteroclinic orbit itself accumulates on the corresponding non-hyperbolic periodic orbit placed on $\mathbf{SN_1}$, as can be seen in Figs. 3(e) and 3(f) when $b = 5.4$. We have drawn, respectively, the phase portraits of the degenerate symmetric periodic orbit that exists when $\rho \approx 33.413688$ on the curve $\mathbf{SN_1}$ and of the heteroclinic orbit on the curve **He** for $\rho \approx 33.414582$ (in this accumulation process, the heteroclinic orbit performs more and more windings around the non-hyperbolic periodic orbit). On the other hand, in Fig. 3(d) we have also drawn the curves of the other bifurcations present in the diagram of Fig. 3(b). Thus, the torus bifurcation **HH** exists between the curves $\mathbf{SN_2}$ and **PPO**. The endpoints of **HH** correspond to Takens–Bogdanov bifurcations of periodic orbits **TBPO** (double +1 Floquet multiplier with geometric multiplicity one). Examples of this situation can be found for the Lorenz system in [20,45]. Although in this work we do not focus on them, it should be noted

that the cascades of period-doubling bifurcations, exhibited by the asymmetric periodic orbits emerged from the symmetry-breaking bifurcations **PPO**, give rise to a sequence of Takens–Bogdanov bifurcations of periodic orbits (with double -1 Floquet multiplier). The complex dynamics present in this scenario is illustrated, for instance, in the figures of the works [20,45].

A similar accumulation process, but relative to a curve of homoclinic connections, has been found in [57] where a curve of homoclinic orbits accumulates on a segment in parameter space while the homoclinic orbit itself approaches a saddle periodic orbit. A theoretical study of this type of behavior has been carried out in [58]. It is interesting to note the following fact. Although in our case there is no saddle periodic orbit in the region where the curve ends up accumulating over a segment of $\mathbf{SN_1}$ (the saddle periodic orbit exists in the region between the curves $\mathbf{SN_1}$ and $\mathbf{SN_2}$), however, the heteroclinic orbit behaves in a similar way to the homoclinic orbit studied in [57,58]. Let us discuss those details.

In the accumulation process of the curve **He**, the maxima and the minima (with respect to ρ) converge to separate points on $\mathbf{SN_1}$ (that limit the accumulation segment of **He**). To understand the evolution of the heteroclinic orbit along the curve **He** we are going to look at how it changes in the first minima, marked as (**1**), (**2**) and (**3**) in Fig. 3(d). In Figs. 4(a) and 4(c) we have drawn, for $\sigma = 0.3$, the projections on the (x, z)-plane of the heteroclinic orbits labelled (**1**) and (**3**), placed respectively at $(\rho, b) \approx (30.0154396, 4.6367200)$ and $(\rho, b) \approx (32.1468879, 5.1240339)$. Their temporal profiles t-z appear in Figs. 4(b) and 4(d). As can be seen in these figures (similarly as it occurs in [57, Fig. 10] with the homoclinic orbits), if we start from the heteroclinic orbit (**1**), to go around each of the non-trivial equilibria $E_{3,4}$ (black bullets) one more time, we have to go to the point (**3**) of the curve **He**, that is, go through two oscillations on such a curve. We note that the projection onto the (x, z)-plane of the heteroclinic orbit corresponding to the point (**2**), placed at $(\rho, b) \approx (31.6099774, 4.9976719)$, surrounds equilibrium E_3 twice and equilibrium E_4 only one time.

In [57, Table 1] (inspired by the results of the theoretical analysis carried out in [58]) the authors build a table to check if consecutive maxima (or minima) of the homoclinic curve converge to their limit with a rate given by the stable eigenvalue of the saddle-periodic orbit to which the homoclinic orbit approaches. Their table contains data of the distances dist(i) between the ith and the $(i-1)$st maximum of the homoclinic curve. The numbers dist(i) were determined as the Euclidean distances between fold points (LP) detected by AUTO/HomCont during continuation of the homoclinic curve. It seems that the ratios converge (within numerical accuracy) to the stable Floquet multiplier. In our case, as the periodic orbit to which the heteroclinic orbit approaches is non-hyperbolic (it is on the curve $\mathbf{SN_1}$), we want to check if the ratios of the distances converge to the Floquet multiplier 1. We consider the minima (with respect to ρ) of Fig. 3(d), where the point labelled (**1**) is the first minimum ($i = 1$). The results appear in Table 1 and, according to them, it is plausible that the ratios converge to 1.

Table 1 For $\sigma = 0.3$ and $D = 0.1$, distances dist(i) between the $(i+1)$th and the ith minimum of the curve **He** and their ratios, dist(i)/dist$(i-1)$. The point labelled (**1**) in Fig. 3(d) is the first minimum. It seems that the ratio approaches the Floquet multiplier +1 of the non-hyperbolic periodic orbit on which the heteroclinic orbit accumulates.

i	dist(i)	dist(i)/dist$(i-1)$
1	1.6348813716	
2	0.5515797634	0.3373821324
3	0.2510243729	0.4551007660
4	0.1345820461	0.5361313904
5	0.0803617162	0.5971206302
6	0.0518220796	0.6448602905
10	0.0142412156	0.7614073846
20	0.0022340045	0.8692080074
40	3.2262084789e-04	0.9306352572
60	1.0097576035e-04	0.9526560989
100	2.2851831113e-05	0.9709947053

When $D = 0.1$, to verify the above and determine the existence of other degeneracies on the curve **He**, we have drawn in Fig. 5(a), for $\sigma = 0.3$, the value of the product δ_{12} at the points of the curve **He** in a wider range than that of Fig. 3(a), namely when $b \in (0, 2.5]$. In fact, in this figure it can be observed that, in the neighborhood of the point **DZ**, the product $\delta_{12} < 1$ for the points of the curve **He**. Subsequently, there is a value (red bullet) where $\delta_{12} = 1$, being both saddle-node equilibrium points (this point of the graph corresponds to the lowest point **DHe** of the curve **He** in the first quadrant in Fig. 3(a)). Next, in the zone where $\delta_{12} > 1$, the existence of a maximum is observed. This maximum corresponds to the point $\mathbf{DHe^2}$ in Fig. 3(a) on the curve **He** where a double eigenvalue $\lambda_1^* = \lambda_2^*$ appears. Finally, the existence of another point (blue bullet) is observed where, being the equilibrium E_1 a real saddle and E_2 a saddle-focus, it is true that $\delta_{12} = 1$. This point on the graph corresponds to the upper point **DHe** for $(\rho, b) \approx (5.225, 0.5951172)$ which appears in Fig. 3(a). As we will see later, this degeneration is not related to the double-zero degeneracy **DZ** analyzed in this work. In the remaining points it is observed that $\delta_{12} < 1$ and its value decreases as b increases.

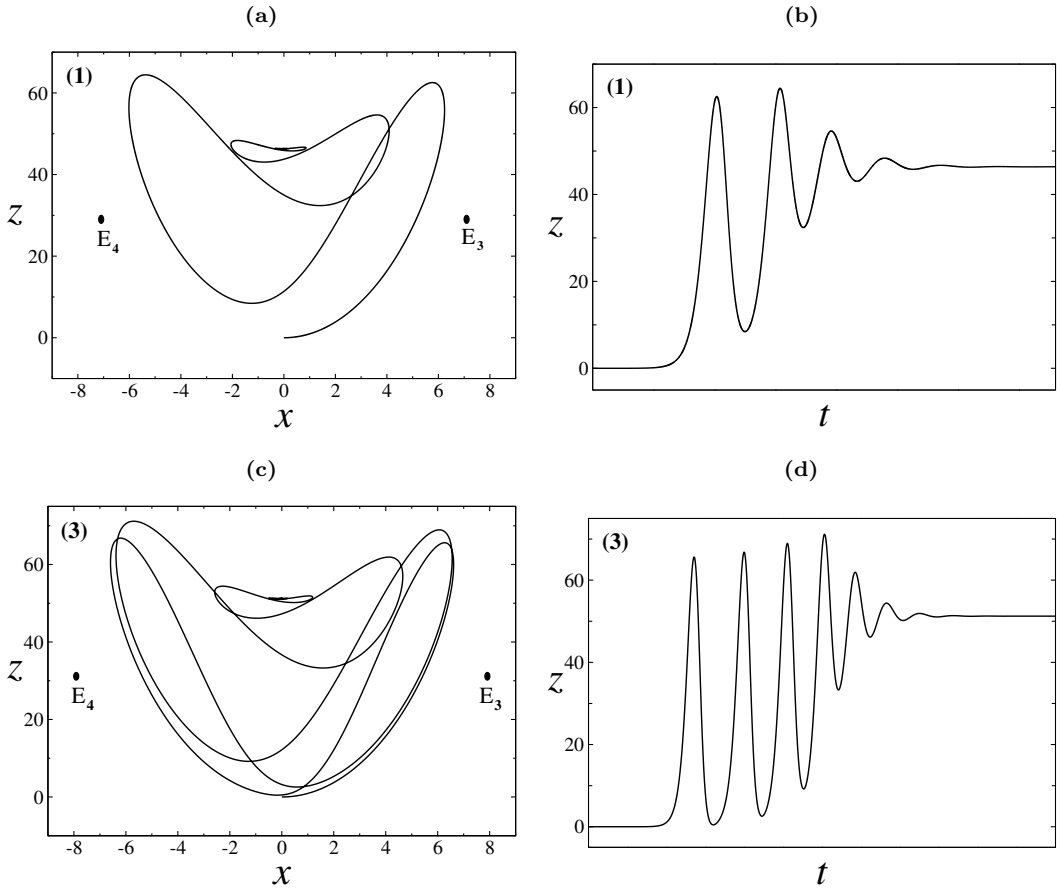

Fig. 4 For $\sigma = 0.3, D = 0.1$: (a) Projection on the (x, z)-plane of the heteroclinic orbit labelled (**1**) in Fig. 3(d). (b) Temporal profile $z(t)$ of heteroclinic orbit (**1**). (c) Projection on the (x, z)-plane of the heteroclinic orbit labelled (**3**). (d) Temporal profile $z(t)$ of heteroclinic orbit (**3**). Note that, to simplify the drawings, we have not included the heteroclinic connection located on the z-axis which joins E_2 and E_1 (it is structurally stable). This does appear drawn in Fig. 3(f).

In Fig. 5(b) we have made a similar graph for $\sigma = 0.2$, maintaining the same range for the parameter b. In this case, it is observed that at all points of the curve **He**, since it arises from the degeneracy **DZ**, it is true that $\delta_{12} < 1$. As before, this graph presents a local maximum where a degeneration of the same type occurs as in the previous case. At this point $\mathbf{DHe^2}$, for $(\rho, b) \approx (6.643798, 0.7443798)$ from the curve **He** it is verified that $\lambda_1^* = \lambda_2^* = -0.6$, and from that point on the heteroclinic cycle the equilibrium E_2 changes from real saddle to saddle-focus. As a consequence of the above, and due to the continuity of the function δ_{12} with respect to the parameters, there must exist a value in the three-parameter space (ρ, b, σ) where a codimension-three degeneracy occurs, since the degeneracies $\mathbf{DHe^2}$ and $\delta_{12} = 1$ coincide at this point. Indeed, as can be seen in Fig. 5(c) at the point $\mathbf{DDHe^2}$, for $(\rho, b, \sigma) \approx (6.1866153, 0.6915487, 0.2126370)$, when $D = 0.1$, the heteroclinic cycle **He** undergoes a double degeneracy since the equilibrium E_2 changes from real saddle to saddle-focus and also the product $\delta_{12} = 1$.

Now we fix $\sigma = 0.4$, that is, we move to the other side of the critical value $\sigma = 1/3$, where the degeneracy **DDZ** of the double-zero bifurcation of the origin occurs. In Fig. 6(a) we have represented the curves of Hopf bifurcation **h** and of heteroclinic connections **He**. Note that in the range shown in this figure these curves do not intersect and, in a neighborhood of the point **DZ**, they have their positions exchanged with respect to those in Fig. 3(a) (since now the curve **h** arises from **DZ** to the left of the curve **He**, as can be seen in Fig. 1 when $\sigma > 1/3$). In addition, the Hopf bifurcation **h** now appears supercritical and, at the point **Dh**, for $(\rho, b) \approx (4.4526922, 0.5295297)$, it changes its character because another degeneracy $a_1 = 0$ occurs. We note that this degeneracy is also present for $\sigma = 0.3$ (it corresponds to the second point **Dh** marked in Fig. 3(a)), but it is not related to the degenerate double-zero bifurcation **DDZ** (the degeneracy **Dh** appears due to the minimum of the curve **Dh** with respect to σ, see Fig. 7). Indeed, when $\sigma \approx 1/3$ this second degeneracy

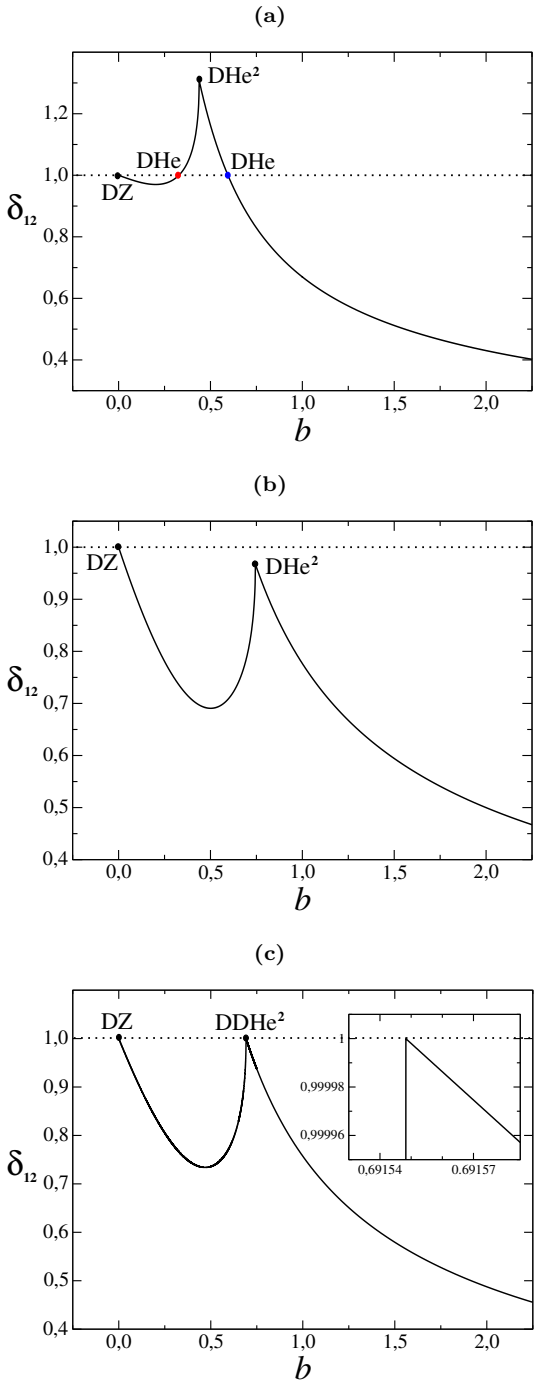

Fig. 5 For $D = 0.1$, product of saddle quantities δ_{12} versus parameter b on the points of the curve **He** when: (a) $\sigma = 0.3$. (b) $\sigma = 0.2$. (c) $\sigma \approx 0.212637$.

$a_1 = 0$ is experienced at the point **Dh** which occurs at $(\rho, b) \approx (4.4094488, 0.5046604)$.

As we can see in Fig. 6(b), in a neighborhood of **DZ**, $\delta_{12} > 1$ for this heteroclinic cycle. In this situation, the periodic orbit arising from the curve **He** is attractive and, as expected, there is no longer a point on that curve where $\delta_{12} = 1$ when both equilibria are real saddle. As in the previous case, in the region where $\delta_{12} > 1$, there is a point **DHe²**, which occurs at $(\rho, b) \approx (3.0167880, 0.3241788)$, where a maximum exists. At this point a double eigenvalue occurs, $\lambda_1^* = \lambda_2^* = -0.7$, and by increasing the value of b, the equilibrium E_2 changes from real saddle to saddle-focus. In this zone we see that for $\sigma = 0.4$ there is still a point **DHe**, when $(\rho, b) \approx (4.675, 0.5451430)$, where $\delta_{12} = 1$. This fact confirms that this degeneracy is not related to **DDZ**, as can be seen in Fig. 7. In fact, when $\sigma \approx 1/3$ the degeneracy $\delta_{12} = 1$, being E_2 a saddle-focus equilibrium, is experienced at $(\rho, b) \approx (5, 0.5740328)$.

In Fig. 6(a) we have marked the degeneracy **DHe²** (as we said before, we conjecture that an infinite sequence of curves of homoclinic connections arises from it). We have also drawn the first curve of homoclinic connections of the origin **Ho** (blue color) that emerges from **DHe²** (see the inset of Fig. 6(a)) and we have detected a degenerate point **DHo**, which occurs at $(\rho, b) \approx (9.1386649, 1.2353206)$, where $\lambda_3 = -\lambda_1 = -b$, and consequently $\delta_1 = 1$. Although we have preferred not to draw it so as not to overcomplicate Fig. 6(a), we remark that a second homoclinic connection to the origin arising from **DHe²** ends spiraling in a T-point **TP**, which occurs at $(\rho, b) \approx (15.3331808, 2.0863007)$. As we are going to see in Sect. 4.2, the interaction between the curves emerged from the degenerate points **DHe²**, **DHo** and **TP** is crucial to explain the disposition in the Lorenz system of the family of infinitely many homoclinic orbits previously found in the literature [47, Fig.6], [48, Fig.8(B)], [17, Fig. 3].

That is why, in the second part of this numerical study, we analyze the existence of the degeneracy **DHe²** when $D = 0$ (Lorenz system). This will allow us to find its relationship with the sequence of homoclinic connections of the origin present in [17, Figs. 3-4], including the homoclinic connection that ends at the T-point heteroclinic loop **TP**.

Now we are going to determine in the (ρ, b, σ)-space, when $D = 0.1$, the loci where the degenerate bifurcations that we have found occur. We represent in Fig. 7 the projections onto the (ρ, σ)- and the (b, σ)-planes of the bifurcation curves corresponding to the four codimension-two degeneracies that exist in the first quadrant of Fig. 3(a), namely **Dh** (degenerate Hopf bifurcation of the equilibria $E_{3,4}$; green color), **DHe** (degeneracy condition $\delta_{12} = 1$ on the curve of heteroclinic connections **He** between E_1 and E_2 when the equilibrium E_2 is a real saddle (red color) and when it is a saddle-focus (orange color)), **DHe²** (degeneracy on the curve **He** when E_2 changes from real saddle to saddle-focus; black color) and **DZ** (double-zero bifurcation of the equilibrium E_1; blue color). We have also drawn

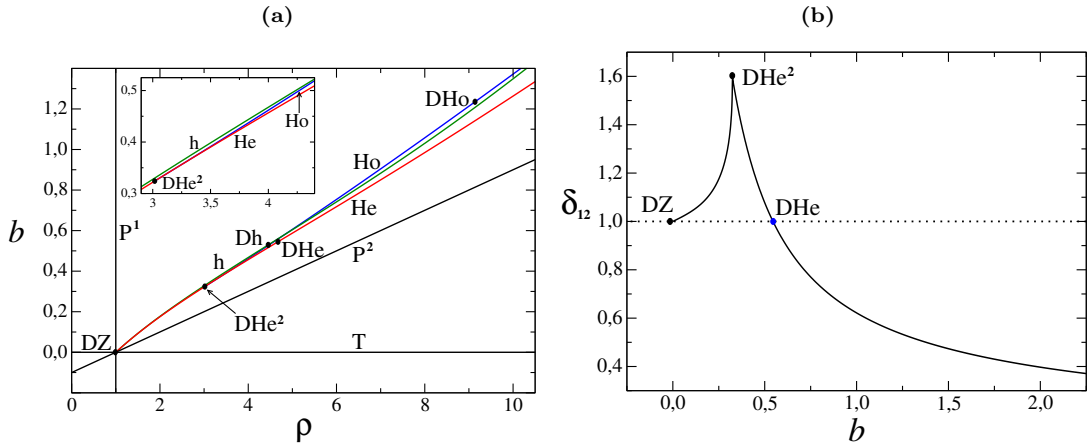

Fig. 6 For $\sigma = 0.4$, $D = 0.1$: (a) Partial bifurcation set in a neighborhood of the point **DZ**. Other four codimension-two bifurcations are also present: **Dh**, **DHe**, **DHe²** and **DHo**. (b) Product of saddle quantities δ_{12} versus parameter b on the points of the curve **He**.

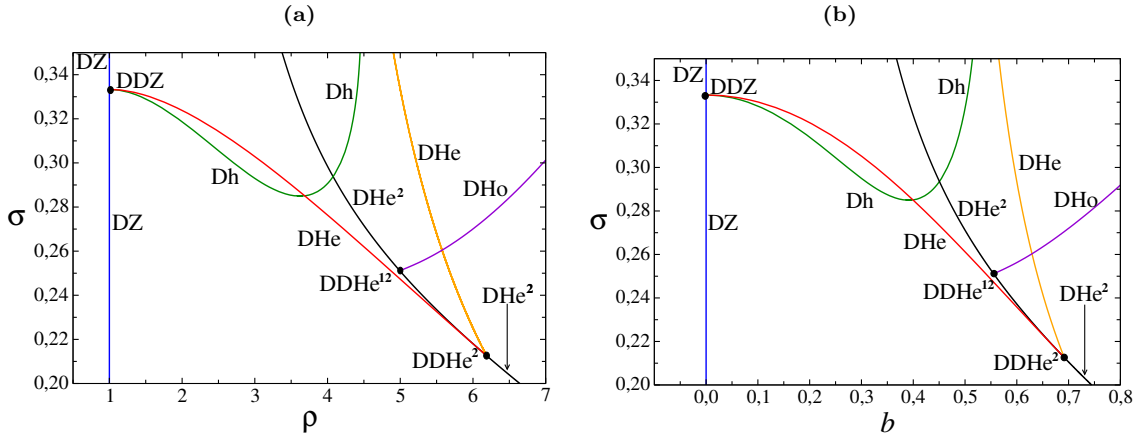

Fig. 7 For $D = 0.1$, projection in the vicinity of the degenerate bifurcation point **DDZ** of the curves **Dh** (degenerate Hopf bifurcation of the equilibria $E_{3,4}$; green color), **DHe** (degeneracy condition $\delta_{12} = 1$ on the curve of heteroclinic connections **He** when the equilibrium E_2 is real saddle (red color) and when it is saddle-focus (orange color)), **DHe²** (degeneracy on the curve **He** when E_2 changes from real saddle to saddle-focus; black color), **DZ** (double-zero bifurcation of the equilibrium E_1; blue color) and **DHo** (degeneracy $\delta_1 = 1$ on the homoclinic connection to the origin; magenta color) onto: (a) the (ρ, σ)-plane. (b) the (b, σ)-plane. The codimension-three degeneracies **DDHe²** and **DDHe¹²** are also marked.

the degeneracy **DHo** (degeneracy condition $\delta_1 = 1$ on the curve of homoclinic connections of the origin **Ho**; magenta color) which we can see in Fig. 6(a).

In Fig. 7 we observe that the curves **Dh** and **DHe** emerge from the point **DDZ** which occurs at $(\rho, b, \sigma) = (1, 0, 1/3)$. Remark that both curves are tangent at **DDZ** and the equilibria E_1 and E_2 are real saddle.

The red curve **DHe** ends at the point **DDHe²**, which is located on the curve **DHe²**, being tangent to it. Let us remember that at **DDHe²** a double degeneracy occurs on the heteroclinic cycle **He** ($\delta_{12} = 1$ and the equilibrium E_2 changes from real saddle to saddle-focus). From that point, the other curve **DHe** (of equation (15) in the case of Fig. 7(a), where $\delta_{12} = 1$) also emerges. This curve is located to the right of the curve **DHe²**, in the area where the equilibrium E_2 is saddle-focus, although in this case it is not tangent to the curve **DHe²** at **DDHe²**. Now we see that the two degenerate points **Dh**, that exist on the curve **h** in the range of Fig. 3(a) for $\sigma = 0.3$, belong to the same branch of the curve **Dh** and, due to a lack of transversality with respect to the parameter σ, these two degeneracies disappear when the value of σ decreases.

Finally, we note that on the curve **DHe²** there are other codimension-three degeneracies of the heteroclinic cycle **He**. Specifically, in Fig. 7 we have marked the point **DDHe¹²**, located at $(\rho, b, \sigma) \approx (4.9938042, 0.5552146, 0.2511140)$, where $\delta_1 = 1$ (since $\lambda_1 = -\lambda_3 = 1$). As can be seen, from **DDHe¹²** the curve **DHo** of degenerate homoclinic connections **Ho** emerges. We remark that $\delta_1 < 1$ at the points of the curve **DHe²** above **DDHe¹²** while $\delta_1 > 1$ for those below **DDHe¹²**. Thus, $\delta_1 < 1$ at

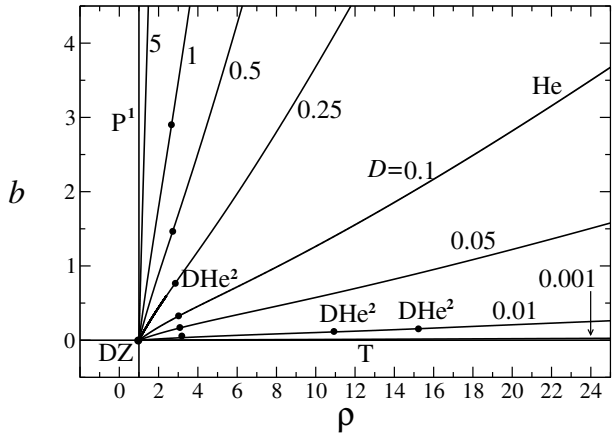

Fig. 8 For $\sigma = 0.4$, curves of nondegenerate heteroclinic cycles **He**, related to **DZ**, for $D = 0.001$, 0.01, 0.05, 0.1, 0.25, 0.5, 1, 5, in the first quadrant of the (ρ, b)-plane.

the points $\mathbf{DHe^2}$ shown in Figs. 3(a) and 6(a). As we are going to see in Sect. 4.2, the type of global bifurcations that emerge from $\mathbf{DHe^2}$ will depend on the value of δ_1.

Until now we have done our numerical study by setting $D = 0.1$. We are going to end this subsection by looking at how the curve **He** evolves when D varies. In Fig. 8, for $\sigma = 0.4$, we have represented in the (ρ, b)-plane the curves where the global connections **He** occur for the values $D = 0.001, 0.01, 0.05, 0.1, 0.25, 0.5, 1, 5$. We recall that $\mathbf{DHe^2}$ (marked with black bullets in this figure) corresponds to a degeneracy on the curve **He** because the equilibrium E_2 changes from real saddle to saddle-focus.

As shown in Fig. 8, in the (ρ, b)-plane all the curves **He** arise from the double-zero degeneracy **DZ**. It is true that, setting a value of b, as the value of the D increases, the component $z = \frac{b}{D} > 0$ of E_2 decreases. Thus, this equilibrium approaches E_1 and, as a consequence, the value of ρ in the points of the curves **He** corresponding to these heteroclinic cycles approaches the value $\rho = 1$ where these cycles disappear. On the other hand, when $D \longrightarrow 0^+$, the curves **He** are approaching the ρ-axis. This fact leads us to conjecture that the heteroclinic cycles corresponding to the value $D = 0$ (Lorenz system) are located on the axis $b = 0$ being therefore degenerate.

4.2 Approaching the Lorenz system ($D = 0$)

The main objective of this subsection is to see how the global connections related to the double-zero bifurcation of system (2) allow to explain the origin of the global connection curves present in the partial bifurcation set found in the Lorenz system for $\rho = 50$ (see [17, Figs. 1 and 3]). We note that this complex distribution of the homoclinic connections in the Lorenz system has been previously found in the literature [47, 48], although the reason for this complicated behavior was unknown. Specifically, we want to analyze the evolution of these global connection curves when $D \neq 0$ (keeping $\rho = 50$, we will start with $D = 0.5$ and we will decrease the value of D until we reach $D = 0$) and then to determine if some of the curves in the Lorenz system are related to the degeneracies found here on the curve **He**. In what follows, we will see that the degeneracies $\mathbf{DHe^2}$, **DHo** and **TP** play a key role in justifying the presence of the curves drawn in [17, Figs. 1 and 3] for the Lorenz system.

In Fig. 9(a) we have represented a partial bifurcation set in the (b, σ)-parameter plane, for $\rho = 50$, $D = 0.5$ (three zooms of this bifurcation set appear in Figs. 9(b)-(d)). The curve **h** of supercritical Hopf bifurcation of $E_{3,4}$, given by (13), has a vertical asymptote when $b = 2D(\rho - 1) = 49$ and ends at the point $(b, \sigma) = (48, 0)$ (outside the range of the figure), since now the condition $2D(\rho - 1) - b - \sigma - 1 \neq 0$ of (13) is not fulfilled. A degenerate point $\mathbf{DHe^2}$, which it placed at $(b, \sigma) \approx (50.34911853,$
$204.78806517)$, appears on the heteroclinic curve **He**. At this point the equilibrium E_2 changes from real saddle to saddle-focus, whereas E_1 is real saddle with $\delta_1 > 1$. From $\mathbf{DHe^2}$, as we said above, we conjecture that an infinite sequence of curves of homoclinic connections to the origin emerges, in addition to other bifurcation curves. We have only represented the first three curves of this infinite sequence, namely **Ho**, $\mathbf{Ho^0_{TP}}$ and $\mathbf{Ho^0_{TPS}}$. The periodic orbits that arise from any of these homoclinic connections are attractive since $\delta_1 > 1$ holds for all their points.

The notation we will employ from now on for the curves of homoclinic connections to the origin is similar to that used in [17]. On the one hand, we use a superscript to give information about the shape of the homoclinic orbit in the upper zone of the range of existence of the homoclinic curve (when it emerges from $\mathbf{DHe^2}$). On the other hand, the subscript informs about the shape of the homoclinic connection in the lower part of the region shown in the parameter plane (sometimes the curve ends in a codimension-two point and, in other cases, it leaves the region drawn in the figure). Specifically, in $\mathbf{Ho^i_j}$, the superscript i (the same explanation is valid for the subscript j) indicates the number of turns around one of the non-trivial equilibria $E_{3,4}$, in our case E_4, given by the projection in the (x, z)-plane of the homoclinic orbit whose leading unstable manifold arises towards the positive semi-axis $x > 0$ (note that

because of the symmetry a pair of the corresponding orbits exists).

The difference between the homoclinic connections corresponding to these three curves, **Ho**, $\mathbf{Ho^0_{TP}}$ and $\mathbf{Ho^0_{TPS}}$, can be seen in Fig. 9(e) where we have drawn their projection on the (x, z)-plane for $\sigma = 100$. As can be observed, the homoclinic orbit corresponding to the curve **Ho** (green) whose leading unstable manifold arises towards the positive semi-axis $x > 0$ does not cross the z-axis and reaches equilibrium E_1 on its right hand side. On the contrary, the homoclinic orbit corresponding to the curve $\mathbf{Ho^0_{TP}}$ (black) crosses the z-axis once (red line in the inset of Fig. 9(e)), close to E_2 (black bullet), and enters E_1 from its left side. For its part, the homoclinic orbit corresponding to the curve $\mathbf{Ho^0_{TPS}}$ (blue) crosses the z axis twice before entering E_1 on its right side. According to their shape, the corresponding superscript is "0" in the three cases (to simplify the notation of the principal homoclinic orbit to the origin we use **Ho** instead of $\mathbf{Ho^0_0}$). The curves $\mathbf{Ho^0_{TP}}$ and $\mathbf{Ho^0_{TPS}}$ end, respectively, at the principal T-point **TP**, which occurs at $(b, \sigma) \approx (51.8873485,$ $14.3396057)$ (bullet orange), and at the secondary T-point **TPS**, situated at $(b, \sigma) \approx (52.2305506, 6.8452189)$. The projection onto the (x, z)-plane of these two heteroclinic cycles can be seen in Figs. 9(f)-(g). Although in these two cases the subscript should be "∞" (because the homoclinic curves end spiraling at the T-points), we prefer to use "TP" and "TPS" to distinguish both curves.

As was the case with the heteroclinic connection curve in Figs. 3(c)-(d), the curve **He** accumulates on a line segment on a saddle-node bifurcation curve of symmetric periodic orbits $\mathbf{SN_1}$ (see Fig. 9(b)). This saddle-node curve arises from the cusp bifurcation point **CU**, which occurs at $(b, \sigma) \approx (55.0074131, 11.8687941)$. To the right of **CU** there is another bifurcation curve $\mathbf{SN_2}$ of the same type.

In what follows, we are going to focus on seeing the evolution of the curves **Ho** and $\mathbf{Ho^0_{TP}}$ as well as of other new homoclinic curves which, as we will see, emerge from $\mathbf{DHe^2}$ (we will no longer show the curve $\mathbf{Ho^0_{TPS}}$ because it is not relevant to the results we present). Thus, keeping $\rho = 50$, we decrease the value of the parameter to $D = 0.21$ and draw the partial bifurcation set of Fig. 10(a). As in Fig. 9(a), the bifurcation curves **h**, **He**, **Ho** and $\mathbf{Ho^0_{TP}}$ are also present. The Hopf bifurcation curve **h** now ends, for the same reason as before, at the point $(b, \sigma) = (19.58, 0)$, and the point of codimension two $\mathbf{DHe^2}$ continues to exist on the curve **He**, for $(b, \sigma) \approx (20.8579428, 199.2891303)$. However, while E_1 is still a real saddle, now $\delta_1 < 1$ (which implies an important change as we will discuss below). From point $\mathbf{DHe^2}$ the homoclinic connections to the origin $\mathbf{Ho^0_{TP}}$ and **Ho** continue to emerge but, as can be seen in the figure, a new degeneration **DHo** appears on the curve **Ho**, when $(b, \sigma) \approx (30.2447608, 50.3854047)$. At this point, $\delta_1 = 1$ (since $\lambda_2 < \lambda_3 = -\lambda_1 = -b$). So, from **Ho**, a non-stable periodic orbit arises between the points $\mathbf{DHe^2}$ and **DHo** (since $\delta_1 < 1$) whereas this periodic orbit is stable below the point **DHo** ($\delta_1 > 1$). As a consequence of this, for this value of D there is a new infinite sequence $\{\mathbf{Ho^i_i}\}$ of homoclinic connections to the origin (apart from other bifurcation curves such as saddle-node of periodic orbits, symmetry-breaking of symmetric periodic orbits, etc.) that join $\mathbf{DHe^2}$ and **DHo**. In Fig. 10(a) we have represented the first three curves of the sequence, namely $\mathbf{Ho^1_1}$, $\mathbf{Ho^2_2}$ and $\mathbf{Ho^3_3}$ (dashed line).

As seen in Figs. 10(d), 10(e) and 10(f), for $\sigma = 100$, these homoclinic connections are different from those that exist in the **Ho** (see Fig. 10(c)) and $\mathbf{Ho_{TP}}$ curves (see Fig. 9(e)) in the sense that their projection onto the (x, z)-plane surrounds both non-trivial equilibria $E_{3,4}$ (black bullets). Note that, although we have not represented them in Fig. 10(a), on the curve $\mathbf{Ho^0_{TP}}$ there are several points **DHo** (the intersection points of this curve with the curve $\delta_1 = 1$), where the same degeneracy present on curve **Ho** is experienced.

To see the relationship that exists between the periodic orbits that arise from these homoclinic connections, and justify the previously mentioned difference, we draw in Fig. 10(b) the bifurcation diagram for $\sigma = 100$. An asymmetric non-stable periodic orbit arises from **Ho**, which after undergoing a saddle-node bifurcation of periodic orbits **sn** (for $b \approx 25.6078095$) disappears as a stable periodic orbit at the supercritical Hopf bifurcation **h**. Due to the symmetry, a non-stable symmetric periodic orbit also arises from **Ho** [59], which undergoes a symmetry-breaking bifurcation **PPO**, for $b \approx 25.1363078$. The attractive periodic orbit arising from **PPO** undergoes a saddle-node bifurcation **SN** in which it becomes a saddle. Finally, it ends in the homoclinic connection $\mathbf{Ho^0_{TP}}$.

The saddle asymmetric periodic orbit that emerges from the bifurcation **PPO** is the one that ends in the homoclinic connection $\mathbf{Ho^1_1}$ and, as it arises from the symmetry breaking of a symmetric periodic orbit whose projection on the (x, z)-plane surrounds both non-trivial equilibria $E_{3,4}$, the projection of this homoclinic connection also does. Finally, the saddle asymmetric periodic orbits arising from $\mathbf{Ho^2_2}$ and $\mathbf{Ho^3_3}$ also end, without undergoing any bifurcation, on the homoclinic connection **Ho**. As far as we know, this is the first example of a system in which infinitely many periodic orbits bifurcate from a homoclinic connection to a real saddle

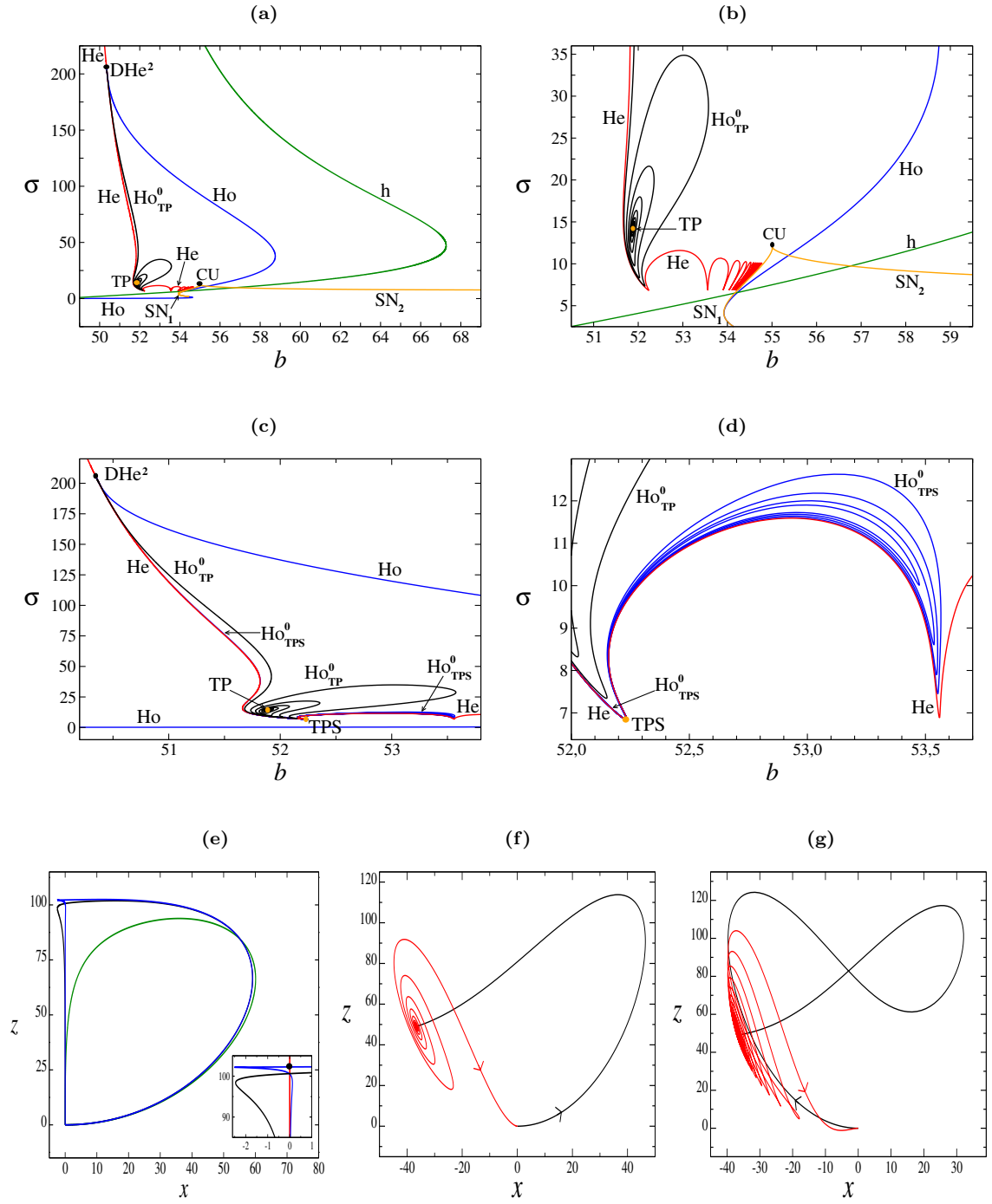

Fig. 9 For $\rho = 50, D = 0.5$: (a) Partial bifurcation set in the (b, σ)-plane with the curves **h** (supercritical Hopf bifurcation of the nontrivial equilibria $E_{3,4}$; green), **Ho**, $\mathbf{Ho^0_{TP}}$ (homoclinic connections to the origin; blue and black, respectively), **He** (heteroclinic connections between E_1 and E_2; red) $\mathbf{SN_1}$ and $\mathbf{SN_2}$ (saddle-node bifurcations of symmetric periodic orbits; orange). (b)-(d) Zooms of panel (a) including the curve $\mathbf{Ho^0_{TPS}}$ (blue) of homoclinic connections to the origin. Projection onto the (x, z)-plane of the: (e) homoclinic connections to the origin **Ho** (green), $\mathbf{Ho^0_{TP}}$ (black) and $\mathbf{Ho^0_{TPS}}$ (blue), for $\sigma = 100$; (f) principal T-point **TP** between E_1 and E_4 (note that because of the symmetry a pair of the corresponding orbits exists); (g) secondary T-point **TPS** between E_1 and E_4. The black line corresponds to the intersection between the one-dimensional manifolds of the equilibria E_1 and E_4 and the red one to the intersection between the two-dimensional manifolds.

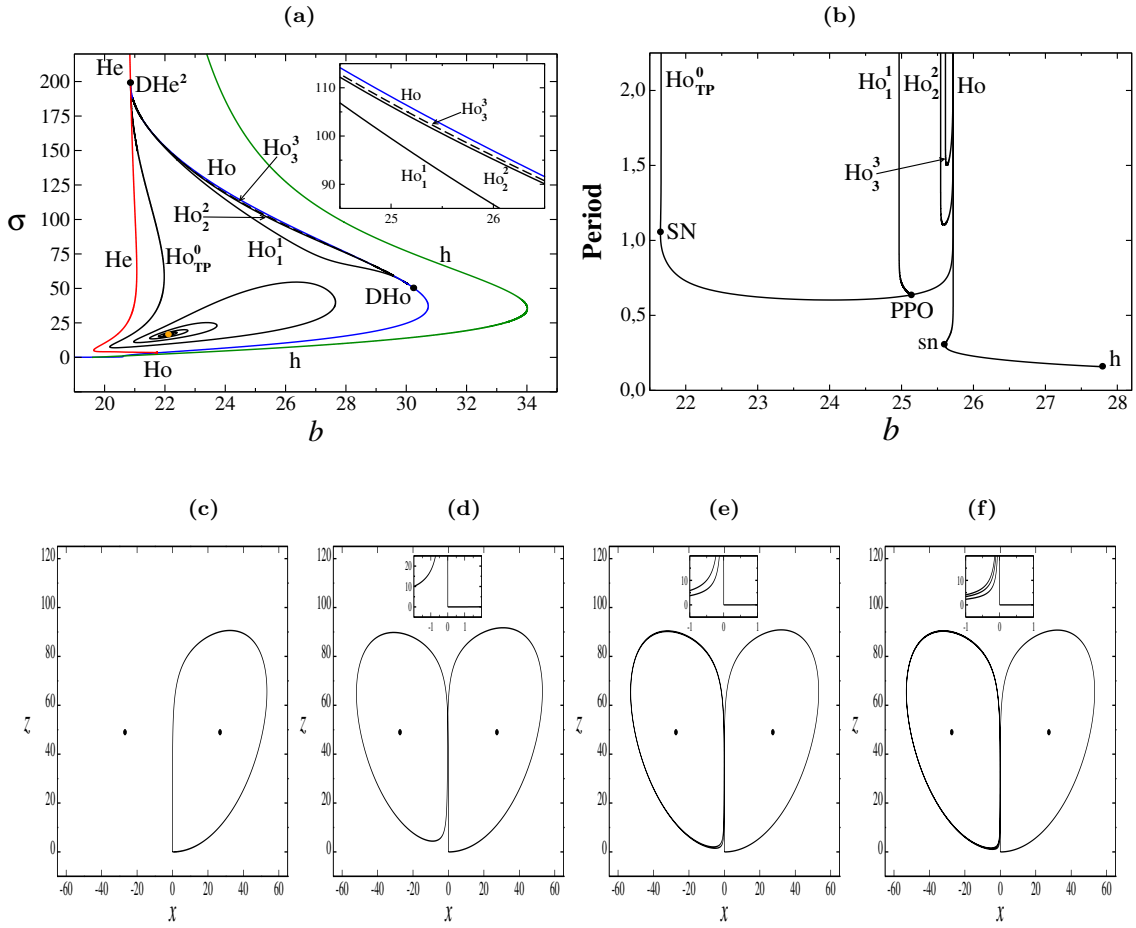

Fig. 10 For $\rho = 50$, $D = 0.21$: (a) Partial bifurcation set in the (b, σ)-plane with the curves **h** (Hopf bifurcation of the nontrivial equilibria $E_{3,4}$), **Ho**, $\mathbf{Ho_1^1}$, $\mathbf{Ho_2^2}$, $\mathbf{Ho_3^3}$, $\mathbf{Ho_{TP}^0}$ (curves of homoclinic orbits to the origin) and **He** (heteroclinic connection between E_1 and E_2). The principal T-point is marked with an orange bullet. (b) For $\sigma = 100$, bifurcation diagram of the symmetric and asymmetric periodic orbits that end at **Ho** and of the asymmetric periodic orbits emerged from **h**, $\mathbf{Ho_1^1}$, $\mathbf{Ho_2^2}$ and $\mathbf{Ho_3^3}$. For $\sigma = 100$, projection onto the (x, z)-plane of the homoclinic orbit corresponding to the curve: (c) **Ho** for $b \approx 25.7178751$; (d) $\mathbf{Ho_1^1}$ for $b \approx 24.965864$; (e) $\mathbf{Ho_2^2}$ for $b \approx 25.543696$; (f) $\mathbf{Ho_3^3}$ for $b \approx 25.610137$.

($\delta < 1$) and its theoretical analysis has not yet been carried out. The three-parameter continuation of **DHo** allows to detect that, for $\rho = 50$, there is a codimension-three degeneracy on the curve **He** when $(b, \sigma, D) \approx (40.6626754, 203.1965805, 0.4054090)$. At this point, **He** exhibits a double degeneracy since $\delta_1 = 1$ for E_1 and, simultaneously, E_2 changes from real saddle to saddle-focus. We called $\mathbf{DDHe^{12}}$ to this codimension-three degeneracy when we found it for $D = 0.1$ (see Fig. 7) which, as far as we know, has not been studied in the literature either. We note that the points where the equilibrium E_1 fulfills that $\delta_1 = 1$ do not depend on the value of the parameter D.

As a consequence, when $D < D_c \approx 0.4054090$, the point **DHo** appears on the curve **Ho** in the (b, σ)-plane. This implies that, in this parameter plane, the bifurcations related to the degeneracy $\mathbf{DHe^2}$ are different on each side of the value D_c. Specifically, new bifurcation curves emerge from $\mathbf{DHe^2}$ when $D < D_c$ (for example, those of the new sequence of homoclinic connections of the origin $\mathbf{Ho_i^i}$) since now $\delta_1 < 1$ for the equilibrium E_1.

Next, to try to explain the origin of the curves that appear in [17, Figs. 1-4] for Lorenz system ($D = 0$), we investigate in Fig. 11 how the bifurcation set evolves as D decreases.

When $D = 0.2$, we see in Fig. 11(a) how a contact has already been produced between the curves $\mathbf{Ho_1^1}$ and $\mathbf{Ho_{TP}^0}$ of Fig. 10(a). This implies that although these curves of homoclinic connections continue to emerge from the point $\mathbf{DHe^2}$, placed at $(b, \sigma) \approx (19.8533783, 199.0625408)$, they have swapped the points of the parameter plane where they now end. Thus, $\mathbf{Ho_1^0}$ ends in **DHo**, situated at $(b, \sigma) \approx (29.5439568, 46.3809284)$ and $\mathbf{Ho_{TP}^1}$ does it in **TP** (orange bullet), located at $(b, \sigma) \approx (21.2063502, 16.809238)$. We note that the con-

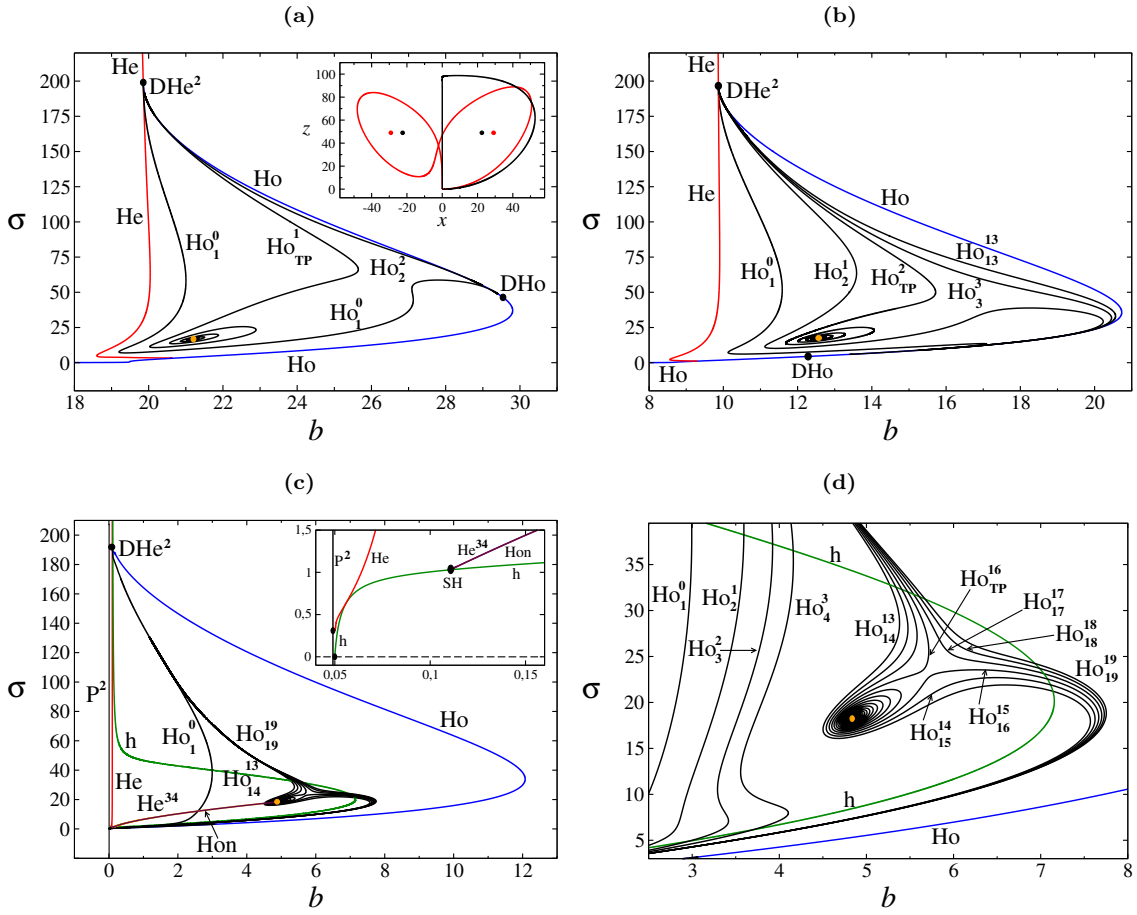

Fig. 11 For $\rho = 50$ partial bifurcation set in the (b, σ)-plane: (a) for $D = 0.2$; (b) for $D = 0.1$; (c) for $D = 0.001$. (d) Zoom of panel (c) in the vicinity of the T-point.

tact between the curves $\mathbf{Ho^0_{TP}}$ and $\mathbf{Ho^1_1}$ occurs near the point **DHo**, in a zone where these homoclinic connections are orientable. The tangency takes place between $\mathbf{Ho^1_1}$ and the outer loop of the spiral curve $\mathbf{Ho^0_{TP}}$, since, in this zone, the projection on the (x, z)-plane of the homoclinic orbit corresponding to these values gives a turn to each of the equilibria $E_{3,4}$. Let us remember that although initially, when it arises from $\mathbf{DHe^2}$, the projection of the homoclinic orbit corresponding to the curve $\mathbf{Ho^0_{TP}}$ only surrounds one of the equilibria $E_{3,4}$, in our case E_3 (see Fig. 9(e)), later the homoclinic orbit turns around the same equilibrium, in our case E_4, one more time (in the phase space) as the curve turns one more time (in the parameter plane) in its spiraling way towards the T-point. In the inset of Fig. 11(a), to illustrate the evolution of the homoclinic orbits along the curve $\mathbf{Ho^0_1}$, we show the projection onto the (x, z)-plane of two of them. The first one (in black), for $\sigma = 150$, $b \approx 20.0900594$, is "close to" $\mathbf{DHe^2}$ (its shape justifies the superscript "0") whereas the second one (in red), $\sigma = 50$, $b \approx 27.0985454$, is "close to" **DHo** (its shape justifies the subscript "1"). Equilibria $E_{3,4}$ are also marked in the corresponding colors.

In Fig. 11(b) we see how, by decreasing the value of the parameter to $D = 0.1$, the same contact process has been repeated between the curve $\mathbf{Ho^2_2}$ (whose projection on the (x, z)-plane gives two turns to the equilibrium E_4 according to Fig. 10(e)) and the outer loop of the spiral curve $\mathbf{Ho^1_{TP}}$ of Fig. 11(a), whose homoclinic orbits have a projection with the same number of turns to each of the equilibria $E_{3,4}$. As a consequence, there is a new curve of homoclinic connections $\mathbf{Ho^1_2}$ that, like the curve $\mathbf{Ho^0_1}$, goes from the point $\mathbf{DHe^2}$, located at $(b, \sigma) \approx (9.8657655, 196.6255324)$, to the point **DHo**, situated at $(b, \sigma) \approx (12.2833185, 4.4438448)$. We also draw in Fig. 11(b) the curves of homoclinic connections $\mathbf{Ho^3_3}$ and $\mathbf{Ho^{13}_{13}}$ that are orientable at all points. Between these two curves are located the curves $\mathbf{Ho^i_i}$ $(i = 4, 5, ..., 12)$ which we have not drawn so as not to overload the figure excessively.

Since we want to keep decreasing D to get closer to $D = 0$, in Fig. 11(c) we have drawn a partial bifurcation set for $D = 0.001$. In this case we have included

the curve $\mathbf{P^2}$ where a pitchfork bifurcation of the equilibrium E_2 takes place when $b = D(\rho - 1) = 0.049$. The Hopf bifurcation curve $\mathbf{h}$ has a vertical asymptote at $b = 2\,D\,(\rho - 1) = 0.098$ and ends by contacting the b axis at the point $(b, \sigma) = (0.04998, 0)$, since now the condition $b(\rho + \sigma) - 2D(\rho - 1)\sigma + D(1 - \rho^2) > 0$ of (13) is not fulfilled (see the inset of Fig. 11(c)). In agreement with what was obtained in Fig. 8 the curve of heteroclinic cycles $\mathbf{He}$ is close to the axis $b = 0$, presenting a vertical asymptote for $b \approx 0.0979964$ very close to the asymptote of the curve $\mathbf{h}$. In this case the degeneracy $\mathbf{DHe^2}$ continues to exist and is placed at $(b, \sigma) \approx (0.09796673, 193.8617781)$. In the region between $\mathbf{Ho}$ and $\mathbf{Ho_1^0}$ we have drawn (see Figs. 11(c)-(d)) the curves $\mathbf{Ho_{14}^{13}}$, $\mathbf{Ho_{15}^{14}}$, $\mathbf{Ho_{16}^{15}}$, $\mathbf{Ho_{TP}^{16}}$, $\mathbf{Ho_{17}^{17}}$, $\mathbf{Ho_{18}^{18}}$ and $\mathbf{Ho_{19}^{19}}$, which all arise from the point $\mathbf{DHe^2}$.

As we can see, the curve $\mathbf{Ho_{TP}^{16}}$, whose orbit makes 16 turns around E_4 when it arises from $\mathbf{DHe^2}$, is the one that now ends at the T-point $\mathbf{TP}$ (orange bullet), placed at $(b, \sigma) \approx (4.837184, 18.241456)$. As can be seen in the inset of Fig. 11(c), the curves $\mathbf{Hon}$ (homoclinic connections to $E_{3,4}$) and $\mathbf{He^{34}}$ (heteroclinic connections between E_3 and E_4) arise from the point $\mathbf{TP}$, with the shape predicted in [11]. As in the Lorenz system, these two curves are so close as to be almost indistinguishable. They end in Shil'nikov-Hopf degenerate points $\mathbf{SH}$ [17,60] when they intersect the Hopf curve $\mathbf{h}$ at $(b, \sigma) \approx (0.1103258, 1.0293202)$. In the zoom of Fig. 11(d) we have also included the first four curves of homoclinic connection $\mathbf{Ho_1^0}$, $\mathbf{Ho_2^1}$, $\mathbf{Ho_3^2}$ and $\mathbf{Ho_4^3}$ (in order not to complicate this figure too much, we have not included the curves $\mathbf{Ho_5^4}$, $\mathbf{Ho_6^5}$, ..., $\mathbf{Ho_{13}^{12}}$ which are placed consecutively between $\mathbf{Ho_4^3}$ and $\mathbf{Ho_{14}^{13}}$).

In Fig. 12(a) we consider $D = 0$ (Lorenz system). Now the Hopf curve $\mathbf{h}$ is bounded and exists between the points $(b, \sigma) \approx (0, 1.089065)$ and $(b, \sigma) \approx (0,$ $45.910935)$, where the condition $b(\rho + \sigma) > 0$ is not satisfied (see [44]). Furthermore, in this case we know that the curve of heteroclinic connections $\mathbf{He}$ no longer exists in the (b, σ) plane, although there are infinitely many heteroclinic cycles joining points of the continuum of equilibria $E_z = (0, 0, z)$ that exists on the z-axis when $b = 0$ [61]. Thus, the three-parameter continuation in the (b, σ, D)-space of the point $\mathbf{DHe^2}$ of the Fig. 11(c) for $D = 0.001$ allows us to obtain the point $\mathbf{DHe_*^2}$, placed at $(b, \sigma_*, D) \approx (0, 193.8318321, 0)$ (see Fig. 12(b)). For $\rho = 50$, as the value of σ increases and reaches σ_*, the equilibrium point $E_z \approx (0, 0, 97.9592478)$ has a double degeneracy since it changes from saddle-focus to real saddle and has a zero eigenvalue. Remember that when $b = 0$ the eigenvalues of the equilibria E_z are [14]

$$\lambda_{1,2} = \frac{-(1+\sigma) \pm \sqrt{(1+\sigma)^2 + 4\sigma(\rho - z - 1)}}{2}, \;\; \lambda_3 = 0. \tag{16}$$

The numerical continuation of the curves $\mathbf{Ho_j^i}$ of Fig. 12(c) shows that all of them arise from the degeneracy $\mathbf{DHe_*^2}$. Also, as can be seen in Fig. 12(d), the curve $\mathbf{Ho_{TP}^{17}}$ ends at the principal T-point, in agreement with the result obtained in [17, Figs. 3-4]. This indicates that there is a parameter value $D \in (0, 0.001)$ where there has been a contact between the curves $\mathbf{Ho_{TP}^{16}}$ and $\mathbf{Ho_{17}^{17}}$ of Fig. 11(d), giving rise to the new curves $\mathbf{Ho_{17}^{16}}$ and $\mathbf{Ho_{TP}^{17}}$ drawn in Fig. 12. Finally we note that the bifurcation set of Figs. 11(c)-(d), for $D = 0.001$, is similar to that of [17, Fig. 4(b)], corresponding to $\rho = 50.1$. This tells us that, given $\rho = 50$, decreasing the value of the parameter D (transition from $D = 0.001$ to $D = 0$) in system (2) produces on the curves $\mathbf{Ho_j^i}$, the same effect as that obtained when the value of ρ is decreased (transition from $\rho = 50.1$ to $\rho = 50$) in Lorenz system (1).

5 Conclusions

In this work, given the difficulties that appear to study the double-zero bifurcation in the Lorenz system (because it is exhibited by a non-isolated equilibrium), we propose the new system (2) which encompasses the Lorenz system. To do this we add the term Dz^2 in the third equation and, since the continuum of equilibria disappears, it is already possible to study the double-zero bifurcation. Once we have shown that the double-zero degeneracy of the origin guarantees, in a certain region of the parameter space, the existence of heteroclinic cycles (see Theorem 1), we carry out a numerical study to see how that heteroclinic connection evolves as it separates from the singularity.

At first, in Sect. 4.1, we have moved to either side of a degeneracy of the double-zero bifurcation which occurs when $\sigma = 1/3$. This has allowed us to find that the curve of heteroclinic connections accumulates on a line segment of the saddle-node curve $\mathbf{SN_1}$ (see Fig. 3(d)). As far as we know, this is the first example in which the accumulation process occurs in the region in which the periodic orbit involved in the saddle-node bifurcation does not exist. Thus, the heteroclinic cycle accumulates on a non-hyperbolic periodic orbit. In addition, we have found the following global bifurcations of codimension two (see Fig. 7):

- $\mathbf{DHe}$, degenerate heteroclinic connection because $\delta_{12} = 1$, being E_2 a real saddle equilibrium. This

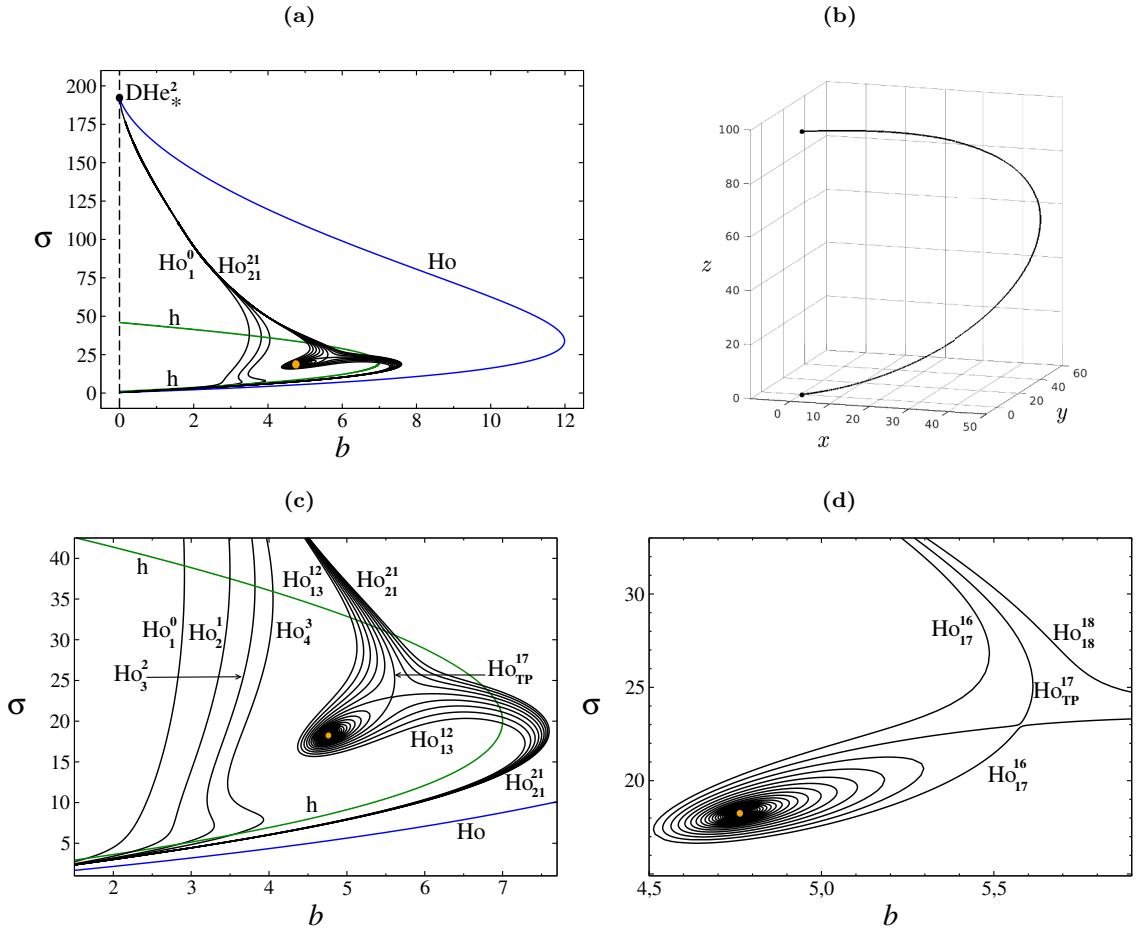

Fig. 12 (a) For $\rho = 50$, $D = 0$, partial bifurcation set in the (b, σ)-plane (b) Phase portrait of $\mathbf{DHe}^2_*$ in (a). (c) Zoom of panel (a) in the vicinity of the T-point (orange bullet). (d) Zoom of panel (c).

curve joins points **DDZ** and $\mathbf{DDHe^2}$. In the parameter plane, a curve of saddle-node bifurcations emanates from **DHe**. We note that from this point $\mathbf{DDHe^2}$ arises another degeneration **DHe**, degenerate heteroclinic connection because $\delta_{12} = 1$, being E_2 a saddle-focus equilibrium.

- $\mathbf{DHe^2}$, degenerate heteroclinic connection because E_2 changes from real saddle to saddle-focus (the double real eigenvalue is negative). As far as we know, this degeneration has not been studied in the literature. From the numerical results we have found, we conjecture the existence of an infinite sequence of bifurcation curves of various types that emanate from this point: saddle-nodes of asymmetric and symmetric periodic orbits, period-doublings of the asymmetric periodic orbits, symmetry-breakings of the symmetric periodic orbits, homoclinic connections of the origin, ... Two degeneracies $\mathbf{DDHe^2}$ and $\mathbf{DDHe^{12}}$ appear on this curve. $\mathbf{DHe^2}$ exhibits even greater bifurcation richness when $\delta_1 < 1$.
- **DHo**, degenerate homoclinic connection of the origin because $\delta_1 = 1$, being a real saddle. In the generic situation for a neutral resonant saddle (see [30, Sect. 2.2.1] and [31, Theorem 5.13]) there are two possibilities. If the homoclinic orbit is nontwisted, an extra curve of saddle-node bifurcation of periodic orbit appears whereas if it is twisted, two curves originate at the critical point (which correspond to a double homoclinic orbit and to a period-doubling bifurcation). However, the bifurcation scenario we have found here is much more complicated (we conjecture that infinitely many curves appear, see Figs. 10(a) and 11(b)) and it deserves to be studied theoretically in the near future. It seems that the structurally stable heteroclinic connection along the z-axis between E_2 and the origin affects the bifurcations involved at this singularity. Remark that the curve **DHo** emerges from the point $\mathbf{DDHe^{12}}$.

The above degeneracies are organized by the codimension-three global bifurcations:

– **DDHe$^{\mathbf{2}}$**, degenerate heteroclinic connection because $\delta_{12} = 1$ and E_2 changes from real saddle to saddle-focus.
– **DDHe$^{\mathbf{12}}$**, degenerate heteroclinic connection between E_1 (with $\delta_1 = 1$) and E_2 (which changes from real saddle to saddle-focus). Due to the richness of the bifurcations that appear around it, the theoretical study of this degeneracy should be addressed in the future.

System (2) is a particular unfolding of the Lorenz system in such a way that, when the continuum of equilibria disappears, it exhibits structurally stable bifurcations. Thus, in subsection 4.2, studying how the bifurcation sets evolve when D tends to zero, we have been able to explain, in the Lorenz system, the origin of the global connections which are related to a T-point, a codimension-two heteroclinic loop. Concretely, we have shown that the degenerate global connection **DHe$^{\mathbf{2}}$** is their main organizing center (see Fig. 12).

It also deserves to be highlighted that, when we introduce the new term Dz^2 in the Lorenz system, one of the two infinite heteroclinic orbits (that connect the origin and one equilibrium on the sphere at infinity, see [14, Theorem 2(b)]) becomes finite.

Authors contribution All authors contributed equally to the present research work. All authors read and approved the final manuscript.

Data availability The data that support the findings of this study are available from the corresponding author upon reasonable request. The numerics of the figures were obtained by AUTO/HomCont and Matlab.

Conflict of interest The authors declare that there is no conflict of interest regarding the publication of the paper.

References

1. Lorenz, E.N.: Deterministic non-periodic flows. J. Atmospheric. Sci. **20**, 130–141 (1963)
2. Haken, H.: Analogy between higher instabilities in fluids and lasers. Phys. Lett. A **53**, 77–78 (1975)
3. Knobloch, E.: Chaos in the segmented disc dynamo. Phys. Lett. A **82**, 43–440 (1981)
4. Gorman, M., Widmann, P.J., Robbins, K.A.: Nonlinear dynamics of a convection loop: a quantitative comparison of experiment with theory. Physica D **19**, 255–267 (1986)
5. Elgin, J.N., Molina-Garza, J.B.: Traveling wave solutions of the Maxwell-Bloch equations. Phys. Rev. A 35, 3986–3988 (1987)
6. Knobloch, E., Proctor, M.R.E., Weiss, N.O.: Heteroclinic bifurcations in a simple model of double-diffusive convection. J. Fluid Mech. **239**, 273–292 (1992)
7. Poland, D.: Cooperative catalysis and chemical chaos: a chemical model for the Lorenz equations. Physica D **65**, 86–99 (1993)
8. Cuomo, K.M., Oppenheim, A.V.: Circuit implementation of synchronized chaos with applications to communications. Phys. Rev. Lett. **71**, 65–68 (1993)
9. Hemati, N.: Strange attractors in brushless DC motors. IEEE T. Circuits-I **41**, 40–45 (1994)
10. Alexeev, I.: Lorenz system in the thermodynamic modelling of leukaemia malignancy. Med. Hypotheses **102**, 150–155 (2017)
11. Glendinning, P., Sparrow, C.: T-points: a codimension two heteroclinic bifurcation. J. Stat. Phys. **43**, 479–488 (1986)
12. Tucker, W.: The Lorenz attractor exists. C. R. Acad. Sci. **328**, 1197–1202 (1999)
13. Barrio, R., Serrano, S.: Bounds for the chaotic region in the Lorenz model. Physica D **238**, 1615–1624 (2009)
14. Messias, M.: Dynamics at infinity and the existence of singularly degenerate heteroclinic cycles in the Lorenz system. J. Phys. A **42**, 115101 (2009)
15. Llibre, J., Messias, M., da Silva, P.R.: Global dynamics of the Lorenz system with invariant algebraic surfaces. Int. J. Bifurc. Chaos **20**, 3137–3155 (2010)
16. Algaba, A., Fernández-Sánchez, F., Merino, M., Rodríguez-Luis, A.J.: Centers on center manifolds in the Lorenz, Chen and Lü systems. Commun. Nonlinear Sci. Numer. Simul. **19**, 772–775 (2014)
17. Algaba, A., Fernández-Sánchez, F., Merino, M, Rodríguez-Luis, A.J.: Analysis of the T-point-Hopf bifurcation in the Lorenz system. Commun. Nonlinear Sci. Numer. Simul. **22**, 676–691 (2015)
18. Creaser, J.L., Krauskopf, B., Osinga, H.M.: α-flips and T-points in the Lorenz system. Nonlinearity **28**, R39–R65 (2015)
19. Doedel, E.J., Krauskopf,B., Osinga,H.M.: Global organization of phase space in the transition to chaos in the Lorenz system. Nonlinearity **28**, R113–R139 (2015)
20. Algaba, A., Gamero, E., Merino, M., Rodríguez-Luis, A.J.: Resonances of periodic orbits in the Lorenz system. Nonlinear Dyn. **84**, 2111–2136 (2016)
21. Leonov, G.A., Kuznetsov, N.V., Korzhemanova, N.A., Kusakin, D.V.: Lyapunov dimension formula for the global attractor of the Lorenz system. Commun. Nonlinear Sci. Numer. Simul. **41**, 84–103 (2016)
22. Algaba, A., Merino, M., Rodríguez-Luis, A.J.: Superluminal periodic orbits in the Lorenz system. Commun. Nonlinear Sci. Numer. Simulat. **39**, 220–232 (2016)
23. Algaba, A., Freire, E., Gamero, E., Rodríguez-Luis, A.J.: Analysis of Hopf and Takens–Bogdanov bifurcations in a modified van der Pol-Duffing oscillator. Nonlinear Dyn. **16**, 369–404 (1998)
24. Algaba, A., Freire, E., Gamero, E., Rodríguez-Luis, A.J.: A three-parameter study of a degenerate case of the Hopf-pitchfork bifurcation. Nonlinearity **12**, 1177–1206 (1999)
25. Algaba, A., Freire, E., Gamero, E., Rodríguez-Luis, A.J.: On a codimension-three unfolding of the interaction of degenerate Hopf and pitchfork bifurcations. Int. J. Bifurc. Chaos **9**, 1333–1362 (1999)
26. Algaba, A., Freire, E., Gamero, E., Rodríguez-Luis, A.J.: A tame degenerate Hopf-pitchfork bifurcation in a modified van der Pol-Duffing oscillator. Nonlinear Dyn. **22**, 249–269 (2000)
27. Gamero, E., Freire, E., Rodríguez-Luis, A.J., Ponce, E., Algaba, A.: Hypernormal form calculation for triple-zero degeneracies. B. Belg. Math. Soc. Sim. **6**, 357–368 (1999)

28. Champneys, A.R., Rodríguez-Luis, A.J.: The non-transverse Shil'nikov-Hopf bifurcation: uncoupling of homoclinic orbits and homoclinic tangencies. Physica D **128**, 130–158 (1999)
29. Freire, E., Rodríguez-Luis, A.J., Gamero, E., Ponce, E.: A case study for homoclinic chaos in an autonomous electronic circuit. A trip from Takens–Bogdanov to Hopf-Šil'nikov. Physica D **62**, 230–253 (1993)
30. Champneys, A.R., Kuznetsov, Y.A.: Numerical detection and continuation of codimension-two homoclinic bifurcations. Int. J. Bifurc. Chaos **4**, 795–822 (1994)
31. Homburg, A.J., Sandstede, B.: Homoclinic and heteroclinic bifurcations in vector fields. In: Broer, H., et al. (eds.) Handbook of Dynamical Systems, vol. 3, pp. 379–524. Elsevier, Amsterdam (2010)
32. Guckenheimer, J., Holmes, P.J.: Nonlinear Oscillations, Dynamical Systems, and Bifurcations of Vector Fields. Springer, New York (1983)
33. Wiggins, S.: Introduction to Applied Dynamical Systems and Chaos. Springer, New York (2003)
34. Kuznetsov, Y.A.: Elements of Applied Bifurcation Theory. Springer, New York (2004)
35. Algaba, A., Gamero, E., Rodríguez-Luis A.J.: A bifurcation analysis of a simple electronic circuit. Commun. Nonlinear Sci. Numer. Simul. **10**, 169–178 (2005)
36. Gazor, M., Moazeni, M.: Parametric normal forms for Bogdanov–Takens singularity; the generalized saddle-node case. Discrete Contin. Dyn. Syst. **35**, 205–224 (2015)
37. Zhan, F., Liu, S., Zhang, X., Wang, J., Lu, B.: Mixed-mode oscillations and bifurcation analysis in a pituitary model. Nonlinear Dyn. **94**, 807–826 (2018)
38. Gazor, M., Sadri, N.: Bifurcation controller designs for the generalized cusp plants of Bogdanov–Takens singularity with an application to ship control. SIAM J. Control Optim. **57**, 2122–2151 (2019)
39. Durga Prasad, K., Prasad, B.S.R.V.: Qualitative analysis of additional food provided predator–prey system with anti-predator behaviour in prey. Nonlinear Dyn. **96**, 1765–1793 (2019)
40. Algaba, A., Chung, K.W., Qin, B.W., Rodríguez-Luis, A.J.: A nonlinear time transformation method to compute all the coefficients for the homoclinic bifurcation in the quadratic Takens–Bogdanov normal form. Nonlinear Dyn. **97**, 979–990 (2019)
41. Algaba, A., Domínguez-Moreno, M.C., Merino, M., Rodríguez-Luis, A.J.: Double-zero degeneracy and heteroclinic cycles in a perturbation of the Lorenz system. Commun. Nonlinear Sci. Numer. Simul. **111**, 106482 (2022)
42. Maurício de Carvalho, J.P.S., Rodrigues, A.A.: SIR model with vaccination: bifurcation analysis. Qual. Theory Dyn. Syst. **22**, 105 (2023)
43. Wang, Q., Huang, W., Feng, J.: Multiple limit cycles and centers on center manifolds for Lorenz system. Appl. Math. Comput. **238**, 281–288 (2014)
44. Algaba, A., Domínguez-Moreno, M.C., Merino, M., Rodríguez-Luis, A.J.: Study of the Hopf bifurcation in the Lorenz, Chen and Lü systems. Nonlinear Dyn. **79**, 885–902 (2015)
45. Algaba, A., Domínguez-Moreno, M.C., Merino, M., Rodríguez-Luis, A.J.: Takens–Bogdanov bifurcations of equilibria and periodic orbits in the Lorenz system. Commun. Nonlinear Sci. Numer. Simul. **30**, 328–343 (2016)
46. Algaba, A., Domínguez-Moreno, M.C., Merino, M., Rodríguez-Luis, A.J.: A Review on Some Bifurcations in the Lorenz System. In: Carmona, V. et al. (eds) Nonlinear Systems, Vol. 1. Understanding Complex Systems, pp. 3–36. Springer, Cham (2018)
47. V. de Witte, W. Govaerts, Y.A. Kuznetsov, M. Friedman, Interactive initialization and continuation of homoclinic and heteroclinic orbits in MATLAB, ACM T. Math. Software 38 (2012) art. no. 18.
48. Barrio, R., Shilnikov, A., Shilnikov, L.: Kneadings, symbolic dynamics and painting Lorenz chaos. Int. J. Bifurcat. Chaos **22**, 1230016 (2012)
49. Fernández-Sánchez, F., Freire, E., Rodríguez-Luis, A.J.: T-Points in a $\mathbb{Z}_2$-symmetric electronic oscillator. (I) Analysis. Nonlinear Dyn. **28**, 53–69 (2002)
50. Algaba, A., Fernández-Sánchez, F., Merino, M., Rodríguez-Luis, A.J.: Structure of saddle-node and cusp bifurcations of periodic orbits near a non-transversal T-point. Nonlinear Dynamics **63**, 455–476 (2011)
51. Rodrigues, A.A.P.: Repelling dynamics near a Bykov cycle. J. Dyn. Diff. Equat. 25, 605–625 (2013)
52. Sparrow, C.: The Lorenz Equation: Bifurcations, Chaos and Strange Attractors. Springer, New York (1982)
53. Keener, J.P.: Infinite period bifurcation and global bifurcation branches. SIAM J. Appl. Math. **41**, 127–144 (1981)
54. Chow, S.N., Li, C., Wang, D.: Normal forms and bifurcation of planar vector fields. Cambridge University Press, Cambridge (1994)
55. Qin, B.W., Chung, K.W., Algaba, A., Rodríguez-Luis, A.J.: High-order approximation of heteroclinic bifurcations in truncated 2D-normal forms for the generic cases of Hopf-zero and non-resonant double Hopf singularities. SIAM J. Appl. Dynam. Syst. **20**, 403–437 (2021)
56. Doedel, E.J., Champneys, A.R., Dercole, F., Fairgrieve, T., Kuznetsov, Y., Oldeman, B.E., Paffenroth, R., Sandstede, B., Wang, X., Zhang, C.: Auto07-P: Continuation and bifurcation software for ordinary differential equations (with HomCont). Technical report, Concordia University (2010)
57. Krauskopf, B., Oldeman, B.E.: Bifurcations of global reinjection orbits near a saddle-node Hopf bifurcation. Nonlinearity **19**, 2149–2167 (2006)
58. Rademacher, J.D.M.: Homoclinic orbits near heteroclinic cycles with one equilibrium and one periodic orbit. J. Diff. Equ. **218**, 390–443 (2005)
59. Glendinning, P.: Bifurcations near homoclinic orbits with symmmetry. Phys. Lett. A **103**, 163–166 (1984)
60. Hirschberg, P., Knobloch, E.: Sil'nikov-Hopf bifurcation. Physica D **62**, 202–216 (1993)
61. Kokubu, H., Roussarie, R.: Existence of a singulary degenerate heteroclinic cycle in the Lorenz system and its dynamical consequences: Part I. J. Dyn. Differ. Equ. **16**, 513–557 (2004)

Informe con el factor de impacto de las publicaciones presentadas.

Double-zero degeneracy and heteroclinic cycles in a perturbation of the Lorenz system

Algaba, A.; Domínguez-Moreno, M. C.; Merino, M.; Rodríguez-Luis, A. J.

Tipo: Artículo
Revista: COMMUNICATIONS IN NONLINEAR SCIENCE AND NUMERICAL SIMULATION (1007-5704 / 1878-7274)
Año de Publicación: 2022
Volumen: 111
Número de artículo: 106482
Acceso abierto: Vía híbrida

Fuente	Nº Citas	Fecha Actualización
scopus	1	27-05-2023
wos	0	28-05-2023

Año: 2021

Journal Impact Factor (JIF): 4,186

Categoría	Edición	Posición	Cuartil	Tercil	Decil
MATHEMATICS, APPLIED	SCIE	9/267	Q1	T1	D1
PHYSICS, MATHEMATICAL	SCIE	4/56	Q1	T1	D1
MATHEMATICS, INTERDISCIPLINARY APPLICATIONS	SCIE	14/108	Q1	T1	D2
PHYSICS, FLUIDS & PLASMAS	SCIE	5/34	Q1	T1	D2
MECHANICS	SCIE	35/138	Q2	T1	D3

Año: 2021

CiteScore: 7,700

Categoría	Posición	Cuartil	Tercil	Decil
Applied Mathematics	23/590	Q1	T1	D1
Modeling and Simulation	19/303	Q1	T1	D1
Numerical Analysis	2/76	Q1	T1	D1

Study of a simple 3D quadratic system with homoclinic flip bifurcations of inward twist case C-in

Algaba, A.; Domínguez-Moreno, M. C.; Merino, M.; Rodríguez-Luis, A. J.

Tipo: Artículo
Revista: COMMUNICATIONS IN NONLINEAR SCIENCE AND NUMERICAL SIMULATION (1007-5704 / 1878-7274)
Año de Publicación: 2019
Volumen: 77
Páginas: 324 - 337

Fuente	Nº Citas	Fecha Actualización
scopus	3	27-05-2023
wos	3	27-05-2023

Año: 2019

Journal Impact Factor (JIF): 4,115

Categoría	Edición	Posición	Cuartil	Tercil	Decil
MATHEMATICS, APPLIED	SCIE	3/261	Q1	T1	D1
MATHEMATICS, INTERDISCIPLINARY APPLICATIONS	SCIE	7/106	Q1	T1	D1
PHYSICS, FLUIDS & PLASMAS	SCIE	2/34	Q1	T1	D1
PHYSICS, MATHEMATICAL	SCIE	1/55	Q1	T1	D1
MECHANICS	SCIE	15/136	Q1	T1	D2

Año: 2019

CiteScore: 7,300

Categoría	Posición	Cuartil	Tercil	Decil
Applied Mathematics	14/510	Q1	T1	D1
Modeling and Simulation	14/274	Q1	T1	D1
Numerical Analysis	2/60	Q1	T1	D1

Takens-Bogdanov bifurcations of equilibria and periodic orbits in the Lorenz system

Algaba, A.; Domínguez-Moreno, M. C.; Merino, M.; Rodríguez-Luis, A. J.

Tipo: Artículo
Revista: COMMUNICATIONS IN NONLINEAR SCIENCE AND NUMERICAL SIMULATION (1007-5704 / 1878-7274)
Año de Publicación: 2016
Volumen: 30
Número: 1-3

- Páginas: 328 - 343

Fuente	Nº Citas	Fecha Actualización
scopus	23	27-05-2023
wos	21	27-05-2023

Año: 2016

Journal Impact Factor (JIF): 2,784

Categoría	Edición	Posición	Cuartil	Tercil	Decil
MATHEMATICS, APPLIED	SCIE	9/255	Q1	T1	D1
PHYSICS, MATHEMATICAL	SCIE	2/55	Q1	T1	D1
MATHEMATICS, INTERDISCIPLINARY APPLICATIONS	SCIE	15/100	Q1	T1	D2
MECHANICS	SCIE	19/133	Q1	T1	D2
PHYSICS, FLUIDS & PLASMAS	SCIE	7/31	Q1	T1	D3

Año: 2016

CiteScore: 6,200

Categoría	Posición	Cuartil	Tercil	Decil
Applied Mathematics	11/408	Q1	T1	D1
Modeling and Simulation	6/225	Q1	T1	D1
Numerical Analysis	2/44	Q1	T1	D1

Study of the Hopf bifurcation in the Lorenz, Chen and Lu systems

Algaba, Antonio; Domínguez-Moreno, María C.; Merino, Manuel; Rodríguez-Luis, Alejandro J.

Tipo: Artículo
Revista: NONLINEAR DYNAMICS (0924-090X / 1573-269X)
Año de Publicación: 2015
Volumen: 79
Número: 2
Páginas: 885 - 902

Fuente	Nº Citas	Fecha Actualización
scopus	21	27-05-2023
wos	17	27-05-2023

Año: 2015

Journal Impact Factor (JIF): 3,000

Categoría	Edición	Posición	Cuartil	Tercil	Decil
ENGINEERING, MECHANICAL	SCIE	8/132	Q1	T1	D1
MECHANICS	SCIE	8/135	Q1	T1	D1

Año: 2015

CiteScore: 5,600

Categoría	Posición	Cuartil	Tercil	Decil
Aerospace Engineering	5/107	Q1	T1	D1
Applied Mathematics	18/407	Q1	T1	D1
Mechanical Engineering	24/533	Q1	T1	D1
Ocean Engineering	2/89	Q1	T1	D1
Control and Systems Engineering	25/214	Q1	T1	D2
Electrical and Electronic Engineering	71/660	Q1	T1	D2